

CHARACTERIZATION OF THE ROLES OF NEURONAL CHOLESTEROL
BIOSYNTHESIS AND ORP4 IN HIPPOCAMPAL NEURONS AND GLIA

by

Laura A. Martin

Submitted in partial fulfilment of the requirements
for the degree of Master of Science

at

Dalhousie University
Halifax, Nova Scotia
October 2016

© Copyright by Laura A. Martin, 2016

TABLE OF CONTENTS

LIST OF TABLES	v
LIST OF FIGURES.....	vi
ABSTRACT	viii
LIST OF ABBREVIATIONS USED	ix
ACKNOWLEDGMENTS	xii
CHAPTER 1: INTRODUCTION	1
1.1 STRUCTURE OF BRAIN AND BRAIN CELL TYPES.....	1
1.1.1 OVERVIEW OF BRAIN STRUCTURE	1
1.1.2 NEURONAL MORPHOLOGY AND SYNAPSE STRUCTURE	2
1.1.3 MECHANISMS OF SYNAPTIC TRANSMISSION	3
1.1.4 GLIAL CELL TYPES AND FUNCTIONS	5
1.2 CHOLESTEROL BIOSYNTHESIS.....	7
1.2.1 OVERVIEW OF THE CHOLESTEROL BIOSYNTHETIC PATHWAY.....	7
1.2.2 NEURONAL AND GLIAL CHOLESTEROL SYNTHESIS.....	9
1.2.3 CHOLESTEROL TURNOVER IN THE BRAIN	13
1.3 REGULATION OF CHOLESTEROL BIOSYNTHESIS.....	14
1.3.1 CONSEQUENCES OF DYSREGULATED CHOLESTEROL HOMEOSTASIS IN THE BRAIN	15
1.4 OXYSTEROL BINDING PROTEINS	17
1.4.1 OSBP AND OSBP-RELATED PROTEIN FAMILY	17
1.4.2 ORP4	19
1.5 RESEARCH OBJECTIVES.....	22
CHAPTER 2: MATERIALS AND METHODS	23
2.1 MATERIALS.....	23
2.2 SOLUTIONS.....	23
2.3 CELL CULTURE	24
2.3.1 Primary Hippocampal Cell Culture	24
2.3.2 Immortalized Cell Lines.....	25

2.4 PLASMIDS AND CLONING	25
2.5 RNA INTERFERENCE (RNAi)	27
2.5.1 Calcium Phosphate (CaPO ₄) Transfection	27
2.5.2 Viral Production	31
2.6 STABLE CELL LINE PREPARATION.....	31
2.6.1 Polyethyleneimine (PEI) Transfection	31
2.6.2 Selection Of Transfected Cells.....	31
2.7 CELL COLLECTION	32
2.8 PROTEIN DETERMINATION.....	32
2.9 SDS-PAGE AND WESTERN BLOTTING	32
2.10 ISOLATION OF RNA AND qPCR	33
2.11 IMMUNOSTAINING	35
2.12 IMAGE ACQUISITION AND ANALYSIS.....	35
2.12.1 Mitochondrial Length	38
2.12.2 Spine Density	38
2.12.3 Neuronal PINK1 And NRF2 Levels	39
2.13 STATISTICS.....	39
 CHAPTER 3: RESULTS.....	 40
3.1. SELECTIVE DOWNREGULATION OF NEURONAL CHOLESTEROL BIOSYNTHETIC ENZYMES.....	40
3.1.1 Expression Of Fluorescent Reporter Constructs For Visualization Of The Effects Of Decreased Neuronal Cholesterol Biosynthetic Enzymes.....	41
3.1.2 Validation Of Short Hairpin Sequences	42
3.1.3 Decreased FDFT1 Or CYP51 Increases Dendritic Spine Density.....	45
3.1.4 Mitochondrial Effects Of Decreased FDFT1 Or CYP51	47
3.2 ORP4 EXPRESSION IN HIPPOCAMPAL CULTURES	49
3.2.1 Transduction With shORP4 Or shORP4L Does Not Affect Cholesterol Biosynthetic Enzyme Expression	50
3.3 TRANSDUCTION WITH shORP4 OR shORP4L DIMINISHES GLIAL POPULATIONS BUT NOT NEURONAL CELL NUMBERS WITHOUT AFFECTING GROSS CELLULAR MORPHOLOGY.....	54

3.3.1 Transduction With shORP4 Or shORP4L Inhibits Proliferation But Does Not Induce Apoptosis	57
3.4 EFFECTS OF shORP4 OR shORP4L ON ORGANELLAR MORPHOLOGY.....	57
3.4.1 Transduction With shORP4 Or shORP4L Elongates Neuritic And Glial Mitochondria	60
3.5 EFFECTS OF shORP4 OR shORP4L ON MITOCHONDRIAL DYNAMICS.....	63
3.6 EFFECTS OF shORP4 OR shORP4L ON NEURONAL PINK1 LEVELS	65
3.7 EFFECTS OF shORP4 OR shORP4L ON NEURONAL NRF2 LEVELS AND LOCALIZATION	67
 CHAPTER 4: DISCUSSION	 73
4.1 OVERVIEW OF RESEARCH OBJECTIVES.....	73
4.2 THE ROLE OF NEURONAL CHOLESTEROL BIOSYNTHESIS IN HIPPOCAMPAL NEURONS	74
4.3 THE ROLE OF ORP4 IN HIPPOCAMPAL NEURONS AND GLIA.....	78
4.3.1 ORP4 Is Required For Glial Cell Proliferation But Not Neuronal Survival.....	79
4.3.2 ORP4 Regulates Glial And Neuritic Mitochondrial Length	81
4.3.3 ORP4 Regulates Neuronal PINK1 And NRF2 Protein Levels	85
4.4 CONCLUSION	87
 REFERENCES	 89

LIST OF TABLES

Table 1. pGipZ Vector Constructs With Promoters, Fluorescent Reporters And Subcellular Localizations.....	28
Table 2. List Of Hairpin Targets, pGipZ Catalogue Variants, Forward Hairpin Sequences And Abbreviations Used In Thesis.....	29
Table 3. List Of Hairpin Targets, Forward Sequences And Abbreviations For pLKO.1 Vectors Used In Thesis.	30
Table 4. Dilutions Of Primary Antibodies Used In Immunoblotting Experiments.	34
Table 5. List Of The Primer Sequences Used In qPCR Experiments.....	36
Table 6. List Of Excitation And Emission Filters Used For All Live And Fixed Cell Images.....	37

LIST OF FIGURES

Figure 1. Simplified Cholesterol Biosynthetic Pathway.....	8
Figure 2. OSBP And ORP4 Share Sequence Similarity	20
Figure 3. Lifeact And Mito Target Subcellular Regions But Ppalm Causes Fluorescent Artefacts.....	43
Figure 4. Two Each Of Three Hairpin Sequences Targeting FDFT1 Or CYP51 Decrease mRNA Levels Of FDFT1 Or CYP51, Respectively.....	44
Figure 5. Decreased FDFT1 Or CYP51 Increases Dendritic Spine Density	46
Figure 6. Decreased FDFT1 Or CYP51 Does Not Alter Mitochondrial Size.....	48
Figure 7. ORP4 Isoforms Are Expressed By Neurons And Co-Cultures At DIV8 And DIV15	51
Figure 8. ORP4 Isoform Expression 48 h After Transduction Of DIV7 Cultures With shORP4 Or shORP4L	53
Figure 9. Transduction With shORP4 Or shORP4L Does Not Alter Cholesterol Biosynthetic Enzyme Expression.....	55
Figure 10. Transduction With shORP4 Or shORP4L Inhibits Glial Proliferation In DIV7 Cultures Without Affecting Gross Glial Morphology	56
Figure 11. Transduction With shORP4 Or shORP4L Does Not Affect Neuronal Cell Numbers Or Gross Neuronal Morphology	58
Figure 12. Transduction With shORP4 Or shORP4L Does Not Induce Apoptosis	59
Figure 13. Transduction With shORP4 Or shORP4L Does Not Alter Gross Cis, Medial-Golgi Morphology.....	61
Figure 14. Transduction With shORP4 Or shORP4L Does Not Alter Gross ER Morphology	62
Figure 15. Transduction With shORP4 Or shORP4L Elongates Mitochondria.....	64
Figure 16. Transduction With shORP4 Or shORP4L Does Not Alter mRNA Levels Of MFN2, FIS1 Or TFAM.....	66

Figure 17. Transduction With shORP4 Or shORP4L Decreases PINK1 Levels In
The Soma 68

Figure 18. Transduction With shORP4 Or shORP4L Does Not Alter mRNA
Levels Of NRF2 Or HMOX1 69

Figure 19. Transduction With shORP4 Increases Somatic NRF2 Levels..... 71

Figure 20. Transduction With shORP4 Or shORP4L Does Not Affect Nuclear
NRF2 Translocation..... 72

ABSTRACT

Cholesterol is an essential component of cell membranes and plays important roles in cell signalling. The brain contains a quarter of the body's total cholesterol pool, all of which is synthesized *in situ* by neurons and glia, which are the structurally and functionally distinct cells of the brain. Neurons synthesize large quantities of cholesterol during development, but rely more so on glial synthesis in the adult brain. Yet neuronal cholesterol synthesis is maintained into maturity, suggesting a specific role for this process. Oxysterol-binding protein-related protein 4 (ORP4) is highly expressed in the hippocampus, and binds and transfers cholesterol and phosphatidylinositol-4-phosphate *in vitro*. I investigated the roles of neuronal cholesterol biosynthesis and ORP4 in hippocampal cells. My findings implicate neuronal cholesterol synthesis in regulating spine density and provide evidence for a role of ORP4 in glial proliferation, mitochondrial morphology, and the regulation of neuronal proteins involved in mitochondrial homeostasis.

LIST OF ABBREVIATIONS USED

24-DHCR	24 dehydrocholesterol reductase
24OHC	24- hydroxycholesterol
25OHC	25-hydroxycholesterol
7-DHCR	7-dehydrocholesterol reductase
ABCA1	ATP-binding cassette protein A1
AD	Alzheimer's Disease
APOE	apolipoprotein E
APP	amyloid precursor protein
ATP	adenosine triphosphate
BBB	blood brain barrier
BCA	bicichoninic acid
BDNF	brain-derived neurotrophic factor
Ca ²⁺	calcium ion
cDNA	complementary DNA
CERT	ceramide transfer protein
CHO	Chinese hamster ovary
CMV	cytomegalovirus
CNS	central nervous system
COPII	coat protein II
CSF	cerebrospinal fluid
CYCLO	cyclophilin
CYP46A1	cytochrome P450 family, protein 46A1 (24S-hydroxylase)
CYP51	cytochrome P450 family, protein 51 (lanosterol-14 α -demethylase)
CYTC	cytosine arabinoside
DEPC	diethylpyrocarbonate
DFBS	dialyzed fetal bovine serum
DHL	25,25-dihydrolanosterol
DIV	day in vitro
DMEM	Dulbecco's modified Eagle's medium
DMSO	dimethyl sulfoxide
DNA	deoxyribonucleic acid
DPP	dimethylallyl pyrophosphate
DRP1	dynamamin-related protein 1
ECL	enhanced chemiluminescence
ER	endoplasmic reticulum
F-actin	filamentous actin
FBS	fetal bovine serum
FDFT1	farnesyl diphosphate farnesyltransferase, (squalene synthase)
FFAT	two phenylalanines in an acidic tract
FIS1	fission protein 1
FPP	farnesyl pyrophosphate
GFAP	glial fibrillary acidic protein
GFP	green fluorescent protein
GGPP	geranylgeranyl pyrophosphate

GPP	geranyl pyrophosphate
HBS	HEPES buffered saline
HD	Huntington's Disease
HEK	human embryonic kidney
HLM	HeLa metastatic
HMG	3-hydroxy-3-methylglutaryl coenzyme A
HMGS	3-hydroxy-3-methylglutaryl coenzyme A synthase
HMOX1	heme oxygenase 1
HRP	horseradish peroxidase
INSIG1	insulin-induced gene 1
IP3R	inositol triphosphate receptor
IPP	isopentenyl pyrophosphate
K ⁺	potassium ion
KEAP1	Kelch-like ECH-associated protein 1
LDLR	low density lipoprotein receptor
LE/L	late endosome/lysosome
LPDS	lipoprotein-deficient serum
LRP1	low density lipoprotein receptor-related protein 1
LS	lanosterol synthase
LXR	liver X receptor
MAM	mitochondria-associated ER membrane
MAP2	microtubule-associated protein 2
MCS	membrane contact site
MEM	minimum essential medium
MFN	mitofusin
mHTT	mutant huntingtin
mV	millivolt
Na ⁺	sodium ion
NB	neurobasal
NPC	Niemann Pick Type C
NRF2	nuclear factor (erythroid-derived 2)-like 2 protein
NT	non-targeting
ORD	oxysterol-binding protein homology domain
ORP	oxysterol-binding protein-related protein
ORP4L	oxysterol-binding protein-related protein 4, long isoform
ORP4S	oxysterol-binding protein-related protein 4, short isoform
OSBP	oxysterol binding protein
PD	Parkinson's Disease
PDI	protein disulphide isomerase
PEI	polyethyleneimine
PH	Pleckstrin homology
PI4P	phosphatidyl inositol-4-phosphate
PINK1	phosphatase and tensin homolog- induced putative kinase 1
PKA	protein kinase A
PSD	postsynaptic density
PVDF	polyvinylidene fluoride

PVP	polyvinylpyrrolidone
qPCR	quantitative polymerase chain reaction
RGC	retinal ganglion cell
RNAi	RNA interference
ROS	reactive oxygen species
RT	room temperature
SCAP	sterol response element binding protein cleavage-activating protein
SDS PAGE	sodium dodecyl sulphate polyacrylamide gel electrophoresis
SEM	standard error of the mean
sh	short hairpin
SLOS	Smith-Lemli-Opitz Syndrome
SRE	sterol regulatory element
SREBP2	sterol regulatory element-binding protein 2
SV	synaptic vesicle
SYN	synapsin
TFAM	mitochondrial DNA transcription factor A
TOM20	translocase of the outer mitochondrial membrane
TRKB	tropomyosin kinase B
VAMP	vesicle-associated membrane protein
VAP	vesicle-associated membrane protein-associated protein
VDAC	voltage-dependent anion channel
v/v	volume/volume
w/v	weight/volume

ACKNOWLEDGMENTS

When I started this process, I was naïve to think that a Masters degree was simply an academic endeavour, because what I gained was so much more than just scientific knowledge and skills. The most difficult things are the ones worth doing, and this was not easy. But none of it was accomplished alone.

I wouldn't be here without my family, both literally and figuratively. To my parents, for your love and undying support, and for driving me from Guelph to Halifax in the worst winter hurricane of 2014 so I could pursue this degree. You are my strength, my motivation and my greatest supporters. To my siblings Christa, Geoff, Sarah and Alan, for the visits, the texts and the laughs. You made sure I never felt alone out here.

To Adrien, my first and best Halifax friend, for all the Saturdays spent ocean-side, the Timbits and IPAs, the failed cakes and the fun. You'll never know how much you did for me. To fellow Guelphite Eric, for always finding time to argue, reminisce and rant with me. To Sarah, for understanding what it's like to be the new girl and for sharing commiserations and celebrations alike. And to all the wonderful people I've been so lucky to meet along the way: Mary, Anna, Colin, Vanessa, Greg and Anto. You made this experience so much more than I expected.

To my past lab mates, Veronique and Barry, for welcoming me into the lab, teasing me about the pronunciation of Donair, and never failing to include me. To my present lab mates, Zoe, Pia and Debbie, for making me laugh, checking on me in Platform 9N $\frac{3}{4}$, and, maybe most importantly, for always returning the good scissors to my desk. I was incredibly lucky to have such an amazing group of people by my side throughout this degree.

Finally, to Dr Barbara Karten, for whom a simple “thank you” does not suffice. Knowing personally the struggles of completing a Masters degree five years out of undergrad with limited knowledge of biochemistry or neuroscience, I can only imagine how difficult it was to take on a student in my position. You pushed me forward, you encouraged me and you believed in my abilities. You invested countless hours and tireless effort in helping me realize my goals. For these things, I can never thank you enough.

Two and a half years, seven computers and three purple pens later, I’m done. After all the trepidation and failure, the cautious optimism and success, this is my contribution to the pool of scientific knowledge.

CHAPTER 1: INTRODUCTION

1.1 STRUCTURE OF BRAIN AND BRAIN CELL TYPES

1.1.1 OVERVIEW OF BRAIN STRUCTURE

The brain is a complex and fascinating organ that rapidly processes sensory information and coordinates responses to stimuli. It is classified into left and right hemispheres and defined by regions: the cerebrum, cerebellum, brainstem and limbic system. The cerebrum enables thoughts and actions, and is classified into lobes based on naturally occurring clefts: the frontal, parietal, temporal and occipital lobes. The cerebellum is responsible for fine movement and balance, and lies at the base of the cerebrum. The brainstem resides next to the cerebellum and coordinates vital functions like breathing and pulse. The limbic system is above the brainstem and within the cerebrum, and is the emotional and behavioural centre of the brain. The hippocampus is a component of the limbic system and is central to learning and memory processes ¹. The increasing prevalence of dementia ² and other cognitive and neurodegenerative disorders has led to intense research on this brain region.

The blood brain barrier (BBB) protects the central nervous system (CNS) from insults to the peripheral circulation. The BBB consists of tight endothelial junctions in the blood vessels supplying the brain and prevents entry of small molecules and infectious agents into the cerebrospinal fluid (CSF) ³. Cholesterol, a lipid molecule essential for all animal membranes, is one such molecule that cannot cross the BBB. Yet the brain is a cholesterol-rich organ, comprising only 2% of the body's weight but containing nearly

25% of the body's total cholesterol pool ⁴. Neurons and glia, the morphologically and functionally distinct cells of the brain, synthesize this cholesterol entirely *in situ*.

1.1.2 NEURONAL MORPHOLOGY AND SYNAPSE STRUCTURE

Neurons are polar cells that consist of a soma (cell body) and neurites, which are protrusions from the soma. Neurites are classified as dendrites and axons based on both structural and functional characteristics. Dendrites are branched and tapered neurites that typically receive input from other neurons and propagate signals toward the soma. Axons are neurites of uniform diameter that protrude from the soma at the axon hillock and propagate signals away from the soma. While a neuron can have numerous dendritic processes, it contains no more than one axon, although the axon can branch into multiple termini and is commonly longer than dendritic processes. The soma contains the nucleus and is the major site of mRNA transcription and protein translation in neurons. Organelles are present in the soma and throughout the neuritic processes, as ER, Golgi and mitochondria have been detected in dendrites and axons ⁵.

Synapses facilitate the transmission of signals through small molecules at specialized neuronal membrane apposition sites that consist of a presynaptic axonal terminus and a postsynaptic dendritic or somatic terminus separated by an extracellular synaptic cleft. While synapses are typically formed between axons and dendrites (axodendritic) or axons and the soma (axosomatic), axon-axon and dendrite-dendrite synapses are also possible, though less common, and largely serve inhibitory functions.

Spines are dynamic, postsynaptic dendritic protrusions present on some neuronal cell types that increase dendritic surface area and sequester subcellular processes ⁶. Spines are highly plastic structures that grow or regress rapidly in response to stimuli

and/or spontaneously, and form at cholesterol- and sphingolipid-rich membrane domains termed lipid microdomains ⁷. Membrane deformation initiates spine formation while filamentous actin (F-actin) polymerization elongates spines ⁸. Dendritic spines are classified into categories according to morphology: filopodia, thin, stubby, mushroom and cup-shaped (reviewed in ⁹); however, these classifications are based on fixed spine images and may only reflect stages of spine formation, maturation or regression without accurately reflecting active or functional spines. Filopodia are the predominant spine type early in development and likely act as the precursors to all mature spine types ^{10, 11}.

1.1.3 MECHANISMS OF SYNAPTIC TRANSMISSION

Neuronal plasma membranes contain voltage-gated ion channels that maintain a membrane potential of -70 mV at rest. When stimulated by another neuron, an electrical signal known as an action potential increases the membrane potential to a threshold potential (-55 mV or higher) that opens ion channels, causes influx of Na⁺, and depolarizes the membrane. This influx of Na⁺ increases the membrane potential and opens K⁺ channels, releasing K⁺ from the neuron and repolarizing the membrane. This ion exchange is facilitated by the Na⁺/K⁺ ATPase, which uses ATP to pump Na⁺ out and K⁺ in to maintain the ion concentration gradient within the cell. Neurons are polar cells and thus, the action potential moves uni-directionally from its site of initiation to the axon terminus ¹². The axon hillock is the initiation site of most action potentials and contains more voltage-gated ion channels than the soma.

Neurotransmission is the process whereby an action potential stimulates release into the synaptic cleft of chemical neurotransmitters, which bind to receptors on the postsynaptic surface and propagate a signal. At the presynaptic terminal, the action

potential depolarizes the membrane and opens voltage-gated Ca^{2+} channels, which causes influx of Ca^{2+} and activation of calcium-sensitive proteins. Synaptotagmin is a calcium-sensitive transmembrane protein of synaptic vesicles (SV), which contain neurotransmitters. When activated by calcium, synaptotagmin interacts with protein complexes on the presynaptic plasma membrane and enables fusion of SVs with this membrane, thus rapidly releasing neurotransmitters into the synaptic cleft via exocytosis. The site of SV fusion and neurotransmitter release is termed the active zone¹³. The SV pool is replenished through SV recycling, which is the process of endocytosing SV components from the plasma membrane, re-acidifying of the SVs and replenishment of their neurotransmitter content¹⁴. After diffusing across the synaptic cleft, these neurotransmitters bind receptors on the postsynaptic neuron, which opens ligand-gated ion channels or alters chemical messenger production, thereby altering the membrane potential and facilitating signal transduction in the receiving cell.

Dendritic spines represent the majority of excitatory postsynaptic termini in the brain¹⁵, although they are not present on all neurons. Approximately 1-10 spines are present per micron of dendrite in mature spiny neurons¹⁶. Spines contain a thin neck and a head; the neck separates the spine from the dendritic shaft, forming a micro-compartment that prevents propagation of action potentials until the threshold potential is reached. The spine head contains the postsynaptic density (PSD), which is a protein-rich region that serves as a platform for neurotransmitter receptors and protein complexes necessary for signalling. The PSD is directly across from the active zone of a presynaptic terminal, ensuring close proximity of neurotransmitters and receptors and thus, efficient neurotransmission. Increases in spine density and size, as well as thickening of the PSD,

increases synaptic strength and the efficacy of neurotransmission, which are key processes underlying learning. Plasticity in spine number and morphology directly influences synapse function and strength, as connections are made and lost as directed by neural activity.

Excessive stimulation of a synapse leads to inhibited neuronal function and cell death. This process is known as excitotoxicity and involves over-activation of neurotransmitter receptors, excessive influx of Ca^{2+} and activation of proteases and endonucleases, which ultimately leads to regulated cell death ¹⁷.

1.1.4 GLIAL CELL TYPES AND FUNCTIONS

Glial cells encompass the proliferative, non-neuronal cells of the brain and serve both structural and functional roles in the CNS. Glia are distinct from neurons in that they are non-synaptogenic and non-polar; however, glia are indirectly involved in neurotransmission by recycling neurotransmitters, supplying molecules essential for synaptogenesis and SV release, insulating axonal processes and clearing neuronal debris (as reviewed in ¹⁸). Glial cells are classified based on structure and function into astrocytes, oligodendrocytes and microglia.

Astrocytes are highly branched cells named for their resemblance to stars and outnumber neurons in the brain ¹⁹. They serve as a scaffold for neuronal outgrowth and regulate blood vessel size through direct contact with vessel walls. Astrocytes also promote synaptogenesis, as evidenced by the increase in synapse number and synaptic efficiency in rat retinal ganglion neurons (RGCs) co-cultured with astrocytes relative to RGCs cultured without astrocytes ^{20, 21}. The effect of astrocytes on synaptogenesis appears to differ among neuronal populations, as isolated hippocampal and cerebellar

neurons from postnatal mice did not require astrocytes for synaptogenesis, but exhibited increased synaptic efficacy when astrocytes were present in culture ²². Synapses of hippocampal neurons also exhibit less astrocytic ensheathment ²³ than synapses of cerebellar neurons (43% versus 87%, respectively) ²⁴ when analyzed by three dimensional reconstruction of electron microscope images, suggesting different levels of astrocyte-synapse interaction and unique requirements for synaptogenesis in neuronal subtypes. In addition to synapse formation, astrocytes prevent neuronal excitotoxicity by taking up and recycling neurotransmitters from the synaptic cleft via membrane transporter proteins ¹⁸.

Oligodendrocytes are cholesterol-rich glial cells that wrap around neuronal axons in a process called myelination. This myelin sheath prevents inadvertent or aberrant propagation of electrical signals by protecting the axon from neighbouring neurons. The discontinuity of the myelin sheath results in uninsulated areas termed nodes of Ranvier, which facilitate rapid propagation of action potentials through saltatory conductance along the axon ²⁵.

Microglia scavenge cellular debris and invading particles in the CNS ²⁶. They are often considered the macrophages of the brain due to the morphological and functional similarities shared by these cell types. Upon insults to the CNS, microglia proliferate and produce molecules involved in immune responses.

1.2 CHOLESTEROL BIOSYNTHESIS

1.2.1 OVERVIEW OF THE CHOLESTEROL BIOSYNTHETIC PATHWAY

Cholesterol biosynthesis is an energetically costly process that employs numerous enzymes and occurs in the endoplasmic reticulum (ER) (as reviewed in ^{27, 28}). Figure 1 illustrates a simplified cholesterol biosynthetic pathway highlighting some of the key intermediates and enzymes. Acetyl-Coenzyme A (acetyl-CoA) is the precursor of cholesterol, and the first step in the biosynthetic pathway is the condensation of two acetyl-CoA molecules to form 3-hydroxy-3-methylglutaryl Coenzyme A (HMG) by HMG synthase (HMGS). HMG is reduced to mevalonate by HMG reductase (HMGR), which is a key regulatory step in the pathway. Condensation of post-mevalonate precursors produces isoprenoids, which are non-sterol intermediates that modify proteins in a process known as prenylation ²⁹ and are necessary for mitochondrial electron transport chain function and DNA synthesis ³⁰. Condensation of isopentenyl pyrophosphate (IPP) and dimethylallyl pyrophosphate (DPP) forms geranyl diphosphate (GPP). Through the tandem action of geranyl diphosphate synthase, GPP is converted to farnesyl diphosphate (FPP) and then geranylgeranyl diphosphate (GGPP).

The conversion of FPP to squalene, which is catalyzed by farnesyl diphosphate farnesyltransferase (FDFT1), is the committed step of cholesterol biosynthesis. Lanosterol is the first sterol intermediate of the cholesterol biosynthetic pathway, and is formed by the conversion of linear 2,3-squalene epoxide to lanosterol by lanosterol synthase (LS).

Demethylation of lanosterol by lanosterol-14 α -demethylase (also known as cytochrome P450, family 51 (CYP51)) gives rise to alternate but parallel and connected

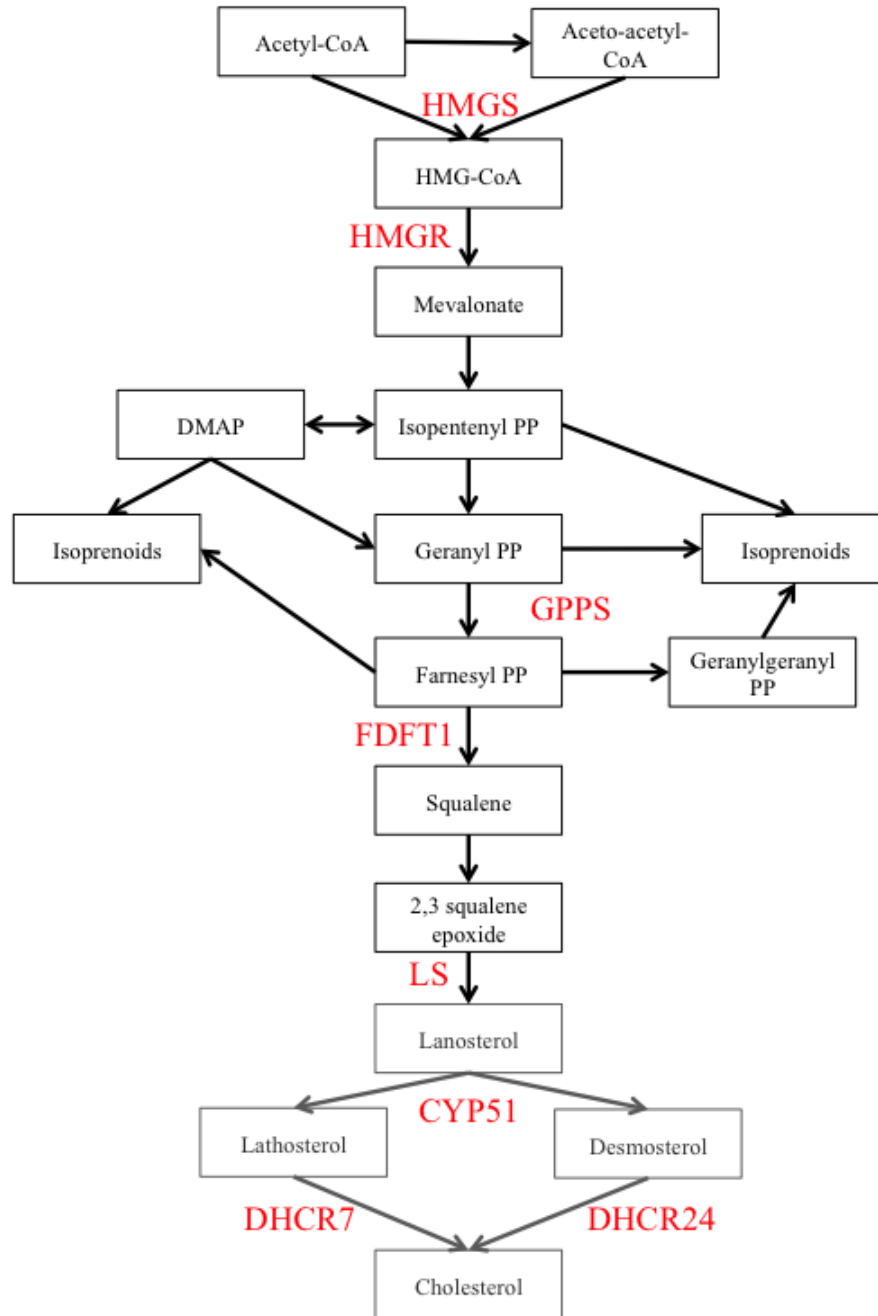


Figure 1. Simplified cholesterol biosynthetic pathway

Cholesterol and isoprenoids are synthesized in a multi-step pathway, involving numerous enzymes (shown in red), and producing both sterol (grey) and non-sterol (black) intermediates.

pathways: the Kandutsch-Russell and Bloch pathways. The primary difference between the pathways is the production of alternate sterol intermediates: predominantly lathosterol in the Kandutsch-Russell pathway and desmosterol in the Bloch pathway. The stage at which the C24 double bond of lanosterol is reduced determines the fate of the pathway: early reduction forms Kandutsch-Russell intermediates while late reduction forms Bloch intermediates ³¹. The pathways are not mutually exclusive and share the same enzymatic steps. Thus, disruptions to either pathway prevent downstream sterol intermediate formation and cholesterol synthesis. Neurons predominantly exhibit intermediates of the Kandutsch-Russell pathway while glia exhibit those of the Bloch pathway ³²; however, the reason for this difference is still unclear. Different dehydrocholesterol reductases (7DHCR and 24DHCR) convert intermediates (7-dehydrocholesterol and 24-dehydrocholesterol, respectively) to the terminal product of the pathway, cholesterol. Disruption of cholesterol biosynthesis at various stages of the pathway can lead to severe and varied neurodevelopmental defects, as cholesterol is imperative for brain function.

1.2.2 NEURONAL AND GLIAL CHOLESTEROL SYNTHESIS

The brain accounts for a quarter of the body's entire cholesterol pool, all of which is synthesized *de novo in situ*. The BBB prevents entry of lipoproteins from the circulation into the brain. Evidence for cholesterol biosynthesis in the brain came from studies as early as 1940 using deuterium in the form of heavy water ³³. In recent decades, studies using intraperitoneal injection of tritium-labelled water into postnatal mouse brains have revealed that brain cholesterol synthesis is highest during the first three postnatal weeks and decreases to low but constant levels by ten weeks, and is unaffected by circulating cholesterol levels ³⁴. The high levels of cholesterol biosynthesis are largely

for myelin synthesis and are dependent on the animal model. Examination of post-mortem human brains using gas chromatography-mass spectrometry revealed that while total cholesterol content in adult brains remains constant, cholesterol biosynthesis decreases with age ³⁵. In the same study, levels of lanosterol and lathosterol were higher in young patients (defined as less than the median age of 38) relative to elderly patients (defined as greater than the median age of 38), illustrating an age-dependent alteration in cholesterol intermediates ³⁵.

The relative contribution of neurons and glia to total cholesterol biosynthesis is unclear and complicated by developmental differences in cellular cholesterol synthesis. Early in development, neuronal membrane expansion and neuritogenesis occur, which requires large quantities of cholesterol. Evidence for neuronal cholesterol biosynthesis in early development comes from studies using cultured sympathetic neurons from newborn rats incubated with radiolabeled acetate, which revealed that cholesterol is synthesized in neuronal cell bodies ³⁶. Studies involving cerebral embryonic rat neurons showed that inhibition of HMGR compromised neuron viability, but supplementation with mevalonate prevented this effect. Additionally, inhibition of FDFT1, which catalyzes squalene synthesis, compromised neuron viability, but supplementation with squalene prevented this effect ³⁷. These results suggest that cholesterol synthesis, and not simply isoprenoid synthesis, is necessary for neuronal survival. Genetic ablation of FDFT1 in embryonic mouse neurons decreased both neuritogenesis and neurite length, which ultimately resulted in neuronal death; however, when FDFT1 was genetically ablated in adult mouse neurons, there were no defects in neurite number or size, and neuronal survival was unaffected ³⁸, suggesting that neuronal cholesterol biosynthesis may not be

essential in the adult brain. Yet experiments involving *in situ* hybridization in the hippocampal neurons of the adult mouse brain revealed that 7DHCR, the final enzyme in the cholesterol biosynthetic pathway, is expressed in hippocampal neurons³⁹, and that all cholesterol biosynthesis and homeostatic genes are expressed^{40,41}. Thus, neurons retain the capacity to synthesize cholesterol into maturity, but the extent of this biosynthesis is unclear, as the presence of cholesterol biosynthetic gene markers does not necessarily reflect active neuronal cholesterol synthesis. Experiments involving radiolabeled acetate or mevalanolactone and highly purified neuronal or glial primary cultures from postnatal rat RGCs revealed that neurons and glia synthesize cholesterol in the adult brain; however, neurons synthesize cholesterol at a lower rate than glia and the cholesterol intermediate profiles differ between cell types³². These results suggest that neurons synthesize large quantities of cholesterol for developmental processes and maintain this cholesterol biosynthetic ability into maturity for as yet undetermined reasons.

As the brain matures, neurons rely on glial synthesis to meet cholesterol demands. Once neurogenesis is nearly complete, glial cells are generated⁴² and become the predominant source of cholesterol synthesis in the brain⁴³. Glia are necessary for neuron survival^{20,44}, as they supply cholesterol to neurons through apolipoprotein E (ApoE), which is expressed predominantly by glia⁴⁵ and is the principal cholesterol transport protein in the brain. While oligodendrocytes are the most cholesterol-rich glial type, they are not directly involved in supplying cholesterol to neurons. Astrocytes, and to a lesser degree microglia⁴⁶, are the glial types responsible for efflux of cholesterol to neurons. This efflux is achieved through ApoE and ATP-binding cassette protein A1 (ABCA1), which is a membrane-bound transporter protein that lipidates ApoE⁴⁷. Cholesterol-rich

ApoE binds to the low-density lipoprotein receptor (LDLr) and LDLr-related protein 1 (LRP1) on neuronal plasma membranes, which facilitates uptake of astrocyte-derived cholesterol, by a mechanism that presumably involves endocytosis.

The development of synapses succeeds astrocytic differentiation⁴⁸, and astrocytes are necessary for synapse formation independent of their role in neuronal survival⁴⁹. Postnatal rat RGCs cultured in the absence of glia had decreased synaptic activity relative to RGCs cultured with astrocytes, as determined by an increase in frequency and amplitude of excitatory postsynaptic currents, which are postsynaptic potentials capable of inducing an action potential and which reflect functional synapses⁴⁹; however, immunoisolated hippocampal and cerebellar neurons from postnatal mice formed functional synapses in the absence of astrocytes, but exhibited increased synaptic efficacy when astrocytes were present²². Ultimately, these results suggest differential astrocyte requirements for synaptogenesis in different neuronal subtypes. Several lines of evidence have indicated that cholesterol is the glia-derived factor that is necessary for synaptogenesis, as treatment of purified rat RGCs with reconstituted, cholesterol-rich glial lipoproteins promoted synapse formation and improved synapse efficacy²⁰. Additionally, supplementation of cultured postnatal rat RGCs with cholesterol and ApoE, which are the major components of glial lipoproteins, promoted the growth of axons⁵⁰. In adult mouse neurons, genetic ablation of *LRP1* decreased total brain cholesterol levels and dendritic spine numbers⁵¹, providing further evidence for the necessity of glia-derived cholesterol in synaptogenesis.

1.2.3 CHOLESTEROL TURNOVER IN THE BRAIN

Cholesterol synthesis occurs at low levels in the adult brain but total cholesterol levels remain constant. The half-life of cholesterol is estimated at two to four months⁵²; thus, cholesterol is removed or “turned over” to prevent cholesterol accumulation and maintain homeostatic levels. The major mechanism of cholesterol turnover in the brain is oxysterol formation, principally in the form of 24S-hydroxycholesterol (24OHC). Oxysterols are 27-carbon, oxygenated derivatives of cholesterol and cholesterol intermediates, and are more hydrophilic than cholesterol. They are synthesized through either enzymatic (oxidases, hydroxylases) or non-enzymatic (free radical oxidation, auto-oxidation) mechanisms. The neuronal ER-resident enzyme, 24S-hydroxylase (CYP46A1), hydroxylates cholesterol to 24OHC, which promotes cholesterol efflux in glia and crosses the BBB. 24OHC is a ligand for LXR⁵³ and increases expression of cholesterol efflux genes including ABCA1 and ApoE^{54, 55}. Due to the concentration gradient of 24OHC in the brain (0.7 ng/μg wet weight of cerebral and cerebellar brain tissue) relative to the circulation (0.05 ng/μg wet weight of the plasma), there is directional flux of 24OHC from the brain to the periphery, thereby eliminating cholesterol from the brain⁵⁶. Studies involving radiolabeled oxygen showed that two thirds of all brain cholesterol turnover in rats is accomplished through 24OHC production⁵² and these results were corroborated in mice with defects in the *Cyp46* gene⁵⁷. Thus, diffusion of 24OHC across the BBB constitutes a major mechanism of cholesterol removal from the brain, but not the only mechanism. Small amounts of ApoE-bound cholesterol are excreted from the brain into the CSF, with an estimated rate of elimination of 1-2 mg/day⁵⁸. While transcription of *CYP46A1* is regulated by oxidative stress, but not

by cholesterol levels ⁵⁹, transcription of *APOE* is regulated by cholesterol levels through LXR.

1.3 REGULATION OF CHOLESTEROL BIOSYNTHESIS

Cholesterol biosynthesis is a tightly regulated process that is controlled both transcriptionally and post-translationally. A conserved gene element known as the sterol regulatory element (SRE) is present in the promoter region of many genes involved in cholesterol homeostasis. The sterol-regulatory element-binding protein 2 (SREBP2) is a transcription factor that binds the SRE of cholesterol homeostatic genes including, but not limited to, *HMGR*, *FDFT1*, *CYP51*, *DHCR7*, *DHCR24* and *LDLr* ⁶⁰, and upregulates gene expression. Under sufficient cellular sterol conditions, SREBP2 is bound to SREBP-cleavage activating protein (SCAP), which binds cholesterol and is bound to the ER-resident protein, insulin-induced gene 1 (INSIG1), which binds oxysterols. INSIG1 anchors SREBP2-SCAP in the ER and prevents sequestration of this protein complex into coat protein II (COPII)-coated vesicles for transport to the Golgi. When cellular sterol levels are limiting, a conformational change takes place in SCAP ⁶¹, releasing SREBP2-SCAP from INSIG1 and facilitating COP11-coated vesicle-mediated transport to the Golgi where SREBP2 is cleaved from SCAP by site one and site two proteases. Mature SREBP2 then translocates to the nucleus to upregulate cholesterol homeostatic gene expression.

Cholesterol biosynthesis is negatively controlled by oxysterols and biosynthetic intermediates, namely 24,25-dihydrolanosterol (DHL), which is a derivative of lanosterol that differs in side chain saturation ⁶². DHL stimulates ubiquitination and proteasomal degradation of HMGR, likely through direct binding of DHL to HMGR or INSIG1 ⁶³,

thus decreasing cholesterol biosynthesis. Similarly, oxysterols stimulate binding of HMGR and SCAP to INSIG1, which results in HMGR degradation ⁶⁴. Both DHL ⁶⁵ and oxysterols ⁶⁶⁻⁶⁸ are ligands for LXR and upregulate expression of *ABCA1* ⁶⁹.

In addition to endogenous regulatory mechanisms, cholesterol biosynthesis can be controlled pharmacologically. Statins are a class of anti-atherosclerotic drugs that prevent cholesterol biosynthesis by competitively inhibiting HMGR, and increase the clearance of cholesterol-rich LDL from the circulation by increasing LDLr levels ⁷⁰. Statins bind HMGR with higher affinity than HMG ⁷¹, and inhibit synthesis of mevalonate and all subsequent intermediates, which has far-reaching implications as both sterol and non-sterol intermediates have functions outside of cholesterol biosynthesis. Isoprenoids are necessary for DNA synthesis and cell replication ⁷², as well as prenylation of guanine nucleotide-binding regulatory proteins (G-proteins) (as reviewed in ⁷³), which facilitates protein-protein interactions and signalling cascades. As some statins are lipophilic and capable of crossing the BBB, there may be consequences of decreased cholesterol synthesis in an organ that relies exclusively on *de novo* synthesis. For example, in a mouse model of Parkinson's disease (PD), which is a common neurodegenerative disorder, lanosterol protected dopaminergic neurons from cell death by inducing mitochondrial uncoupling and promoting mitophagy to prevent neurodegeneration ⁷⁴. Thus, statin-induced inhibition of lanosterol synthesis could conceivably prevent the neuroprotective effects of lanosterol.

1.3.1 CONSEQUENCES OF DYSREGULATED CHOLESTEROL HOMEOSTASIS IN THE BRAIN

Cholesterol is essential for neuronal and glial cell development and function; intuitively, aberrations in cholesterol homeostasis have widespread and significant

consequences in the brain, as evidenced by the multitude of neurodegenerative diseases arising from defective cholesterol synthesis, transport or metabolism.

Smith-Lemli-Opitz syndrome (SLOS) arises from defects in cholesterol synthesis, particularly as a result of 7DHCR deficiency. In lieu of cholesterol, 7DHC incorporates into membranes, which inhibits receptor function and protein localization in the membrane and leads to a range of physical and intellectual disabilities ⁷⁵; however, both the decrease in brain cholesterol levels and the incorporation of 7DHC into membranes are believed to be factors in this disease ⁷⁶.

Niemann Pick Type C (NPC) disease arises from impaired intracellular cholesterol trafficking and pathophysiological cholesterol accumulation. NPC involves the cholesterol-binding proteins NPC1, which is a late endosomal transmembrane protein, and NPC2, which is a luminal protein of late endosomes/lysosomes (LE/L). Mutations in *NPC1* or *NPC2* impair subcellular cholesterol trafficking and cause accumulation of cholesterol in LE/L ⁷⁷. While NPC1 and NPC2 are ubiquitously expressed, the most severe effects of NPC1 or NPC2 deficiency are largely neurological; Purkinje neurons of the cerebellum are lost in NPC disease ⁷⁸, which impairs motor function and leads to premature death in afflicted individuals.

Huntington's Disease (HD) arises from polyglutamate expansions in the *huntingtin* gene and is associated with dysregulated cholesterol homeostasis. Mutant huntingtin (mHTT), which is a hallmark of HD, inhibits SREBP2 processing and decreases cholesterol biosynthetic gene expression and total brain cholesterol levels ⁷⁹. The disruption to cholesterol synthesis has been associated with cognitive impairments, tremors and premature death in individuals afflicted with HD.

Dysregulation of cholesterol homeostasis is implicated in Alzheimer's disease (AD), but the exact mechanisms are multifaceted and not well understood (as reviewed in ⁴⁶); however, isoforms of ApoE are considered independent risk factors in the pathology of AD. In AD, membrane cholesterol levels affect the processing of membrane-bound amyloid precursor protein (APP). Under physiological conditions, APP is proteolytically cleaved by alpha- or beta-secretases. Cleavage products of alpha-secretase are non-amyloidogenic, but cleavage products of beta-secretase, when further cleaved by gamma-secretase, can lead to pathogenic amyloid proteins, which are a hallmark of AD. Elevated membrane cholesterol levels decrease membrane fluidity and prevent alpha-secretase from accessing cleavage sites. Beta-secretase activity then acts on accessible beta-cleavage sites, resulting in the non-physiological production of toxic amyloid-beta molecules, which form pathophysiological plaques and lead to neuronal death.

1.4 OXYSTEROL BINDING PROTEINS

1.4.1 OSBP AND OSBP-RELATED PROTEIN FAMILY

Oxysterol binding protein (OSBP) was first identified as a protein that binds oxysterols ⁸⁰; however, OSBP binds both oxysterols and cholesterol with different affinities ^{81, 82}. OSBP domains include a C-terminal lipid-binding domain (ORD), an N-terminal pleckstrin homology (PH) domain and two phenylalanines in an acidic tract (FFAT) motif. The ORD forms a lipid-binding pocket and facilitates transfer of lipids between membranes. The OSBP PH domain interacts with phosphatidylinositol-4-phosphate (PI4P), which is abundant in Golgi membranes. The FFAT motif interacts with vesicle-associated membrane protein (VAMP)-associated protein (VAP), which resides

in the ER membrane. Cellular cholesterol depletion or addition of 25-hydroxycholesterol (25OHC) initiates translocation of OSBP to the Golgi apparatus⁸³. OSBP simultaneously interacts with the ER and Golgi and transfers cholesterol from the ER to the Golgi in exchange for P14P⁸⁴. The dual membrane tethering is also necessary for the sterol-dependent activation of ceramide transport protein (CERT) activity and translocation to the Golgi for sphingomyelin synthesis⁸⁵.

While oxysterols regulate cholesterol homeostasis by activating LXR⁶⁶ and increasing expression of cholesterol efflux genes⁶⁹, as well as inhibiting activation of SREBP2⁸⁶, and preventing HMGCR expression⁸⁷, OSBP regulates cholesterol homeostasis by directly binding to sterols and regulating intracellular sterol transport⁸⁸. Additionally, the ORD of OSBP decreases protein stability of ABCA1 without affecting *ABCA1* mRNA levels or LXR activity⁸⁹, suggesting a direct role of OSBP in inhibiting cholesterol efflux.

A number of OSBP-related proteins (ORPs) have been identified based on a conserved sequence within the ORD: EQVSHHPP⁹⁰. Including OSBP, the mammalian ORP superfamily encompasses twelve members⁹¹, each of which has varying degrees of similarity to OSBP (as reviewed in⁹⁰). In addition to binding oxysterols and cholesterol, ORPs are capable of binding phosphoinositides, phosphatidic acid and phospholipids⁹². Much of the ORP knowledge currently available has been elucidated from the family of yeast OSBP homologues termed *OSH* proteins. Some commonalities in the ORP family include localization to membrane contact sites (MCS) through simultaneous dual membrane targeting, which is believed to involve lipid transfer or exchange between

membranes. The closest homologue of OSBP is ORP4, also known as OSBP2 or HeLa metastatic (HLM) protein.

1.4.2 ORP4

Although ORP4 shares high sequence homology with OSBP, it does not exhibit the same lipid trafficking/sensing characteristics as OSBP in cultured cell experiments and its function is largely unknown. The ORP4 gene contains three transcription start sites, which encode different ORP4 isoforms. Like OSBP, the full-length isoform of ORP4 (ORP4L) contains a PH domain⁹³ and an FFAT motif, as well as the ORD (Figure 2). The medium isoform (ORP4M) contains a truncated, non-functional PH domain but an intact FFAT motif and ORD. The short isoform (ORP4S) lacks the PH domain completely but contains the FFAT motif and ORD⁹⁴. While other members of the ORP superfamily have overlapping and non-essential individual functions, ORP4 is unique in that it is required for cell proliferation and survival. Specifically, lentivirus-mediated RNAi targeting of exon 1 of ORP4 depletes ORP4L without affecting ORP4M or ORP4S expression, and this led to the discovery that ORP4L, but not ORP4M or ORP4S, is required for cell proliferation and survival of HeLa and HEK293T cells⁹⁴. In cervical carcinoma cell lines, including C33A, HeLa and CaSki, ORP4L promoted cell proliferation by sustaining inositol-1,4,5-triphosphate (IP3) receptor 1 (IP3R) expression and maintaining intracellular Ca²⁺ levels⁹⁵. Additionally, in T-cell acute lymphoblastic leukemia cells, ORP4L depletion decreased IP3 and ATP levels, resulting in inhibited cell proliferation⁹⁶.

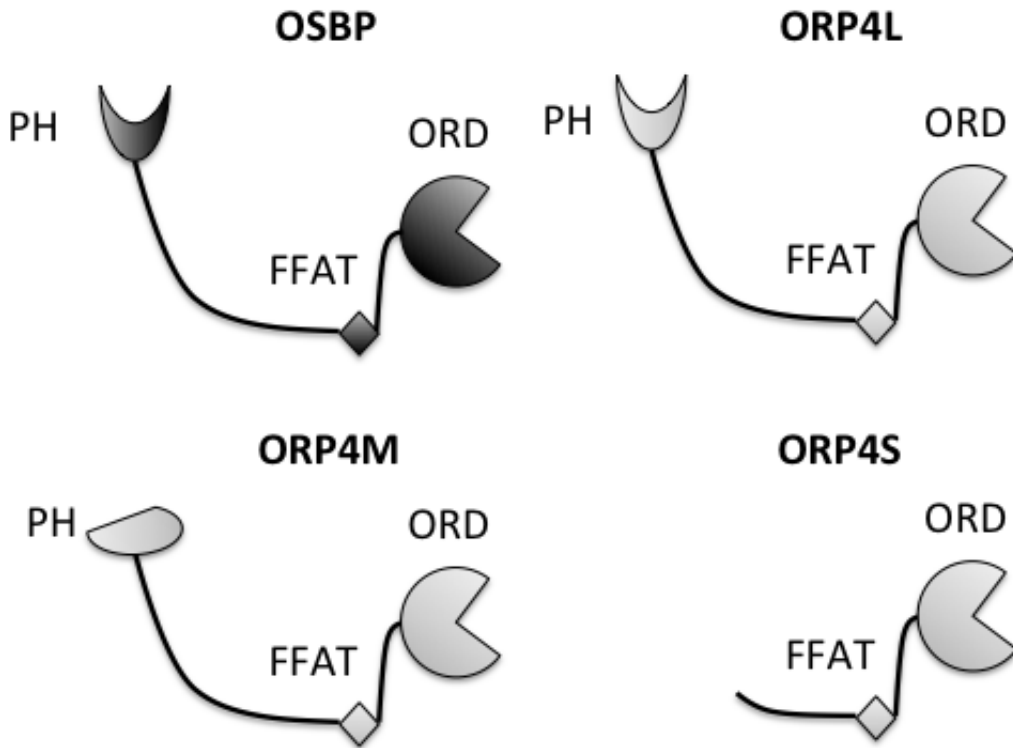


Figure 2. OSBP and ORP4 share sequence similarity

OSBP domains include the pleckstrin homology (PH) domain, two phenylalanines in an acidic tract (FFAT) motif, and the lipid binding domain (ORD). ORP4L contains the PH, FFAT and ORD domains and is the closest homolog of OSBP. ORP4M contains a truncated, non-functional PH domain as well as the FFAT motif and ORD. ORP4S lacks a PH domain but contains the FFAT motif and ORD.

ORP4 is highly expressed in the brain, heart and testis, with lower but detectable expression levels in the kidneys, spleen and skeletal muscle⁸¹. Due to the presence of the ORD, ORP4 isoforms are capable of binding cholesterol, oxysterols such as 25OHC, and PI4P. While most tissues predominantly or exclusively express ORP4L, the brain exhibits comparable expression levels of ORP4S and ORP4L mRNA⁸¹. Overexpression of ORP4S aggregates vimentin, a Type III intermediate filament, likely as a result of excessive interactions of the ORD with vimentin, either directly or indirectly through a binding partner⁹⁷. In the brain, vimentin is expressed by neurons during development and by glial cells throughout their lifetime. It provides mechanical strength, regulates mitochondrial motility and organization, and provides structural integrity for the proper localization of organelles and subcellular components.

ORP4 is also necessary for male fertility in mice, as *ORP4*^{-/-} mice produced sperm with mislocalized mitochondria, elevated levels of apoptosis and differentiation defects⁹⁸. These mice also showed abnormalities in the apical dendrites of hippocampal neurons, though the significance of these abnormalities is still unclear. The recurring theme of ORP4-mediated cell proliferation has been strengthened with the discovery of ORPphilins, naturally occurring products used in the treatment of cancers due to their anti-proliferative effects. ORPphilins inhibit ORP4L and OSBP activity, thereby inhibiting cell proliferation⁹⁹.

1.5 RESEARCH OBJECTIVES

In neurons of the hippocampus, cholesterol biosynthesis is maintained into maturity, as evidenced by the expression of mRNA for cholesterol biosynthetic genes in neurons of the adult brain, and the synthesis of cholesterol from radiolabeled acetate in highly purified neuronal cultures from postnatal rat RGCs. Yet cholesterol is readily acquired from the surrounding glial cells, and glia-derived cholesterol is necessary for synaptogenesis and SV release. Therefore, the maintenance of neuronal cholesterol biosynthesis in the mature brain may be functionally advantageous for neuronal cells. As cholesterol is important in the developing brain and spine formation occurs early in development, I sought to determine whether neuronal cholesterol biosynthesis is maintained in part for the development and maturation of spines. I sought to define a role of neuronal cholesterol biosynthesis by assessing the effects of inhibited biosynthesis on dendritic spines, lipid microdomains and mitochondria. Ultimately, I describe the effects of decreased FDFT1 or CYP51 on dendritic spine density and mitochondrial size.

The high expression levels of ORP4 in the hippocampus suggest an essential role of this protein in brain function. Given the dual membrane-targeting motifs, and the cholesterol- and oxysterol-binding capacities of ORP4, this protein may act as a lipid sensor or transfer protein like its closest homologue, OSBP; however, a role of ORP4 has not been fully elucidated. I sought to define a role of ORP4 in hippocampal cells by decreasing total ORP4 or ORP4L expression, and assessing the effects on neurons and glia.

CHAPTER 2: MATERIALS AND METHODS

2.1 MATERIALS

Minimum essential medium (MEM), OptiMEM, penicillin/streptomycin (p/s), Neurobasal medium (NB), B27 supplement, glutamax and Dulbecco's Modified Eagle Medium (DMEM) were obtained from Life Technologies. Fetal bovine serum (FBS) and cytosine arabinoside (cytC) were purchased from Sigma-Aldrich. Nu serum was purchased from Corning. All chemicals were from Sigma-Aldrich or Thermo Fisher Scientific, unless otherwise indicated. Anti-TOM20 (sc-11415), anti-NRF2 (sc-722) and anti-ACTIN (sc-1616) antibodies were obtained from Santa Cruz Biotechnologies. Anti-CYP51 (ab175863), anti-Calnexin (ab22595), anti-FDFT1 (ab195046), anti-MAP2 (ab75713) were from Abcam. Anti-PINK1 (P0051-25UL) was from Sigma-Aldrich and anti-GFAP (556327) was from BD Biosciences. Anti-ORP4 and anti-GIANTIN antibodies were a gift from the laboratory of Dr Neale Ridgway. MitoTimer (#50547), pLifeAct-mTurquoise2 (#36201), pPalmitoyl-mTurquoise2 (#36209), packaging (psPAX, #12260) and envelope (pMD.2G, #12259) vectors were purchased from Addgene. All restriction enzymes, restriction digest buffers, T4 DNA ligase and ligase buffers were obtained from New England Biolabs.

2.2 SOLUTIONS

Borate buffer (1X): 75 mM boric acid, 6.5 mM sodium tetraborate, pH adjusted to 8.5.

Poly-D-Lysine (PLL) (1X): 0.5 mg/mL poly-D-lysine (Peptides International) in borate buffer.

Phosphate-buffered saline (PBS) (1X): 137 mM NaCl, 2.7 mM KCl, 10 mM Na₂HPO₄, 2 mM KH₂PO₄, pH adjusted to 7.4.

Luria Bertani broth (LB) (1X): 1% (w/v) tryptone, 0.5% (w/v) yeast extract, 1% (w/v) NaCl

TAE (1X): 40 mM Tris, 1 mM EDTA

HEPES- buffered saline (HBS) 0/2 (10X): 1.24 M NaCl, 30 mM KCl, 50 mM D-glucose, 100 mM HEPES, 20 mM MgCl₂•6H₂O, pH adjusted to 6.7, osmolarity adjusted to 260-280 mOsm

HBS 2/1 (10X): 1.24 M NaCl, 30 mM KCl, 50 mM D-glucose, 100 mM HEPES, 20 mM CaCl₂•2H₂O, 10 mM MgCl₂•6H₂O, pH 7.4, osmolarity adjusted to 260-280 mOsm

Sample buffer (5X): 62.5 mM Tris-HCl, 10% (v/v) glycerol, 2% sodium dodecyl sulphate (SDS), 5% β-mercaptoethanol

Running buffer (1X): 25 mM Tris, 192 mM glycine, 0.1% SDS

Transfer buffer (1X): 25 mM Tris, 250 mM glycine, 20% methanol, 5% isopropanol

HeBs (2X): 271 mM NaCl, 10 mM KCl, 1.4 mM Na₂HPO₄, 15 mM D-glucose, 42 mM HEPES, pH adjusted to 7.1.

Tween-Tris Buffered Saline (TTBS) (10X): 153 mM Tris, 1.5 M NaCl, 1% Tween-20, pH adjusted to 7.5

2.3 CELL CULTURE

2.3.1 Primary Hippocampal Cell Culture

In accordance with procedures approved by the animal ethics committee of Dalhousie University (protocol #15-113 Krueger/Fawcett) and standards set by the

Canadian Council of Animal Care, hippocampal cells were harvested from embryonic day 17 Sprague-Dawley rats (Jackson Laboratories) by Annette Kolar of Dr. Stefan Krueger's laboratory and gifted to us for use.

Dissociated cells in MEM + 5% FBS + p/s were plated at a density of 50,000 cells/mL on preconditioned dishes as follows: 12- or 24-well culture dishes with sterile coverslips were coated with PLL for 1 h at 37°C or overnight at room temperature (RT), before conditioning with MEM + 5% FBS + p/s overnight. The cultures were incubated at 37°C and 5% CO₂ for 3 h and the medium was replaced with serum-free NB medium supplemented with 2% B27, p/s, 0.5 mM glutamine and 0.25µM glutamate, or NB electro medium supplemented with 2% B27, p/s and glutamax.

2.3.2 Immortalized Cell Lines

C6 rat glioma cells were grown in DMEM + 10% FBS + p/s. HEK 293T cells were grown in DMEM + p/s and either 10% FBS or 10% Nu serum.

2.4 PLASMIDS AND CLONING

The pGipZ vectors were from Thermo Fisher Scientific and originally modified by Matthew Taylor using a two-digest approach. Specifically, a non-targeting pGipZ vector was digested with XbaI and NotI to remove the CMV promoter and GFP. The CMV promoter was amplified by PCR and an AgeI site was introduced at the 3' end. mCherry containing AgeI and NotI restriction sites was amplified from a separate vector. The CMV promoter amplicon was ligated into the vector, and the vector was digested with AgeI and NotI in order to introduce mCherry. The resulting plasmid was digested with XbaI and NotI to cut out the CMV-mCherry cassette, which was cloned into the

same restriction sites in pGipZ vectors encoding shFDFT1. The Syn promoter was amplified from a Syn-driven Synaptotagmin-pHluorin vector with primers introducing XbaI and AgeI restriction sites and ligated into the vectors containing mCherry and shFDFT1. Restriction digests were performed at 37°C for 2 h in a Thermocycler (MJ Mini, BioRad), and ligations were performed at 16°C overnight using T4 DNA ligase and ligase buffer. The Syn-Mito-shNT was created by inserting a pre-synthesized mitochondrial targeting sequence into Syn-mCherry-shNT after digestion with AgeI and dephosphorylation with calf intestinal phosphatase (NEB BioSciences). LifeAct and pPalm targeting sequences were amplified by PCR from original Addgene vectors and AgeI and NotI restriction sites were introduced. The Syn-mCherry vectors encoding sh46, sh47, sh48 or sh05 sequences were digested with AgeI and NotI, allowing exchange of mCherry for LifeAct, Mito or pPalm. CMV-mCherry-sh78 with perfect complementarity to rat CYP51 was created by digesting a pGipZ-CMV-mCherry vector with XhoI and MluI, and ligating a synthetic sh78 oligonucleotide sequence using a Gibson Assembly (New England Biolabs). The Syn-sh76 and Syn-sh78 vectors containing LifeAct, Mito or pPalm were created by digesting Syn-mCherry-sh76, CMV-mCherry-sh78 Syn-pPalm-shNT, Syn-LifeAct-shNT and Syn-Mito-shNT with XbaI and BsrGI, and ligating the isolated Syn/reporter cassette into the sh76 and sh78 vectors.

The products of digestion (DNA fragments) were separated by electrophoresis in agarose gels prepared with TAE buffer and visualized by staining in GelRed (Biotium) for 30 min and imaging with the Versadoc imaging system (BioRad). Extraction and purification of DNA from agarose gels was accomplished via the QIAEX II Gel Extraction kit (Qiagen). All DNA sequencing was outsourced to Eurofins Genomics. The

plasmids were transformed into Top10 electrocompetent *E. coli* (Life Technologies), grown in LB broth and selected on agar plates with antibiotics. Preparations of plasmids employed Mini Prep kits (Bioneer) or Maxi Prep kits (Thermo Fisher Scientific), as per the manufacturers' instructions. Table 1 illustrates the pGipZ vectors with targeted fluorescent reporter constructs and promoters used in this thesis. Table 2 and 3 list the forward shRNA hairpin sequences of the pGipZ vectors and pLKO.1 vectors, respectively.

2.5 RNA INTERFERENCE (RNAi)

2.5.1 Calcium Phosphate (CaPO₄) Transfection

The calcium phosphate transfection method is effective for transfecting neurons but not the surrounding glial cells (reviewed in ¹⁰⁰). Neurons were transfected at DIV7 unless otherwise indicated. Neuron-conditioned medium (NCM) was replaced with MEM + 2% B27, and NCM was stored at 37°C after addition of glutamate-free NB to replenish volumes lost to evaporation. DNA was added to 2.5 M CaCl₂ in water and added incrementally to 2X HeBS with vortexing after each addition. The transfection mixture was incubated at RT for 20 min, then added to cultures and incubated at 37°C and 5% CO₂ for 3 h. Cells were washed with HBS 0/2 and glutamate-free NB before replacing the NCM.

Full name	Abbreviated name	Localization
pGipZ_Syn_LifeAct-mTurquoise	LifeAct	Filamentous Actin
pGipZ_Syn_mito-mCherry	Mito	Mitochondrial matrix
pGipZ_Syn_pPalm-mTurquoise	pPalm	Targets of Palmitoylated proteins (ie: lipid rafts)
pGipZ_Syn mCherry	Syn-mCh	Cytosol
pGipZ_CMV eGFP	CMV-eGFP	Cytosol
pGipZ_CMV mCherry	CMV-mCh	Cytosol

Table 1. pGipZ vector constructs with promoters, fluorescent reporters and subcellular localizations.

Hairpin target	Variants from catalogue	Sequence (5'-3')	Abbreviated name
FDFT1	V3LMM_488746	ATGTCTTCACCAACTATGG	46
	V3LMM_488747	AGCAGGTCTTCAAGCTGCT	47
	V3LMM_488748	AAATCTCTTCTATGTACTG	48
CYP51	V2LMM_247105	TGTTGTATAATTCACAGTG	05
	V3LMM_451176	AAAGCTAAACACAGGTCCA	76
	V3LMM_451178rat	TCAATGATAGAAACATACT	78
Non targeting		TTACTCTCGCCCAAGCGAG	shNT

Table 2. List of hairpin targets, pGipZ catalogue variants, forward hairpin sequences and abbreviations used in thesis.

Hairpin Target	Sequence (5'-3')	Abbreviated name
ORP4	CATCACATCCAATGCTATGAT	shORP4
ORP4L	GCTTCTCAAGTGGACCAACTA	shORP4L
NT	CAACAAGATGAAGAGCACCAAC	shNT

Table 3. List of hairpin targets, forward sequences and abbreviations for pLKO.1 vectors used in thesis.

2.5.2 Viral Production

Viral transduction was employed to increase the proportion of cells expressing the constructs and to avoid cell-type selectivity. Packaging vectors (psPAX and pMD.2G) were combined in OptiMEM with the expression vectors for 5 min at RT before adding to PEI diluted in OptiMEM. The mixture was incubated for 20 min at RT before adding to HEK 293T cells in serum-free DMEM + p/s and incubating for 6 h at 37°C and 5% CO₂. Transfection medium was replaced with DMEM + 10% FBS or 10% Nu + p/s and incubated at 37°C and 5% CO₂ for 48 h. Viral supernatant was collected and concentrated to 40X by centrifugation at 4000 g at 4°C using 100 kDa ultracentrifugal filter units (Pall Life Sciences). Concentrated viral supernatant was added directly to cultures.

2.6 STABLE CELL LINE PREPARATION

2.6.1 Polyethyleneimine (PEI) Transfection

For transfection of C6 glioma cells with plasmids encoding the short hairpin sequences, DNA and PEI were separately diluted in OptiMEM and incubated for 5 min at RT then combined and incubated for 20 min at RT. The transfection mixture was added drop-wise to cells and incubated at 37°C and 5% CO₂. After overnight incubation, transfection medium was replaced with DMEM + 10% FBS + p/s.

2.6.2 Selection Of Transfected Cells

PEI-transfected C6 glioma cells were selected by addition of 2µg/mL puromycin (Invivogen) in DMEM + 10% FBS + p/s for 48 h, and vector expression was confirmed

with fluorescence microscopy of live cells. Colonies were picked by scraping with a p20 pipette tip and transferred into 24 well dishes with DMEM + 10% FBS + p/s. After two days, cells were serially diluted to one cell per well and seeded into 96 well plates. Individual colonies were selected and propagated to produce monoclonal stable knockdown lines. Fresh medium was replaced every three days. When harvesting for protein or RNA analyses, lipoprotein-deficient serum (LPDS), which was prepared by density ultracentrifugation from FBS by Mark Charman according to ¹⁰¹, was added to cultures for 16 h to upregulate cholesterol biosynthesis.

2.7 CELL COLLECTION

Cell monolayers were shaken at RT with PBS + 0.1% SDS containing protease inhibitors including leupeptin (11 μ m), aprotinin (8 μ m), pepstatin A (1 μ m), phenylmethane sulfonyl fluoride (50 μ m) and phosphatase inhibitors including orthovanadate (2 mM), and sodium fluoride (1 mM) after washing with PBS.

2.8 PROTEIN DETERMINATION

Cell protein was measured using the bicinchoninic acid (BCA) assay kit (Pierce, Thermo Fisher Scientific), and a bovine serum albumin (BSA) standard was used as a control. ¹⁰²

2.9 SDS-PAGE AND WESTERN BLOTTING

After determination of protein content, samples were adjusted with loading buffer and boiled for 5 min at 100°C in a water bath. Equal amounts of protein were resolved by

SDS-polyacrylamide gel electrophoresis (PAGE) in 1X SDS running buffer at 100V for 2 h. Proteins were transferred to polyvinylidene fluoride (PVDF) or nitrocellulose membranes in 1 X transfer buffer. Membranes were then blocked in 2% (w/v) PVP in Tween-tris buffered saline (TTBS) and incubated overnight at 4°C with primary antibodies diluted as listed in Table 4. Proteins were detected with horseradish peroxidase (HRP)-conjugated secondary antibodies (Jackson ImmunoResearch), and Clarity Western enhanced chemiluminescence (ECL) substrate (BioRad) using a Kodak 1000CT Developer and CL-X Posure Film (Thermo Scientific), or the Versadoc imaging system. Densitometry was performed using open source ImageJ software.

2.10 ISOLATION OF RNA AND qPCR

RNA was isolated from cell monolayers on ice by harvesting into TriReagent (Sigma-Aldrich) according to the manufacturer's instructions. Briefly, 20% (v/v) chloroform was added to samples in TriReagent. The samples were vortexed and centrifuged at 10,000 rpm and 4°C for 15 min. The aqueous phase was transferred to an RNase-free microcentrifuge tube and RNA was precipitated by addition of an equal volume of isopropanol and centrifugation at 13,000 rpm and 4°C for 15 min. The RNA pellet was washed with 75% ethanol in (DEPC) water, centrifuged at 13,000 rpm at 4°C for 5 min, air-dried and resuspended in DEPC water. RNA concentrations were quantified spectrophotometrically. cDNA was prepared using the ISCRIPt cDNA synthesis kit (BioRad) or the Sensifast cDNA kit (Frogga Bio) according to the manufacturer's instructions. PerfeCTa SYBR Green FastMix (Quanta Biosciences) was used for all qPCR reactions. Reference genes (cyclophilin and actin), which are genes involved in basic cellular functions that are constitutively expressed by all cells of an

Primary Antibody	Dilution
CYP51	1:750
ACTIN	1:2500
ORP4	1:500
GFAP	1:1000
CALNEXIN	1:1000

Table 4. Dilutions of primary antibodies used in immunoblotting experiments.

organism, were employed as reference points of gene expression. Primer sequences for all reference genes and genes of interest are listed in Table 5.

2.11 IMMUNOSTAINING

Cells cultured on glass coverslips were washed with PBS and fixed with 4% paraformaldehyde (PFA) for 8 min, washed thoroughly with PBS and permeabilized with 0.1% Triton X-100 for 5 min. When indicated, rotenone (Enzo Life Sciences) was added to cultures to a final concentration of 200 nM for 30 min immediately prior to washing and fixation with PFA, as a positive effector of mitochondrial dysfunction. Cells were then washed once and incubated for 30 min at RT with blocking buffer (5% (w/v) bovine serum albumin and 1% (v/v) goat serum in PBS). Primary antibodies were diluted in blocking buffer at 1:100 unless otherwise indicated and incubated on cells at 4°C overnight. Cells were washed and incubated with fluorescent secondary antibodies (Jackson ImmunoResearch) diluted in blocking buffer at 1:200 for 2 h at RT. Hoechst dye was diluted in PBS at 1:2500 and incubated on cells for 5 min at RT. Cells were washed thoroughly before mounting with Aquamount (Thermo Fisher Scientific).

2.12 IMAGE ACQUISITION AND ANALYSIS

Fluorescent images were obtained using a Nikon TE2000 epifluorescence microscope with a CCD camera (Orca-AG, Hamamatsu), excitation and emission filters (Semrock), and IPlab software (BD Biosciences). Live cells were imaged in HBS 2/1 recording medium at 37°C using a 60 X oil immersion objective (Plan Apo 60X/1.40 oil, ∞ /0.17 Ph3 DM WD 0.13, Nikon Japan). Table 6 lists the excitation and emission filters

Protein of Interest	Gene name	Forward Primer Sequence (5'-3')	Reverse Primer Sequence (5'-3')
CYCLO	<i>Ppia</i>	TCTTCTTGCTGGTCTTGCCATTCC	TCCAAAGACAGCAGAAAACCTTCG
CYP51	<i>Cyp51</i>	TAATTCTGACCTGCCATAATC	TTGGCCTCAAACCTCTCAATCCT
FDFT1	<i>Fdft1</i>	GTGGCCGTGAAGTGCTTG	GTAACAGGCAGCCAGCGTAG
HMGR	<i>Hmgr</i>	GACTGAAACACGGGCATTG	CGGCACGGAAAGAACCATAG
HMOX1	<i>Hmox1</i>	CGGCGTCCATGTTGACTGAC	TCAAAAGACAGCCCTACTTGGTTAG
mCherry		GAAGGGCGAGATCAAGC	TGTTCCACGATGGTGTAGTC
eGFP		AACACCCGCATCGAGAAG	CGGTGAAGATCACGCTGTC
NRF2	<i>Nfe2l2</i>	CTCGGAAATGGAAGAGCTAG	GCGACAGAGGCTGTACTG
MFN2	<i>Mfn2</i>	GTGTCTGTGCGGAATCAGATAG	GGCCAGGAACCTATTAC
FIS1	<i>Fis1</i>	AGCAGCGGGATTATGTC	GGGCTCAGTCTGTAACAGTC
TFAM	<i>Tfam</i>	GCGAAGTGATCTCATCCGTC	CAGCTTCTTGTGCCAATCC
ORP4	<i>Osbp2</i>	AGCTGAAGTTCGTGCCCTACA	TGGCTGGCAGCGTCTGGTAC
ORP4L	<i>Osbp2</i>	CTGGGCAGGAATCGGAATC	GACTGTCCTGGTCGCAGAAC
ACTIN	<i>Actin</i>	AGCCTTCCTTCTTGGGTATGG	ACACAGAGTACTTGCCTCAG

Table 5. List of the primer sequences used in qPCR experiments.

Fluorophore	Excitation filter (nm)	Emission Filter (nm)
mTurquoise	427/10	472/30
Dy549, Texas Red, mCherry, CMXRos	585/29	527/42
Dy488, Cy2, eGFP	474/23	527/42
AMCA, Hoechst	387/11	447/60
Cy5	628/40	692/40

Table 6. List of excitation and emission filters used for all live and fixed cell images.

for all fluorophores used in the thesis. All live and fixed cell images were analyzed using open source ImageJ software after background subtraction with a rolling ball algorithm.

2.12.1 Mitochondrial Length

Individual mitochondria were traced using the line tool to measure the length of mitochondria. Approximately 50-100 mitochondria/image were selected randomly over the total image field of 3-10 blinded images per coverslip, with duplicate or triplicate coverslips per experiment. The mean mitochondrial length per image was calculated for all constructs and expressed as percent control.

To determine the proportion of elongated mitochondria, the mean mitochondrial length of the control was calculated and mitochondrial lengths exceeding 1.5 times the mean control length were considered elongated. The proportion of elongated mitochondria per total mitochondria was calculated for each condition.

2.12.2 Spine Density

Spines were counted with the cell counter plugin created by Kurt de Vos, (available online at <http://rsbweb.nih.gov/ij/plugins/cell-counter.html>). All spine types were counted along a length of dendrite, which was measured using the freehand line tool, with a maximum of two dendritic regions per neuron. Spine counts were obtained from 4-5 neurons per construct per coverslip, with duplicate or triplicate coverslips per experiment. As the plasmids encoding LifeAct and the shFDFT1 or shCYP51 sequences were generated over several weeks, a total of 5 neuronal preparations were employed for duplicate experiments of spine density analyses. The spine density was calculated by

determining the spine count per 20 μm length, and the mean spine density was calculated. Spine densities were expressed as percent control.

2.12.3 Neuronal PINK1 And NRF2 Levels

Neurons were detected by the presence of MAP2 through immunostaining with anti-MAP2 antibodies. Mean fluorescence intensity of PINK1 or NRF2 was calculated in ImageJ by outlining all soma in an image with the brush tool. Nuclei were detected by staining with Hoechst dye and nuclear NRF2 levels were assessed by outlining all nuclei of MAP2+ cells. Approximately 5-6 images on duplicate coverslips were used for each construct (shORP4, shORP4L and shNT). The mean of the shNT intensities was calculated and individual intensities were expressed as percent of the average shNT.

2.13 STATISTICS

Data from all experiments are presented as the mean \pm SEM and statistical significance was determined by two-tailed Student's t-test with equal variance. An independent experiment was defined as an individual preparation of hippocampal cells.

CHAPTER 3: RESULTS

3.1. SELECTIVE DOWNREGULATION OF NEURONAL CHOLESTEROL BIOSYNTHETIC ENZYMES

Hippocampal neurons maintain the capacity to synthesize cholesterol into maturity, even in the presence of adequate glia-derived cholesterol, suggesting a specific role of neuronal cholesterol biosynthesis. Hippocampal cultures contain both neurons and glia, and we aimed to decrease neuronal synthesis without disrupting glial synthesis to investigate a role of neuronal cholesterol biosynthesis. Inhibitors of cholesterol biosynthesis, such as statins and anti-fungals, are widely available and inhibit various enzymes of the pathway. Use of cholesterol biosynthetic inhibitors to investigate neuronal cholesterol biosynthesis presents limitations, as these inhibitors prevent synthesis in both cell types, necessitating a more selective means of decreasing neuronal cholesterol biosynthesis. I targeted neuronal cholesterol biosynthetic enzymes, namely squalene synthase (FDFT1) or lanosterol-14 α -demethylase (CYP51) for genetic downregulation using modified pGipZ RNAi vectors.

Commercially available pGipZ RNAi vectors contain a cytomegalovirus (CMV) promoter, and encode enhanced green fluorescent protein (eGFP), puromycin N-acetyltransferase, which confers puromycin resistance, and a multiple cloning site for insertion of a microRNA-based short hairpin (shRNA) for RNA interference (RNAi). To achieve selective downregulation of cholesterol biosynthetic enzymes in neurons, the CMV promoter of pGipZ vectors obtained from the GipZ lentiviral shRNAmir library (Open Biosystems) encoding a non-targeting short hairpin (shNT) or shRNA against the late-stage cholesterol biosynthetic enzymes, FDFT1 (shFDFT1) or CYP51 (shCYP51), was exchanged for a human Synapsin (Syn) promoter, which is recognized in neurons but

not glia. Moreover, the sequence encoding eGFP was exchanged for a fluorescent reporter construct. To decrease the probability of off-target effects, one unique sequence per construct was employed, with a total of three constructs per enzyme, as listed in Table 2. This approach allowed neuronal cholesterol biosynthetic enzymes to be targeted for inhibition without affecting glial cholesterol biosynthetic enzymes, and the effects could be visualized on subcellular neuronal regions.

3.1.1 Expression Of Fluorescent Reporter Constructs For Visualization Of The Effects Of Decreased Neuronal Cholesterol Biosynthetic Enzymes

To determine the effects of decreased FDFT1 or CYP51 on specific subcellular structures, fluorescent reporter constructs were used to visualize filamentous actin (F-actin), mitochondria or targets of palmitoylated proteins such as membrane lipid microdomains.

I aimed to determine the effects of decreased FDFT1 or CYP51 on dendritic spine dynamics and mitochondrial morphology using LifeAct and Mito vectors, respectively. LifeAct encodes a fluorescent protein linked to a targeting sequence that binds to F-actin and allows visualization of dendritic spines while Mito encodes a peptide with a mitochondrial-targeting sequence that allows visualization of the mitochondrial matrix. Transfection of DIV7 cultures with pGipZ vectors encoding LifeAct or Mito effectively targeted dendritic spines and mitochondria, respectively (Figure 3). I also aimed to determine the effects of decreased FDFT1 or CYP51 on lipid microdomains using pPalm vectors, which express a fluorescently tagged peptide that is palmitoylated post-translationally. Lipid microdomains serve as platforms for protein-protein associations and are the targets of palmitoylated proteins ¹⁰³. While punctae possibly indicative of

lipid microdomains were apparent in transfected neurons, many proximal neurites and cell bodies exhibited fluorescent tubules, which were deemed non-physiological artefacts of pPalm expression (Figure 3C). Assessment of the effects of decreased FDFT1 or CYP51 using pPalm expression vectors was not pursued further.

3.1.2 Validation Of Short Hairpin Sequences

To validate the efficacy of the shRNA sequences, rat C6 glioma (C6) cells were transfected with pGipZ vectors containing a CMV promoter and encoding eGFP or mCherry as well as shNT or shFDFT1 or shCYP51. Monoclonal stable lines were established and RNA was isolated to assess the efficacy of gene silencing. Assessment of mRNA levels of FDFT1 and CYP51 in these stable lines with qPCR revealed a mild decrease in gene expression relative to actin as a reference gene (Figure 4); however, this was only apparent with two each of the three hairpins employed for each enzyme. Inhibition of FDFT1 with hairpin variant 47 (5'-AGCAGGTCTTCAAGCTGCT-3') or 48 (5'-AAATCTCTTCTATGTAAGT-3') decreased mRNA levels of FDFT1, while inhibition of CYP51 with hairpin variant 76 (5'-AAAGCTAAACACAGGTCCA-3') or 78 (5'-TCAATGATAGAAACATAACT-3') decreased mRNA levels of CYP51.

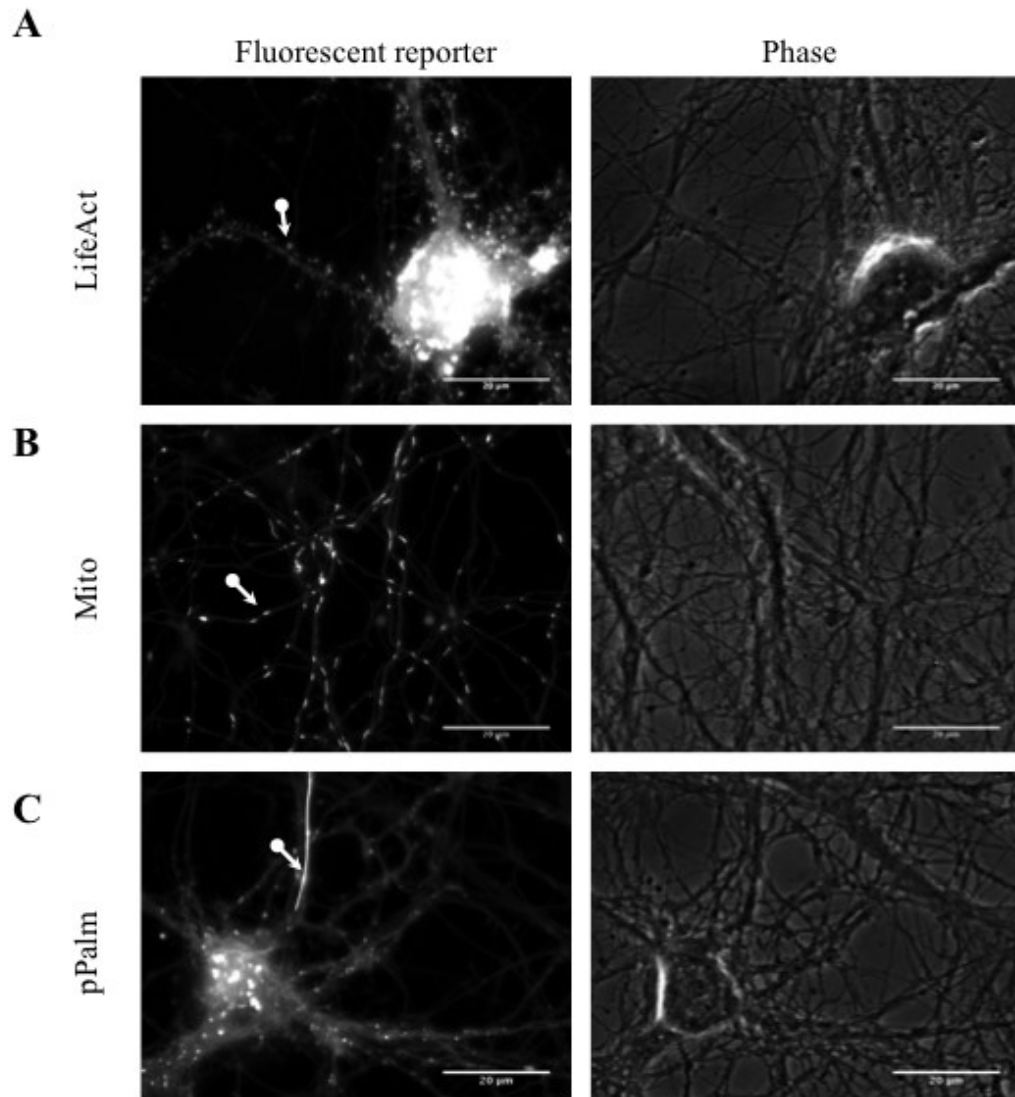


Figure 3. LifeAct and Mito target subcellular regions but pPalm causes fluorescent artefacts

Cultures were transfected with pGipZ vectors containing a Syn promoter and fluorescent reporter construct: A) LifeAct, B) Mito or C) pPalm at DIV7 and imaged live ten days later. A) LifeAct targeted F-actin. Arrow indicates dendritic spine. B) Mito targets mitochondrial matrix. Arrow indicates mitochondrion. C) pPalm produced artefacts. Arrow indicates non-physiological fluorescent tubule. Scale bars are 20 μ m.

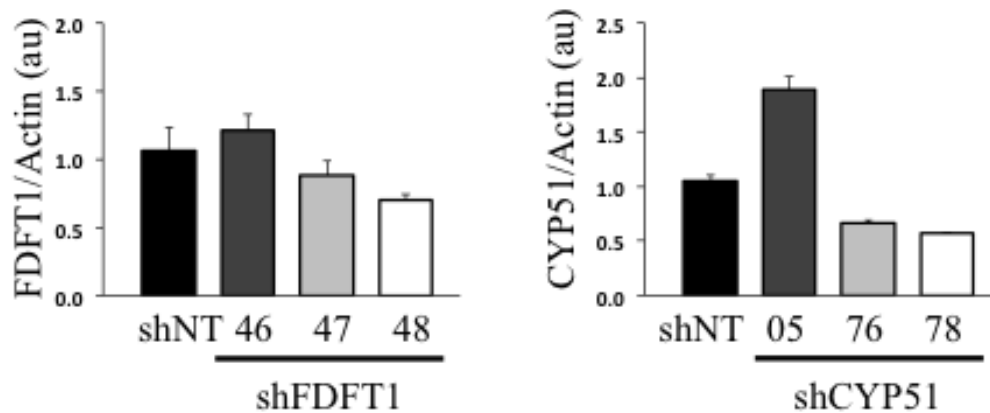


Figure 4. Two each of three hairpin sequences targeting FDFT1 or CYP51 decrease mRNA levels of FDFT1 or CYP51, respectively
 RNA was isolated from rat C6 glioma cell lysates stably expressing different hairpin sequences against FDFT1 or CYP51. Relative mRNA levels were assessed with qPCR and expressed per actin reference gene. Data represent the mean \pm SEM of one experiment in duplicate and are representative of two independent experiments in duplicate.

3.1.3 Decreased FDFT1 Or CYP51 Increases Dendritic Spine Density

Spines are specialized, post-synaptic dendritic protrusions that receive chemical stimuli and facilitate neurotransmission. Spines are classified into categories based on morphology: filopodia, thin, stubby, mushroom and cup-shaped, and form at cholesterol- and sphingolipid-rich regions of dendritic membranes¹⁰³. Spine density steadily increases from 1-3 weeks *in vitro*, with a high proportion of long, immature spines at this stage of development¹⁰⁴.

The effects of decreased FDFT1 or CYP51 on dendritic spines were investigated using LifeAct vectors. Cells were transfected at DIV7 with pGipZ vectors containing LifeAct and shFDFT1 or shCYP51, and imaged live at DIV16 or DIV17. Spines are immature and developing at DIV7, and I predicted that a decrease in FDFT1 or CYP51 at this developmental stage would affect spine development and maturation. Thus, I imaged neurons at DIV16 or DIV17, which represents a developmental stage where spines are mature. Given that the fluorescent reporter was still expressed at DIV16/17, I concluded that the shRNA was still expressed and that FDFT1 or CYP51 were indeed decreased.

All dendritic spines along a length of neurite were counted for 4-5 neurons per coverslip over duplicate or triplicate coverslips, and 5 separate neuronal preparations were employed. The spine number per 20 μm length was calculated and expressed as percent shNT. Neurons transfected with shFDFT1 or shCYP51 exhibited a higher dendritic spine density than control for two each of the three hairpin sequences employed (Figure 5). The hairpin sequences that did not decrease relative mRNA levels of FDFT1

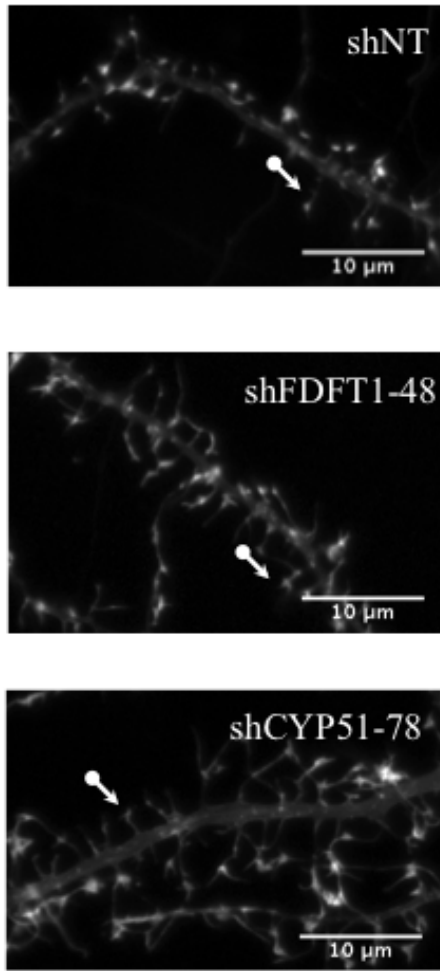
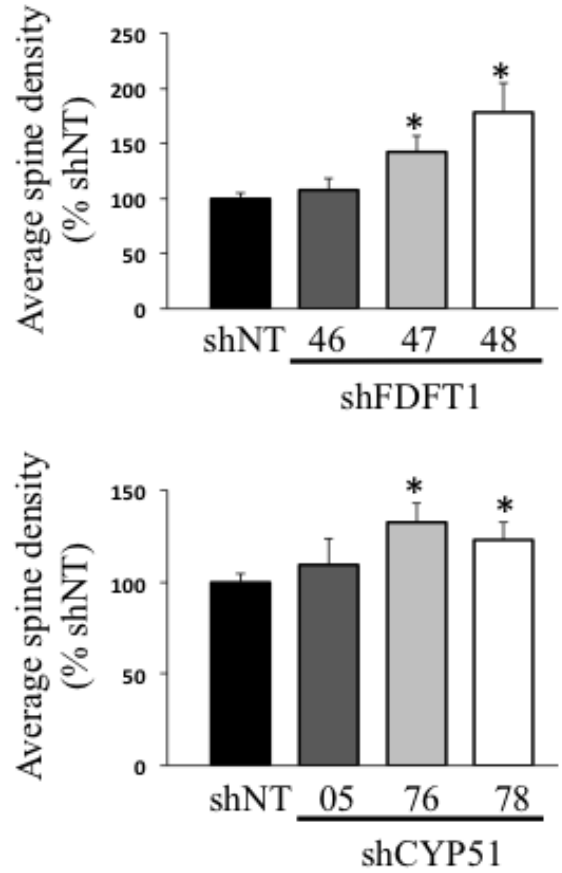
A**B**

Figure 5. Decreased FDFT1 or CYP51 increases dendritic spine density

Cultures were transfected at DIV7 with LifeAct vectors encoding shNT, shFDFT1 or shCYP51. A) Live cells were imaged at DIV16 or DIV17. Arrows indicate dendritic spines. B) Spine density was calculated for 4-5 neurons per coverslip and expressed as % shNT. Data shown are the mean \pm SEM of two experiments in triplicate utilizing five different hippocampal preparations. * $p < 0.05$. Scale bars are 10 μ m.

or CYP51 (Figure 4) did not increase spine densities. Decreased FDFT1 or CYP51 also appeared to increase spine length and/or the number of long spines, which could be indicative of an increase in immature filopodia spines, but this was not quantified and requires further investigation. These results suggest that neuronal cholesterol biosynthesis is involved in the regulation of spine development and/or maturation.

3.1.4 Mitochondrial Effects Of Decreased FDFT1 Or CYP51

Statins inhibit cholesterol biosynthesis and have been associated with mitochondrial effects (as reviewed in ¹⁰⁵). Specifically, statins decrease levels of coenzyme Q10 ¹⁰⁶, which is the oxidized form of the isoprenoid ubiquinone and is necessary for electron transport chain function and ATP production. Statins inhibit HMGR, which also prevents isoprenoid formation and subsequent protein prenylation, suggesting that the mitochondrial effects associated with statins may be a result of decreased isoprenoid levels and/or decreased cholesterol biosynthesis. I investigated the effects of decreased FDFT1 or CYP51 on mitochondria with Mito vectors. Cells were transfected with pGipZ vectors containing Mito and shFDFT1 or shCYP51 at DIV7, and imaged live at DIV16 or DIV17. Mitochondrial length was measured for 50-100 mitochondria per image and 8-10 images were taken per coverslip, with duplicate or triplicate coverslips per experiment. A total of 9 different neuronal preparations were employed. Mitochondrial length was averaged for each image and expressed as percent shNT (Figure 6). Preliminary experiments revealed a decrease in mitochondrial size upon transfection with shFDFT1 or shCYP51; however, these decreases were not consistently apparent with subsequent experiments, suggesting that cell health and density likely affect mitochondrial dynamics and mitochondrial length assessments. Thus, decreased

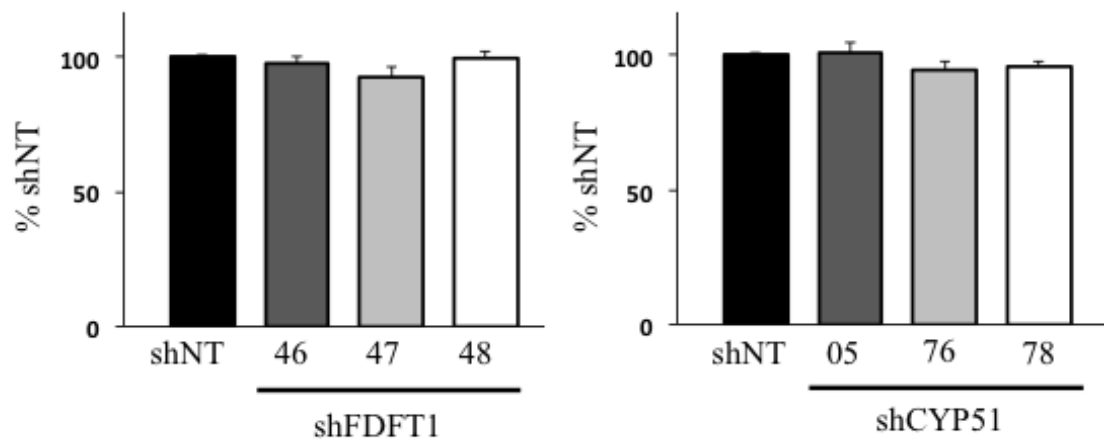


Figure 6. Decreased FDFT1 or CYP51 does not alter mitochondrial size
 Cultures were transfected at DIV7 with Mito vectors encoding shNT, shFDFT1 or shCYP51 and live cells were imaged at DIV16 or DIV17. Mitochondria (50-100/image) were measured over 5-10 images per construct per coverslip, with triplicate coverslips per experiment. The mean mitochondrial size was calculated per image and expressed as % shNT. Data shown are the mean +/- SEM of three independent experiments in triplicate using nine different hippocampal preparations.

FDFT1 or CYP51 did not significantly alter mitochondrial size relative to control. To determine the effects of reduced expression of FDFT1 or CYP51 on mitochondrial function, I attempted to explore mitochondrial turnover with MitoTimer, a doxycycline-inducible sensor of mitochondrial turnover and transport. MitoTimer is a mutant of DsRed that is expressed as a mitochondrially-targeted green fluorescent protein that turns red when oxidized ¹⁰⁷. Neurons were transfected with MitoTimer at DIV8 and imaged at DIV14 to assess baseline turnover of mitochondria in hippocampal cultures; however, MitoTimer was constitutively expressed without doxycycline, preventing controlled expression and accurate analysis of mitochondrial turnover. Functional effects of decreased neuronal cholesterol biosynthesis on mitochondria were not further explored.

3.2 ORP4 EXPRESSION IN HIPPOCAMPAL CULTURES

ORP4, a homolog of the well-known cholesterol sensor/trafficker OSBP, is highly expressed in the hippocampus ^{81,98}, and *ORP4*^{-/-} mice exhibit defects in apical dendrites of the hippocampus ⁹⁸. ORP4 contains an OSBP homology domain (ORD) that binds cholesterol, PI4P and 25OHC; however, the specific role of ORP4 is not yet known. To determine the role of ORP4 in the hippocampus, I first aimed to detect ORP4 in hippocampal cells *in vitro*. Given that hippocampal cultures contain both neuronal and glial cells, and the cell types exhibit different properties at different stages of development *in vitro*, cells were harvested at different developmental stages, DIV8 or DIV15. Glia are proliferating at DIV8, and one expects more neurons than glia in these cultures; however, at DIV15 glia have ceased/slowed proliferation, and one expects more glia than neurons in these cultures. Cultures treated with cytosine arabinoside (cytC), which is an inhibitor of glial proliferation, contain mainly neurons at both DIV8 and

DIV15. Immunoblotting of cell lysates of untreated DIV8 and DIV15 cultures with anti-ORP4 antibodies revealed that the long (ORP4L) and short (ORP4S) isoforms of ORP4 were detected at both developmental stages (Figure 6A). CytC effectively decreased glial proliferation, as evidenced by undetectable GFAP expression in +cytC cultures, and this allowed assessment of predominantly neuronal ORP4 isoform expression. ORP4L and ORP4S were detected in both DIV8 and DIV15 cultures after treatment with cytC, suggesting that neurons express both isoforms (Figure 7A). The levels of ORP4L/actin were significantly lower in DIV8 +cytC cultures relative to DIV8 –cytC cultures, while the levels of ORP4S/actin were similar at this age (Figure 7B). At DIV15, there were no differences in the levels of ORP4L/actin or ORP4S/actin between +cytC and –cytC cultures, which could suggest comparable ORP4 isoform levels in neurons and non-proliferating glia at this developmental stage (Figure 7B). Additionally, the levels of ORP4L/actin and ORP4S/actin were not significantly altered between DIV8 and DIV15 +cytC cultures, nor between DIV8 and DIV15 –cytC cultures (Figure 7C), suggesting that neuronal and glial ORP4 isoform levels do not significantly change with age.

3.2.1 Transduction With shORP4 Or shORP4L Does Not Affect Cholesterol Biosynthetic Enzyme Expression

Cholesterol levels regulate the localization of OSBP, which is a cholesterol sensor/transfer protein, and OSBP regulates cholesterol distribution between the ER and Golgi. *In vitro* studies showed that cholesterol depletion with statins ¹⁰⁸ and treatment with 25-hydroxycholesterol (25OHC) ⁸³, an inhibitor of cholesterol synthesis, caused Golgi localization of OSBP. Chinese hamster ovary (CHO) cells overexpressing OSBP

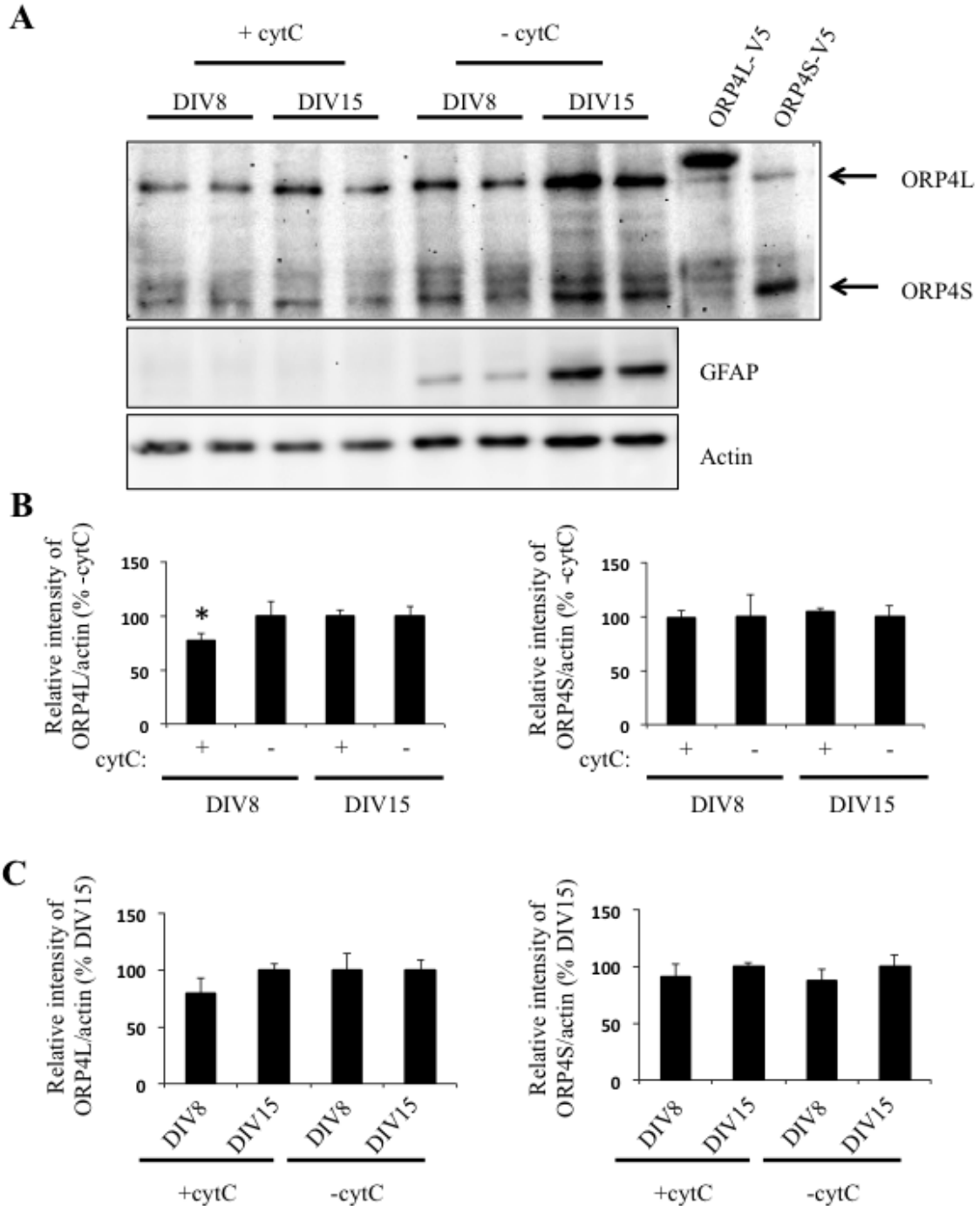


Figure 7. ORP4 isoforms are expressed by neurons and co-cultures at DIV8 and DIV15

Cultures were treated with cytC or left untreated and harvested for protein at DIV8 or DIV15. A) Cell lysates were analyzed by immunoblotting with anti-ORP4 antibodies, and ORP4L and ORP4S isoforms were confirmed by comparison to pcDNA3.1 vectors expressing ORP4L-V5 and ORP4S-V5, respectively. B and C) Quantification of band intensity using densitometry. Data shown are the mean \pm SEM of three independent experiments in duplicate using three different hippocampal preparations.

exhibited increased mRNA levels of LDLr, HMGR and HMGS ¹⁰⁹. However, silencing of OSBP did not affect cholesterol synthesis ¹¹⁰, suggesting that OSBP does not regulate cholesterol levels directly. Given the high sequence similarity between ORP4 and OSBP, it is possible that the function of ORP4 involves cholesterol sensing or transfer in a manner similar to OSBP. I sought to determine whether inhibition of cholesterol biosynthesis influences ORP4 localization similar to OSBP, and whether ORP4 isoform levels regulate cholesterol biosynthetic enzyme expression. However, I was unable to visualize ORP4 localization based on poor specificity of the antibody by immunostaining. Thus, I focused on determining whether ORP4 regulates cholesterol biosynthetic enzyme levels.

I first aimed to decrease total ORP4 or ORP4L isoform expression using lentivirus-mediated RNAi. I used lentivirus-competent pLKO.1 RNAi vectors encoding shRNA targeting exon 3 of the ORP4 transcript to decrease expression of ORP4L and ORP4S (shORP4) or shRNA targeting exon 1 of the transcript to decrease expression of only ORP4L (shORP4L), which effectively decreased total ORP4 or ORP4L expression, respectively, in HEK 293T, HeLa and CHO cells ⁹⁴. Cultures were transduced with shORP4 or shORP4L at DIV7 for 48 hours and protein levels were assessed by immunoblotting with anti-ORP4 antibodies (Figure 8).

I assessed relative mRNA levels of cholesterol biosynthetic genes 48 h after transduction with shORP4 or shORP4L by qPCR. Relative mRNA levels of early- (HMGR) and late-stage (CYP51, FDFT1) cholesterol biosynthetic enzymes were not altered with shORP4 or shORP4L relative to cyclophilin as a reference gene (Figure 9A).

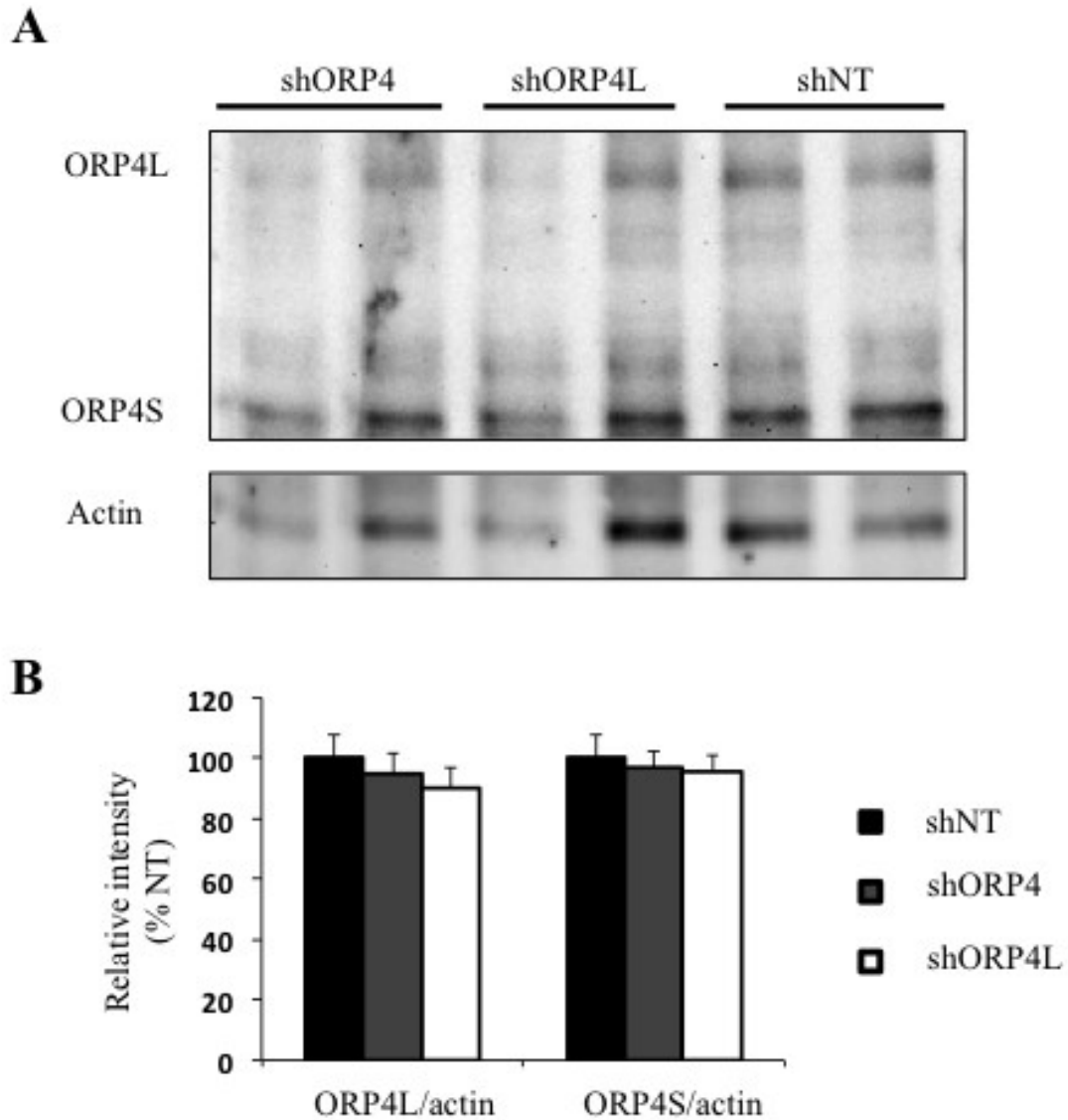


Figure 8. ORP4 isoform expression 48 h after transduction of DIV7 cultures with shORP4 or shORP4L

Cultures were transduced at DIV7 for 48 h. A) Cell lysates were analyzed by immunoblotting with anti-ORP4 antibodies. Actin was used as a loading control. Image is representative of three independent experiments in duplicate. B) Quantification of band intensity using densitometry. Data shown are the mean \pm SEM of three experiments in duplicate using three different hippocampal preparations.

Similarly, protein levels of CYP51 were unaltered after transduction with shORP4 or shORP4L relative to control (Figure 9B and C).

3.3 TRANSDUCTION WITH shORP4 OR shORP4L DIMINISHES GLIAL POPULATIONS BUT NOT NEURONAL CELL NUMBERS WITHOUT AFFECTING GROSS CELLULAR MORPHOLOGY

Inspection of culture health after transduction with shORP4 or shORP4L at DIV7 revealed that glial populations appeared diminished relative to control. In HEK 293T and HeLa cells, depletion of ORP4 inhibited cell proliferation⁹⁴, and I speculated that glial cell proliferation could be inhibited by decreased ORP4, since DIV7 glial cells are proliferative. Additionally, the decrease in glial populations could help to explain the minor decreases in ORP4 isoform expression upon transduction with shORP4 or shORP4L, as protein levels were assessed from not only fewer cells, but only the cells surviving the transduction, which could be a result of increased ORP4 expression. I sought to determine the effects of shORP4 or shORP4L on hippocampal cell proliferation and/or survival. Immunostaining with anti-GFAP antibodies revealed that transduction with shORP4 or shORP4L at DIV7, but not at DIV14, decreased the number of GFAP+ cells, which are indicative of glia (Figure 10). Gross glial morphology was not altered after transduction with shORP4 or shORP4L (Figure 10).

Unlike glial cells, neurons do not proliferate. To determine the effects of shORP4 or shORP4L on neuronal cell numbers, cultures were transduced at DIV7 or DIV14 for 48 h and immunostained with anti-MAP2 antibodies. Neuronal cell numbers were assessed by counting the number of MAP2+ cells in 5-6 images per coverslip over two

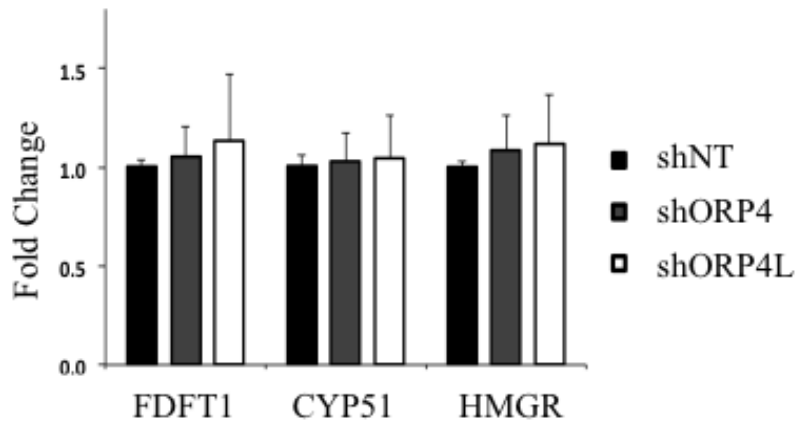
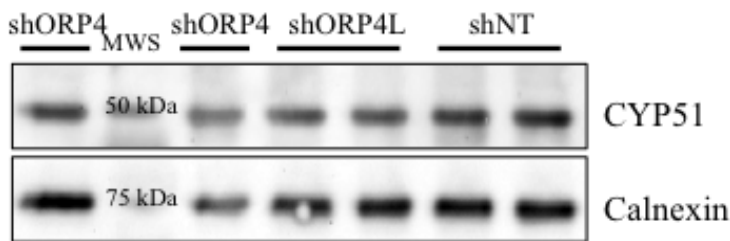
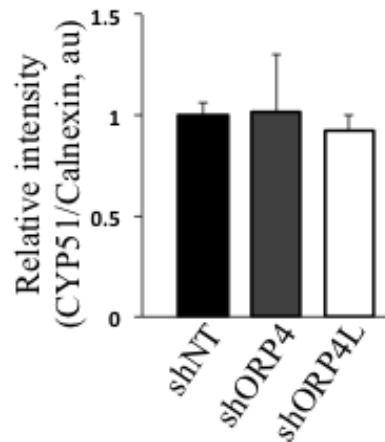
A**B****C**

Figure 9. Transduction with shORP4 or shORP4L does not alter cholesterol biosynthetic enzyme expression

Cultures were transduced at DIV7 for 48 h and RNA was extracted. Relative mRNA levels of FDFT1, CYP51 and HMGR were assessed with qPCR. Data shown are the mean \pm SEM for three independent experiments in duplicate using 3 different hippocampal preparations. B) Cell lysates were analyzed by immunoblotting with anti-CYP51 antibodies. Calnexin was used as a loading control. Image is representative of three independent experiments in duplicate using three different hippocampal preparations. C) Quantification of CYP51 expression shown in B using densitometry.

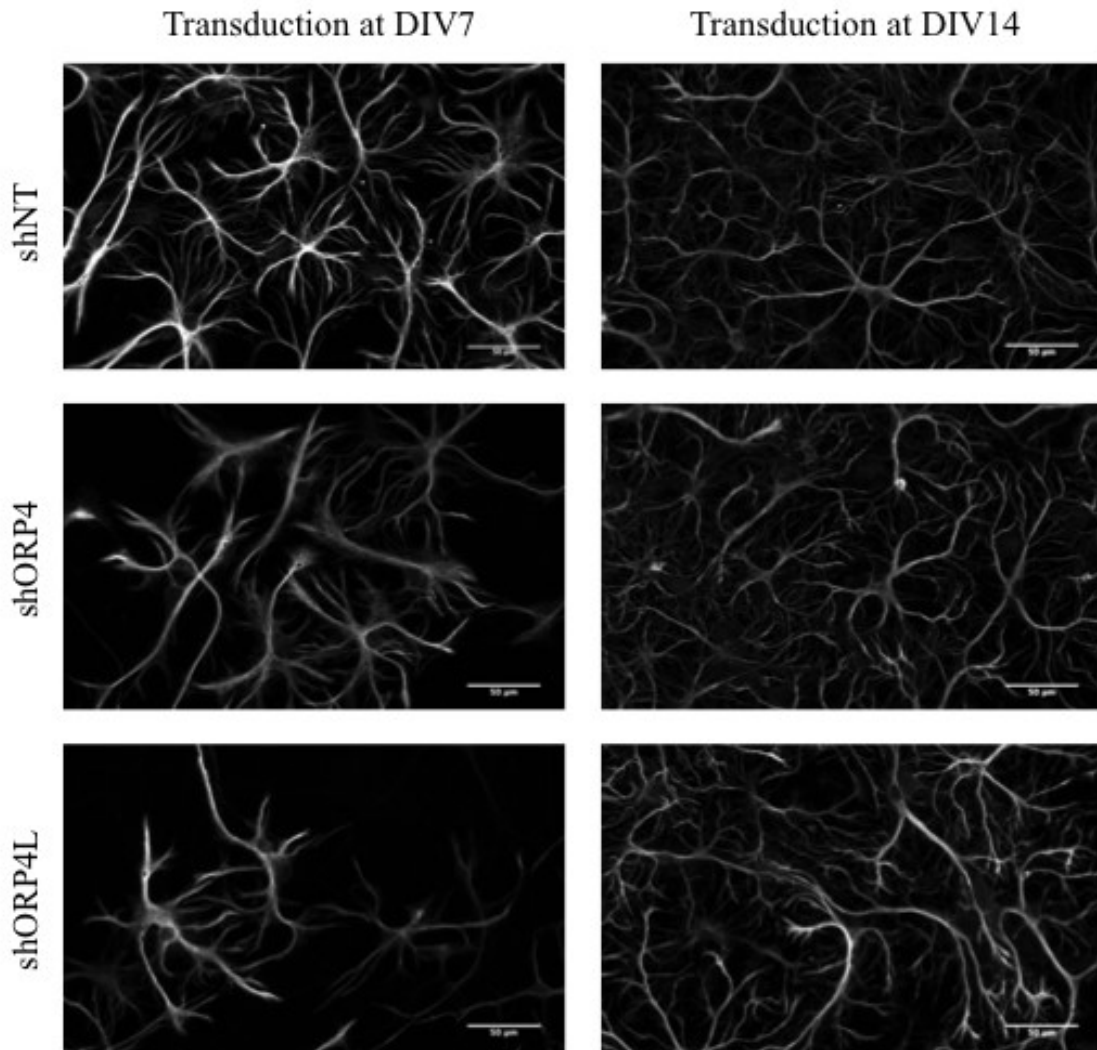


Figure 10. Transduction with shORP4 or shORP4L inhibits glial proliferation in DIV7 cultures without affecting gross glial morphology
 Cultures were transduced at DIV7 or DIV14 for 48 h, fixed and immunostained with anti-GFAP antibodies. Brightness and contrast settings were constant among all DIV7 images and among all DIV14 images. Images are representative of three independent experiments in duplicate. Scale bars are 50 μm .

coverslips per construct per experiment, and expressed as a percent of the control. Neuronal morphology was unaltered with downregulation of total ORP4 or ORP4L expression (Figure 11A) nor were neuronal cell numbers significantly altered (Figure 11B).

3.3.1 Transduction With shORP4 Or shORP4L Inhibits Proliferation But Does Not Induce Apoptosis

To determine whether transduction with shORP4 or shORP4L decreased GFAP⁺ populations due to apoptosis or inhibited proliferation, transduced cultures were stained with Hoechst dye, which binds to DNA and allows detection of nuclei. Apoptotic nuclei exhibit DNA fragmentation and nuclear condensation, which is detected with Hoechst staining as small, intensely fluorescent nuclei. There were no significant differences in percent apoptotic cells with shORP4 or shORP4L relative to control (Figure 12A), nor were there differences after treatment with rotenone to induce mitochondrial dysfunction and cell death in these cultures (Figure 12B). Ultimately, these results suggest that the diminished GFAP⁺ populations were due to inhibited proliferation rather than induction of apoptosis.

3.4 EFFECTS OF shORP4 OR shORP4L ON ORGANELLAR MORPHOLOGY

OSBP contains a PH domain and an FFAT motif, which facilitate interaction with the Golgi and ER, respectively. OSBP is present at ER-Golgi MCS to facilitate transfer/exchange of sterols and PI4P between these organelles⁸⁴. Indeed, depletion of OSBP inhibits lipid transfer and decreases cholesterol levels in the Golgi¹¹¹.

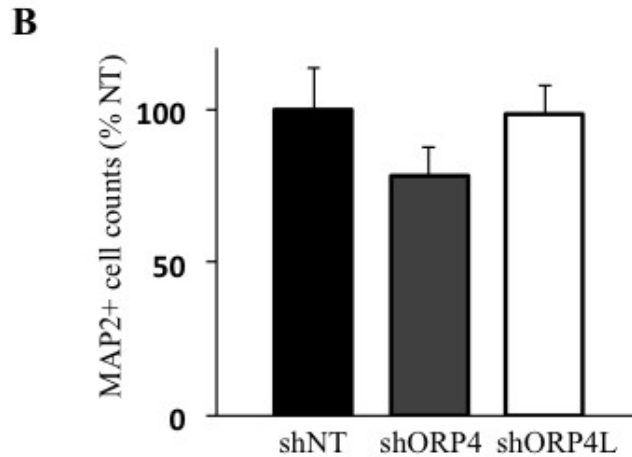
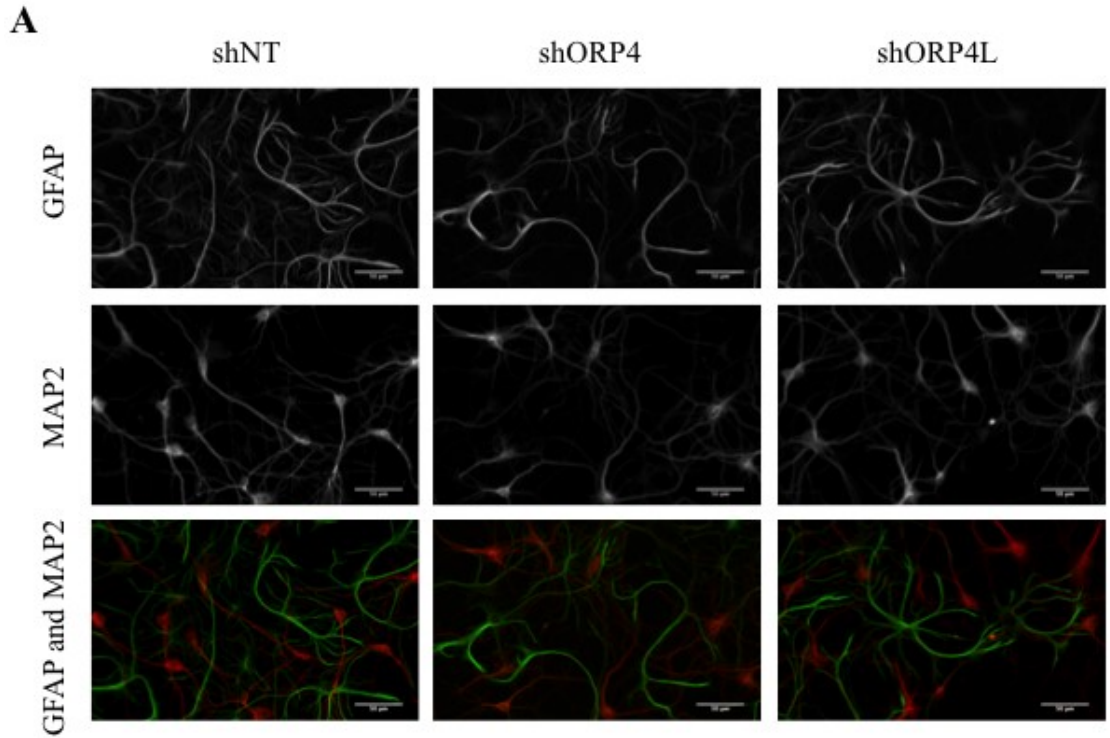


Figure 11. Transduction with shORP4 or shORP4L does not affect neuronal cell numbers or gross neuronal morphology

Cells were transduced at DIV7 for 48 h, fixed and immunostained with anti-GFAP and anti-MAP2 antibodies. A) Contrast was enhanced for each image to illustrate cell morphology. Images are representative of three independent experiments in duplicate. B) All neurons were counted in 20-24 images per construct and expressed as % shNT. Data shown are the mean \pm SEM of three independent experiments in duplicate using three different hippocampal preparations. Scale bars are 50 μ m.

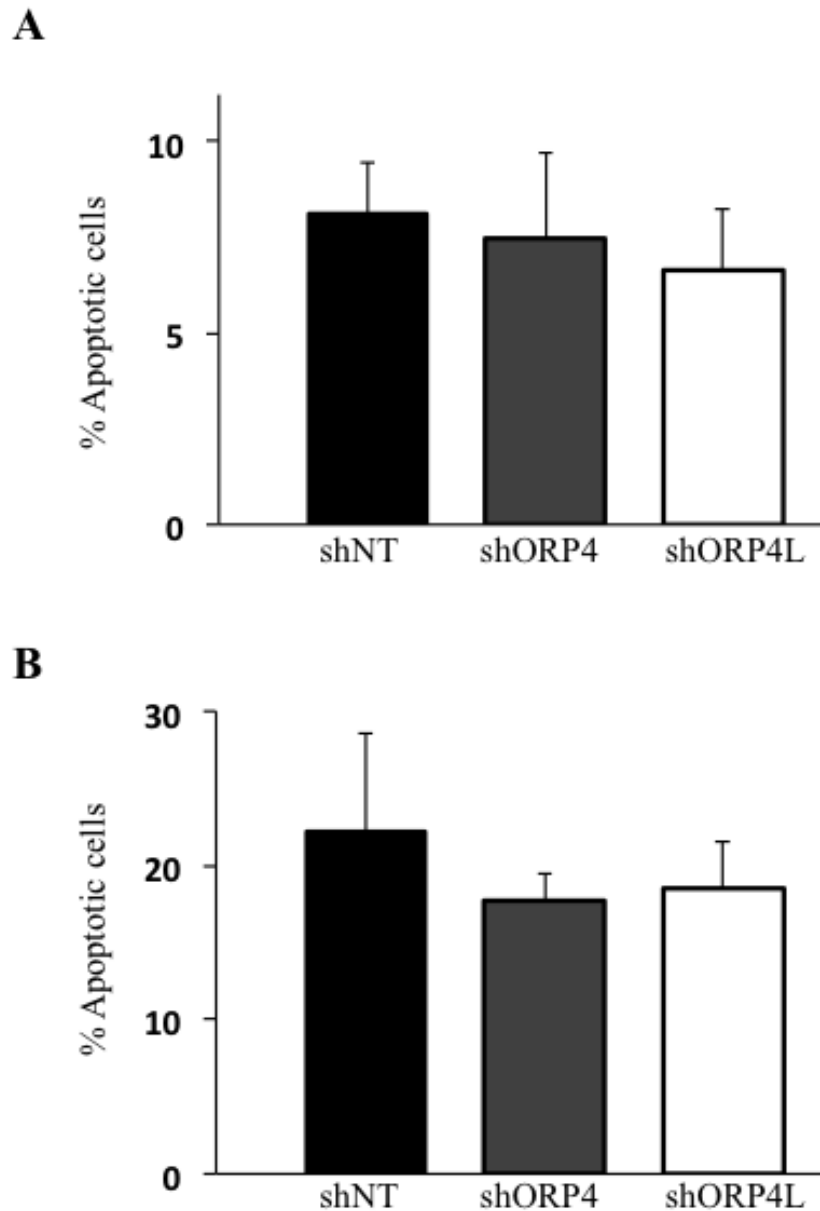


Figure 12. Transduction with shORP4 or shORP4L does not induce apoptosis

Cultures were transduced at DIV7 for 48 h, fixed and stained with Hoechst dye. Apoptotic nuclei were counted and expressed as a percentage of total nuclei. Data shown are the mean \pm SEM of three independent experiments in duplicate using three different hippocampal preparations.

Phosphorylation of OSBP at Ser242 by protein kinase D (PKD) inhibits 25OHC-induced translocation of OSBP to the Golgi and leads to Golgi fragmentation ¹¹², suggesting that OSBP regulates Golgi morphology. ORP4 is highly similar to OSBP, with approximately 63% similarity at the protein level ⁹³; both ORP4L and ORP4S contain an FFAT motif, which facilitates interaction with the ER, but only ORP4L contains a PH domain, which facilitates interaction with the Golgi. Thus, I sought to determine if alterations in total ORP4 or ORP4L would affect gross ER and Golgi organelle structure. Cultures were transduced at DIV7 for 48 hours and immunostained with antibodies against Giantin, which is a cis, medial-Golgi protein, or protein disulphide isomerase (PDI), which is an ER-resident protein. Qualitative assessment of Golgi (Figure 13) and ER (Figure 14) revealed no alterations in gross morphology of these organelles after transduction with shORP4 or shORP4L. Cell type was determined by co-immunostaining with anti-GFAP and anti-MAP2 antibodies, as shown in Figure 13.

3.4.1 Transduction With shORP4 Or shORP4L Elongates Neuritic And Glial Mitochondria

Brain cells have high energy demands, with neurons predominantly relying on mitochondrial oxidative phosphorylation ¹¹³ and glia relying on glycolysis for ATP production ¹¹⁴. While there are no reports of OSBP directly affecting mitochondrial structure or function, two ORPs (ORP5 and ORP8), localize to ER-mitochondria contact sites and regulate phospholipid synthesis at the mitochondria ¹¹⁵. I sought to determine the effects of decreased ORP4 on mitochondrial morphology. Mitochondrial lengths vary

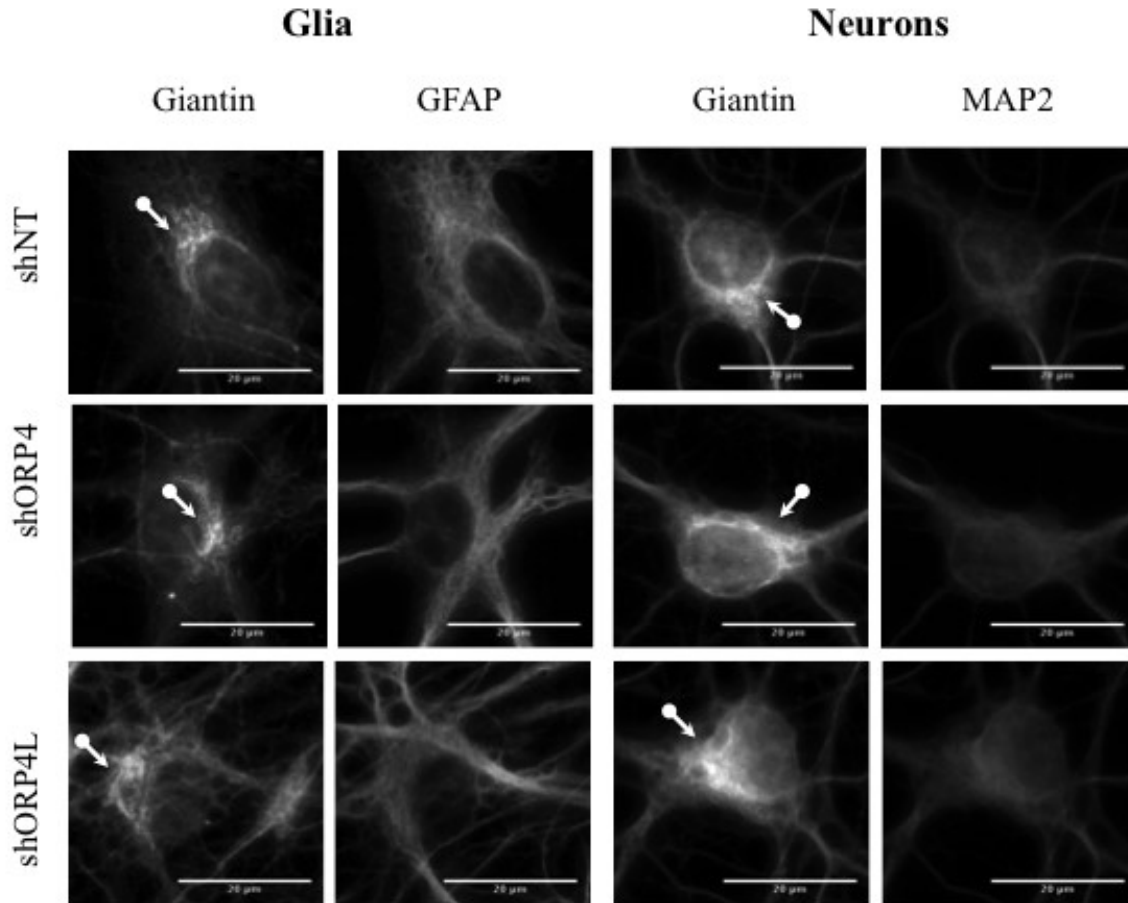


Figure 13. Transduction with shORP4 or shORP4L does not alter gross cis, medial-Golgi morphology

Cultures were transduced at DIV7 for 48 h, fixed and immunostained with anti-Giantin, anti-GFAP and anti-MAP2 antibodies. Contrast was enhanced for each image to illustrate cell morphology. GFAP+ cells are glial while MAP2+ cells are neuronal. Arrows indicate Giantin. Images are representative of two independent experiments in duplicate using two different hippocampal preparations. Scale bars are 20 μ m.

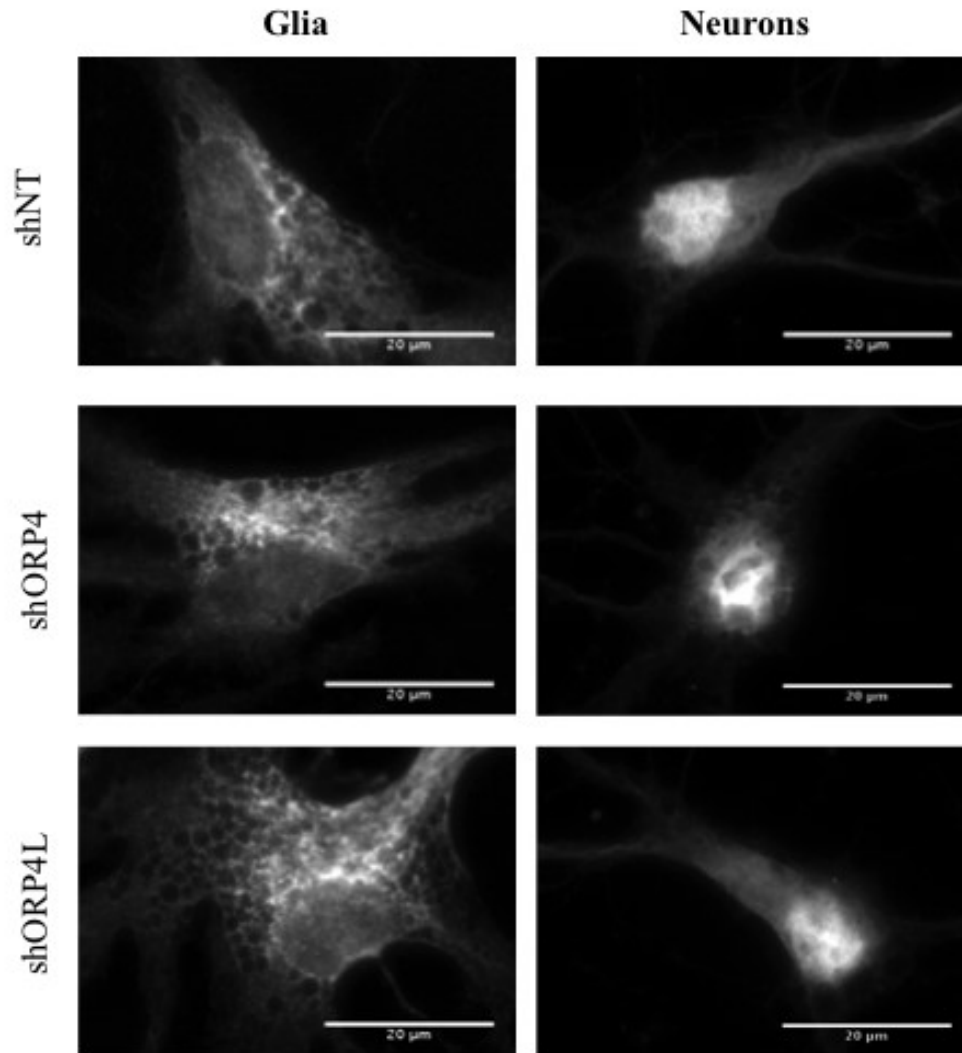


Figure 14. Transduction with shORP4 or shORP4L does not alter gross ER morphology

Cultures were transduced at DIV7 for 48 h, fixed and immunostained with anti-PDI antibodies. Contrast was enhanced for each image to illustrate cell morphology. Cell type was determined by co-immunostaining with anti-GFAP and anti-MAP2 antibodies (not shown) indicative of glia and neurons, respectively. Images are representative of two independent experiments in duplicate using two different hippocampal preparations. Scale bars are 20 μ m.

greatly within a cell, but average neuritic mitochondrial length has been shown to be approximately 2 μm ¹²⁸. Thus, I defined “elongated mitochondria” as mitochondria 1.5 times the average mitochondrial length of the control. Cultures were transduced at DIV7 for 48 hours and immunostained with antibodies against the mitochondrial marker TOM20, which allowed detection of both neuronal and glial mitochondria. I measured neuritic and glial mitochondria in image fields outside of neuronal and glial cell bodies and found that the proportions of elongated mitochondria were significantly increased upon transduction with shORP4 or shORP4L relative to control (Figure 15A and 15B). Additionally, the variation in mitochondrial lengths increased and shifted upward toward a more elongated phenotype when cultures were transduced with shORP4 or shORP4L relative to control (Figure 15C).

3.5 EFFECTS OF shORP4 OR shORP4L ON MITOCHONDRIAL DYNAMICS

Mitochondrial morphology is dynamically regulated to respond to metabolic demands and cellular stresses. Mitochondrial elongation can indicate dysregulated mitochondrial homeostatic mechanisms, such as decreased fission and/or increased fusion events. Fission functions to sequester damaged mitochondrial components for degradation whereas fusion promotes redistribution and sharing of functional mitochondrial components. Under normal physiological conditions, mitochondrial fission and fusion processes are balanced to maintain homeostasis, but impairments to either process dysregulate mitochondrial size and lead to metabolic consequences. Additionally,

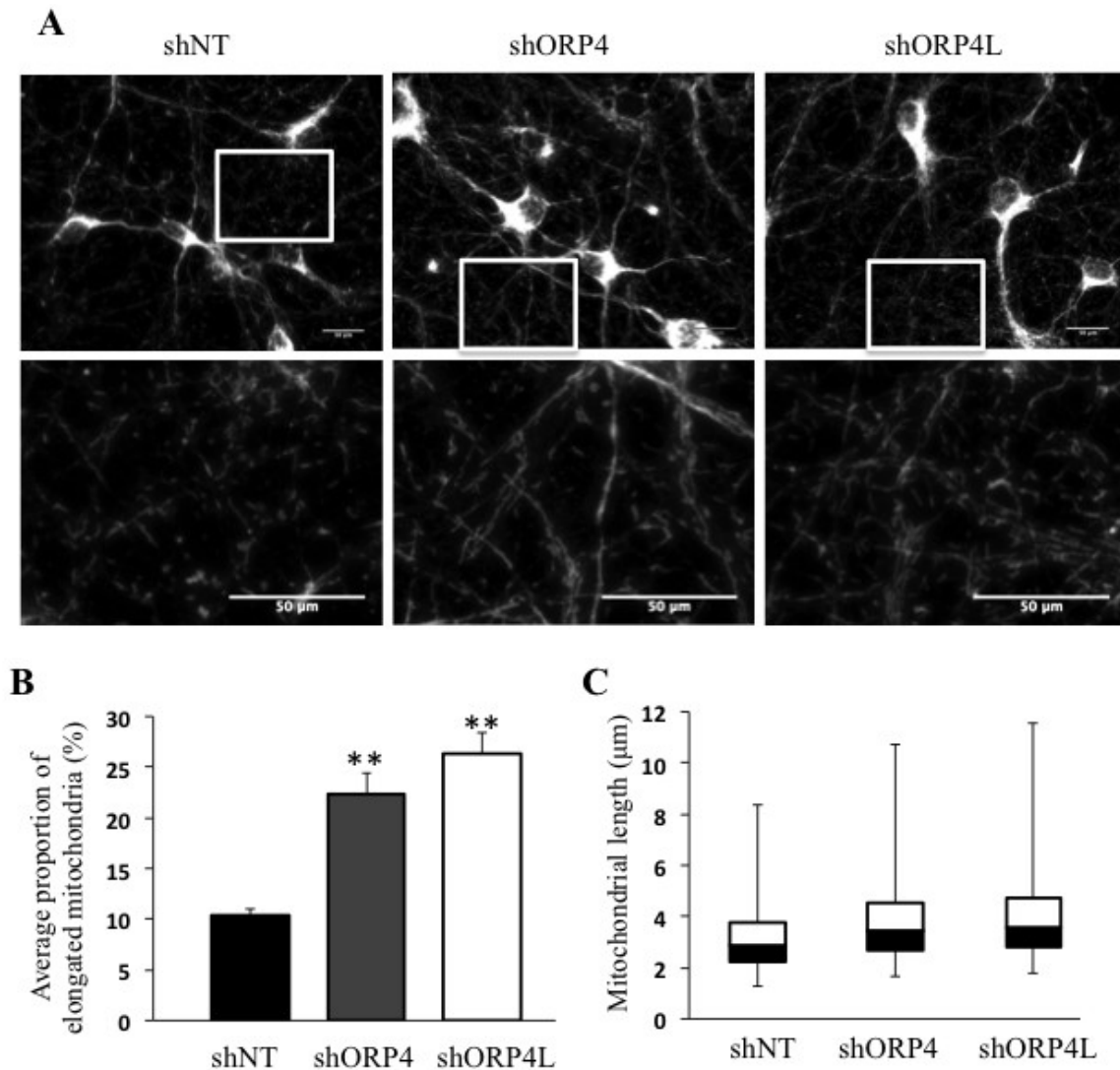


Figure 15. Transduction with shORP4 or shORP4L elongates mitochondria
 Cultures were transduced at DIV7 for 48 h, fixed and immunostained with anti-Tom20 antibodies. A) Contrast was constant among upper panels and cell bodies were overexposed to illustrate mitochondrial morphology. The lower panels show area within the white box enlarged and with enhanced contrast. B) Mitochondrial lengths (50-200/image) were measured across 3-7 images per construct on duplicate coverslips. The number of mitochondria with lengths greater than 1.5 times the average shNT length were calculated as a proportion of total mitochondria counted. Data shown are the mean +/- SEM of three independent experiments in duplicate using three different hippocampal preparations. ** $p < 0.01$. Scale bars are 50 μm . C) Range of mitochondrial lengths of all mitochondria counted as described in B. Medians and quartile values are the average of three independent experiments in duplicate using three different hippocampal preparations.

alterations in mitochondrial morphology can be indicative of cellular changes, as mitochondria dynamically respond to metabolic demands and cellular stresses.

To determine whether transduction with shORP4 or shORP4L was associated with alterations in fission or fusion events, cultures were transduced at DIV7 for 48 hours and RNA was isolated. Relative mRNA levels of FIS1, a protein involved in mitochondrial fission, and MFN2, a protein involved in mitochondrial fusion, were unaltered with shORP4 or shORP4L relative to control (Figure 16A), suggesting that fission and fusion gene expression was not primarily affected at the transcriptional level.

TFAM is a mitochondrial transcription factor that regulates mitochondrial DNA (mtDNA) gene expression and biogenesis. Relative mRNA expression levels of TFAM in cultures transduced at DIV7 for 48 hours were unaltered with shORP4 or shORP4L relative to cyclophilin as a reference gene (Figure 16B).

3.6 EFFECTS OF shORP4 OR shORP4L ON NEURONAL PINK1 LEVELS

Mitophagy is the process of targeting dysfunctional mitochondria for degradation through autophagy that maintains mitochondrial homeostasis. PINK1 is a serine/threonine kinase that indirectly targets dysfunctional mitochondria for degradation by phosphorylating mitochondrial outer membrane proteins, which facilitates ubiquitination of these proteins by the E3 ubiquitin ligase, PARKIN. Degradation of these mitochondria occurs predominantly in the soma where autophagic lysosomes are located, but there are reports of local mitophagy in neurons as well ¹¹⁶. PINK1 has roles outside of mitophagy, as it is present in the cytosol and involved in Ca²⁺ efflux from

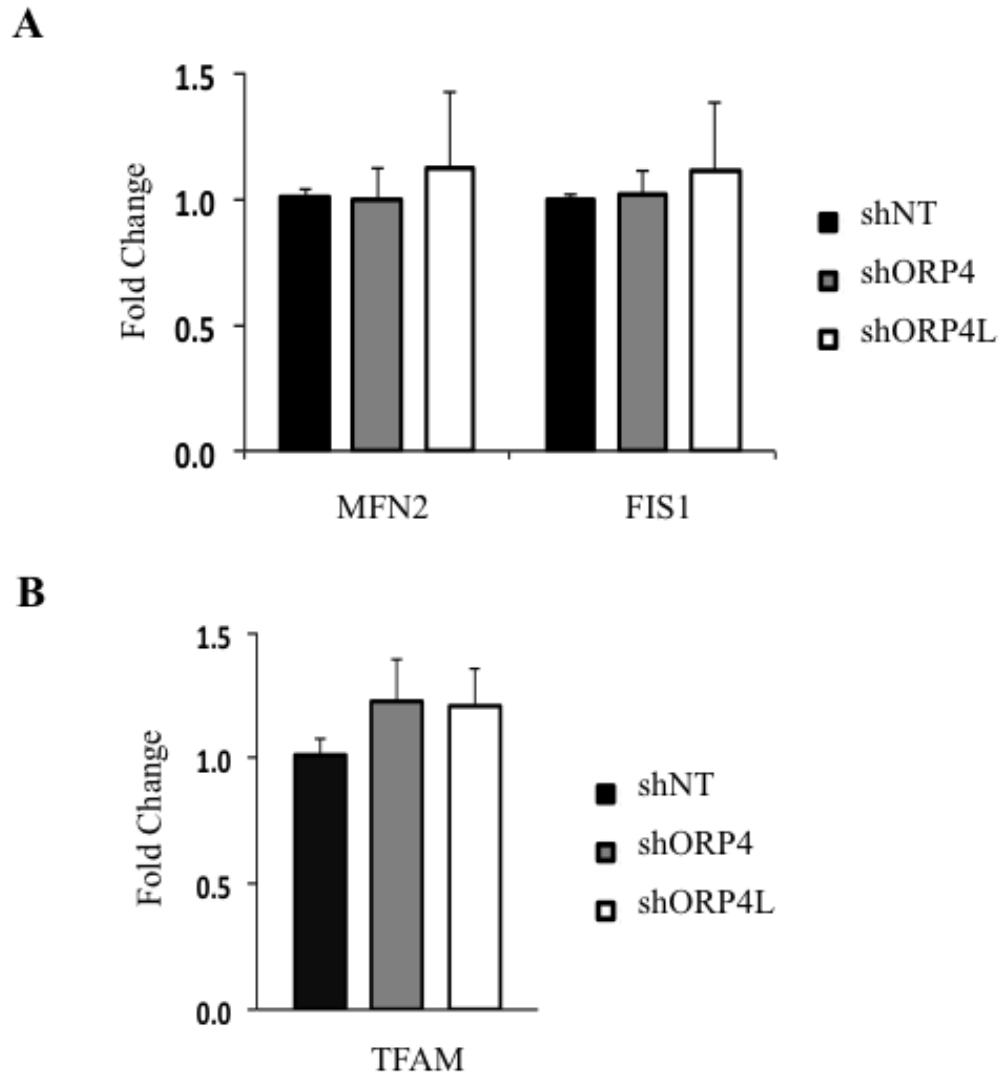


Figure 16. Transduction with shORP4 or shORP4L does not alter mRNA levels of MFN2, FIS1 or TFAM

Cultures were transduced at DIV7 for 48 h and RNA was extracted. Relative mRNA levels were assessed with qPCR and cyclophilin was used as a reference gene. A) Relative mRNA levels of MFN2 and FIS1, mitochondrial fusion and fission proteins, respectively. B) Relative mRNA levels of TFAM, which is a mtDNA transcription factor. Data shown are the mean \pm SEM of three independent experiments in duplicate using three different hippocampal preparations.

mitochondria¹¹⁷. Decreased ORP4L expression decreases IP3R expression, which in turn impairs Ca²⁺ efflux from the ER to cytosol and mitochondria^{95, 96}, and Ca²⁺ regulates mitochondrial morphology, as evidenced by mitochondrial fragmentation upon mitochondrial Ca²⁺-loading¹¹⁸. Thus, I sought to determine whether neuronal PINK1 levels were altered by shORP4 or shORP4L. Cultures were transduced at DIV7 for 48 hours, immunostained with anti-PINK1 antibodies and neurons were detected by co-localization with anti-MAP2 antibodies (Figure 17A). Transduction with shORP4 or shORP4L significantly decreased PINK1 levels in neuronal cell bodies (Figure 17B), suggesting decreased PINK1 expression and/or increased PINK1 processing.

3.7 EFFECTS OF shORP4 OR shORP4L ON NEURONAL NRF2 LEVELS AND LOCALIZATION

Mitochondrial elongation can both contribute to and be a product of excessive reactive oxygen species (ROS) production. Nuclear factor (erythroid-derived 2)-like 2 protein (NRF2) is a transcription factor regulated by ROS and translocates to the nucleus under conditions of oxidative stress to increase expression of antioxidant genes, such as heme oxygenase (*Hmox1*). To determine whether mitochondrial elongation was associated with oxidative stress responses, I assessed mRNA levels of NRF2 and HMOX1 in cultures transduced with shORP4 or shORP4L. Relative mRNA levels of NRF2 and HMOX1 appeared increased with shORP4 but not shORP4L, but these increases were not statistically significant (NRF2, p=0.12, HMOX1, p=0.11) (Figure 18).

Mitochondrial lengths from glia and neurites were included in the assessment of elongated mitochondria in cultures transduced with shORP4 or shORP4L, and thus,

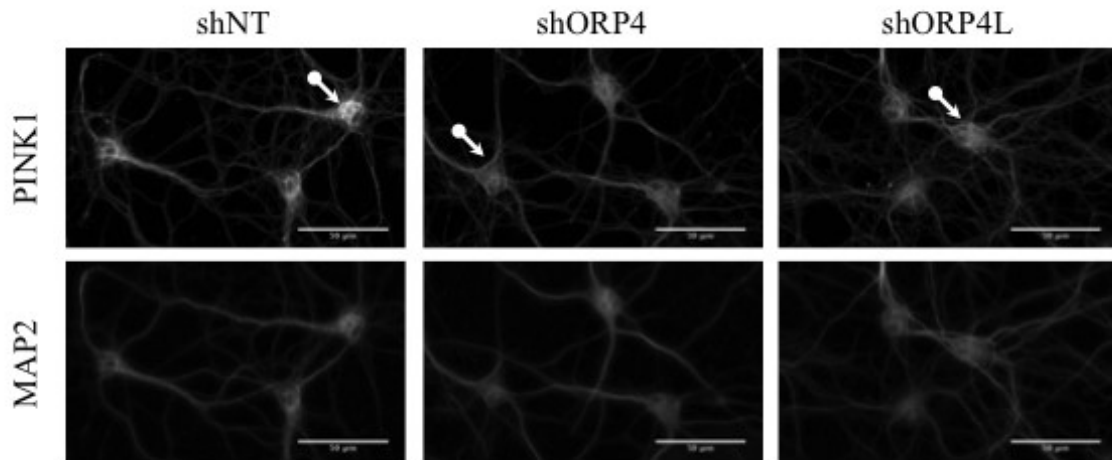
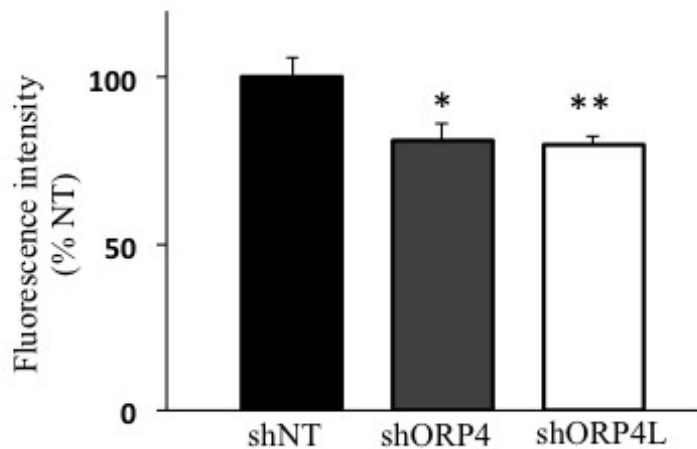
A**B**

Figure 17. Transduction with shORP4 or shORP4L decreases PINK1 levels in the soma

Cultures were transduced at DIV7 for 48 h, fixed and immunostained with anti-PINK1 and anti-MAP2 antibodies. A) Images are shown at equal contrast settings to illustrate relative PINK1 levels. Arrows indicate soma. B) Soma fluorescence intensity was measured in 5-6 images per construct, totaling 50-120 soma per construct per experiment, and expressed as % shNT. Data shown are the mean \pm SEM of three independent experiments in duplicate using three different hippocampal preparations. * $p < 0.05$; ** $p < 0.01$. Scale bars are 50 μ m.

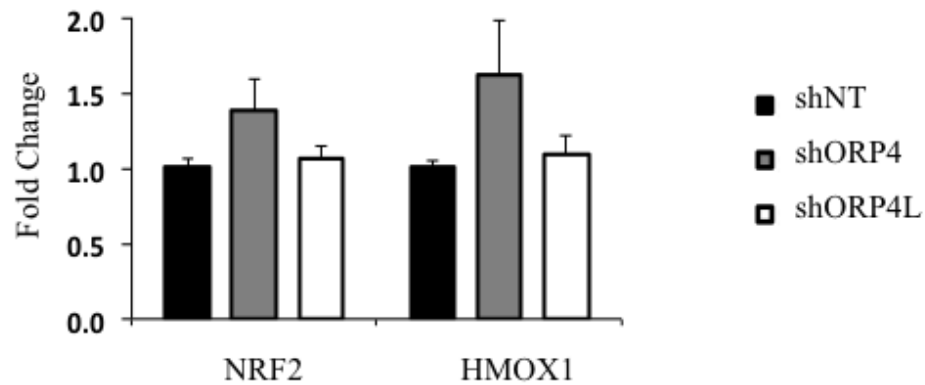


Figure 18. Transduction with shORP4 or shORP4L does not alter mRNA levels of NRF2 or HMOX1

Cultures were transduced at DIV7 for 48 h and RNA was extracted. Relative mRNA levels of NRF2, an antioxidant gene transcription factor and HMOX1, a target of NRF2, were assessed with qPCR relative to a cyclophilin reference gene. Data shown are the mean \pm SEM of three independent experiments in duplicate using three different hippocampal preparations.

mitochondria from each cell type were considered elongated with shORP4 or shORP4L. Neurons and glia exhibit different bioenergetics; neurons rely predominantly on oxidative phosphorylation ¹¹³ while glia rely on glycolysis to meet ATP demands ¹¹⁴. Oxidative phosphorylation is a major source of mitochondrial ROS production ¹¹⁹, and I assessed NRF2 levels in neuronal soma through immunostaining with anti-NRF2 antibodies and co-localizing with anti-MAP2 antibodies (Figure 19A). Transduction with shORP4, but not shORP4L, significantly increased NRF2 levels in the soma relative to control (Figure 19B).

To determine if somatic increases in NRF2 represented NRF2 translocation to the nucleus, I immunostained with anti-NRF2 antibodies and stained with Hoechst dye. The levels of nuclear NRF2 did not change with shORP4 or shORP4L relative to control, suggesting that nuclear import of NRF2 was not impaired (Figure 20). Taken together, these results could suggest that transduction with shORP4 increases or accumulates cytosolic NRF2 without affecting translocation to the nucleus.

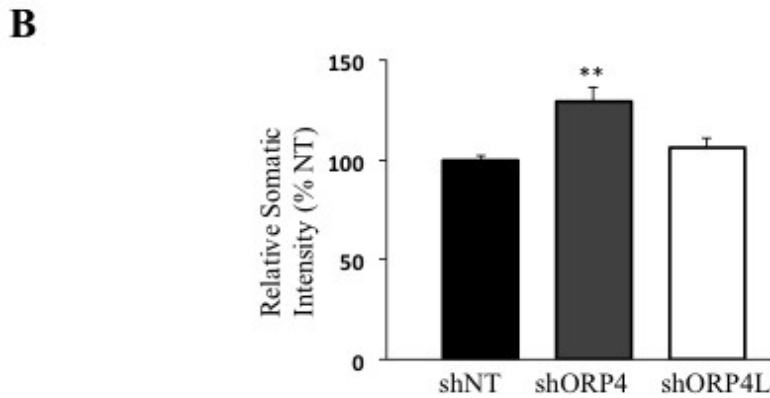
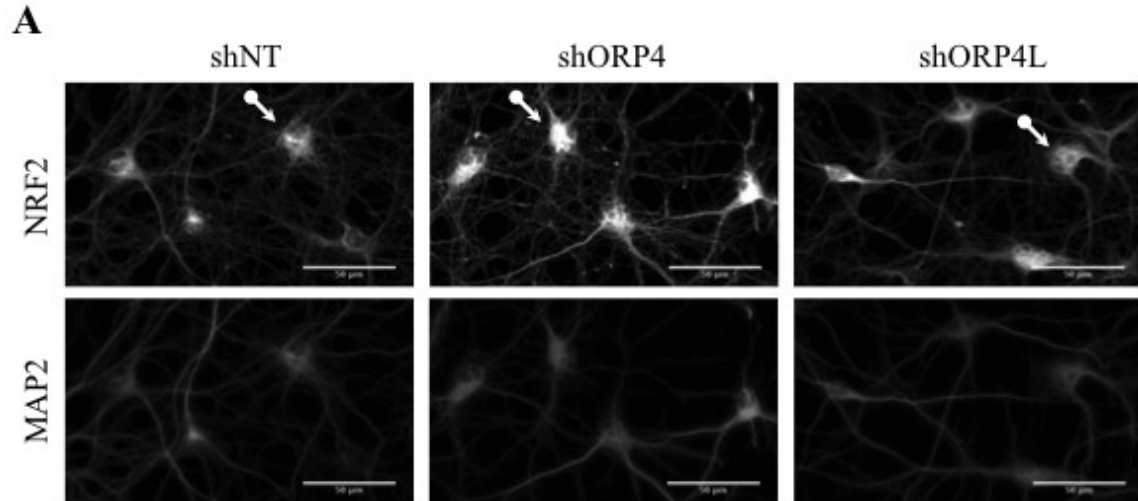


Figure 19. Transduction with shORP4 increases somatic NRF2 levels

Cells were transduced at DIV7 for 48 h, fixed and immunostained with anti-NRF2 and anti-MAP2 antibodies. A) Contrast was constant among NRF2 images to illustrate NRF2 levels. Arrows indicate soma. B) Soma fluorescence intensity was measured in 5-6 images per construct, totaling 190-240 soma per construct per experiment, and expressed as % shNT. Data shown are the mean +/- SEM of three independent experiments in duplicate using three different hippocampal preparations. ** $p < 0.01$. Scale bars are 50 μm .

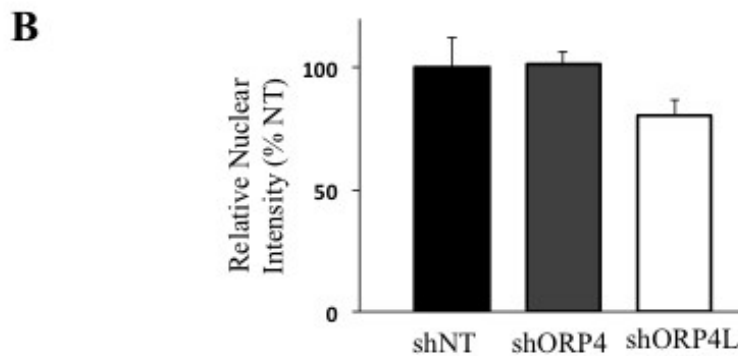
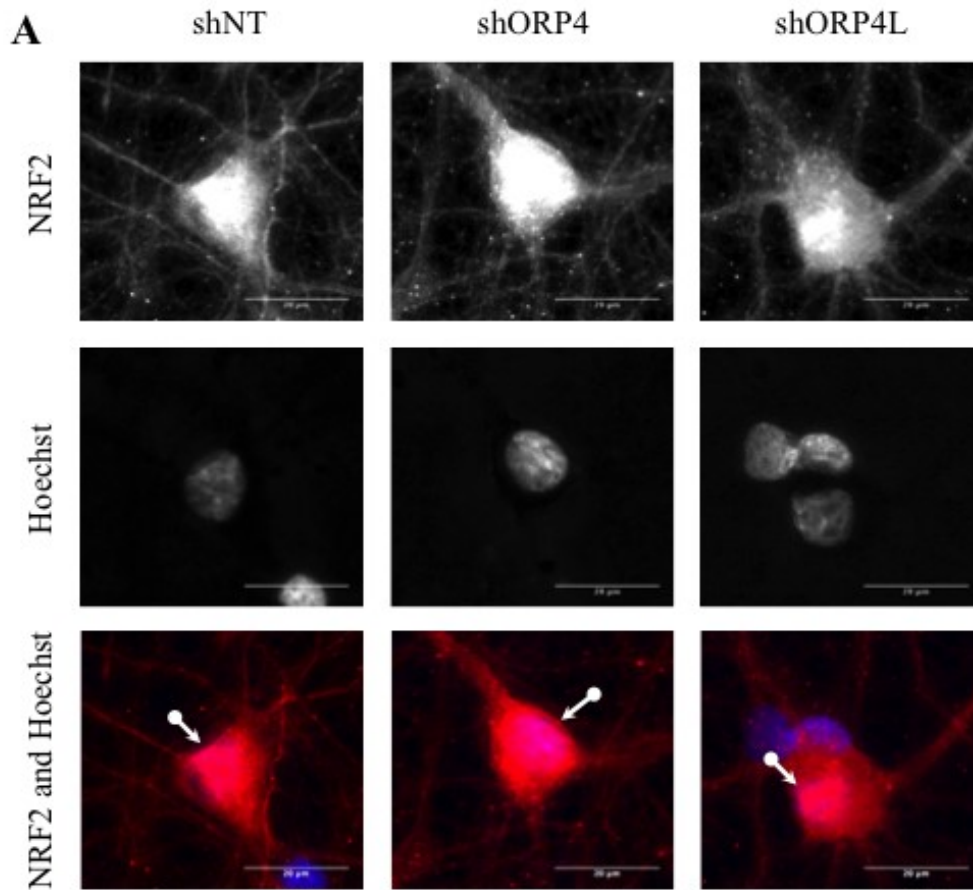


Figure 20. Transduction with shORP4 or shORP4L does not affect nuclear NRF2 translocation

Cells were transduced at DIV7 for 48 h, fixed, immunostained with anti-NRF2 antibodies and stained with Hoechst dye. A) Contrast was constant among NRF2 images to illustrate NRF2 levels. Contrast was enhanced for Hoechst images to illustrate nuclei. Arrows indicate nuclear NRF2. B) Nuclear fluorescence intensity was measured in 5-6 images per construct, totaling 190-240 soma per construct per experiment, and expressed as % shNT. Data shown are the mean +/- SEM of two independent experiments in duplicate using two different hippocampal preparations. * $p < 0.05$. Scale bars are 20 μm .

CHAPTER 4: DISCUSSION

4.1 OVERVIEW OF RESEARCH OBJECTIVES

This thesis investigated the role of neuronal cholesterol biosynthesis on dendritic spines and neuronal mitochondrial size, as well as the role of ORP4 on hippocampal cell survival and mitochondrial dynamics. The brain accounts for a quarter of the body's total cholesterol pool ⁴ all of which is synthesized in situ, and the relative contribution of neurons and glia to brain cholesterol biosynthesis is dependent on the developmental stage. Neurons synthesize large quantities of cholesterol early in development for axon extension and membrane formation, while glial synthesis constitutes the majority of brain cholesterol biosynthesis in maturity and is necessary for synaptogenesis and neuronal survival ^{18, 20, 21}. Yet in hippocampal neurons, neuronal cholesterol synthesis is maintained into maturity for reasons as yet undetermined. I investigated the effects of downregulated late-stage cholesterol biosynthetic enzymes, FDFT1 or CYP51, on dendritic spines and mitochondria to characterize a potential role of neuronal cholesterol biosynthesis in hippocampal neurons.

ORP4 is a sterol-binding protein that is highly expressed in the hippocampus and shares sequence similarity with the sterol sensor/transfer protein, OSBP. The ORP family has functional redundancy but ORP4 is unique in that it is required for cell proliferation and survival ⁹⁴. Additionally, *ORP4*^{-/-} mice exhibit dendritic defects in the hippocampus ⁹⁸; however, very little is known about the function of ORP4. I investigated the role of ORP4 in hippocampal neurons and glia by assessing the effects of lentivirus-mediated RNAi targeting either total ORP4 or ORP4L in these cells.

Here, I discuss the implications of decreased neuronal cholesterol biosynthesis on spine density, and then discuss the role of ORP4 in glial cell proliferation, mitochondrial dynamics and neuronal PINK1 and NRF2 levels.

4.2 THE ROLE OF NEURONAL CHOLESTEROL BIOSYNTHESIS IN HIPPOCAMPAL NEURONS

Previous work in our laboratory found that a statin-induced 50% reduction in cholesterol synthesis impairs synaptic vesicle exocytosis in hippocampal neurons, even in the presence of sufficient exogenous cholesterol from high-density lipoproteins or glial lipoproteins¹²⁰. These results could suggest that the source of cholesterol (neuronal or glial) may dictate its role in hippocampal neurons, or that neuronal cholesterol synthesis serves a specific role in neurons that cannot be compensated for by glial cholesterol. I downregulated neuronal FDFT1 or CYP51 in hippocampal neurons to determine a potential role of neuronal cholesterol synthesis under conditions of adequate glial cholesterol synthesis (Figure 4).

Inhibition of FDFT1 prevents synthesis of squalene and all subsequent sterol intermediates, and some of these late-stage sterol intermediates (ie: 24,25-dihydrolanosterol (DHL), a derivative of lanosterol) regulate early biosynthetic enzyme expression⁶³. Thus, inhibition of squalene formation is expected to decrease levels of DHL, which could upregulate early cholesterol biosynthetic gene expression and promote isoprenoid formation. Inhibition of CYP51 leads to accumulation of lanosterol and prevents synthesis of both Kandutsch-Russell and Bloch pathway sterol intermediates, but presumably does not increase isoprenoid formation since DHL prevents transcription of early cholesterol biosynthetic intermediates and promotes degradation of HMGR.

Thus, downregulation of FDFT1 or CYP51 prevents cholesterol synthesis and simultaneously alters cholesterol biosynthetic intermediate profiles.

Dendritic spines are highly plastic postsynaptic protrusions that grow and regress rapidly, and form at lipid-rich regions of dendritic membranes ^{6, 7}. These regions, known as lipid microdomains, serve as platforms for protein-protein interactions and facilitate the formation of protein complexes involved in signalling, which in turn regulates spine morphology and neurotransmission (as reviewed in ¹²¹). I found that dendritic spine density increased with downregulation of FDFT1 or CYP51 specifically in neurons, and the level of downregulation seemed to inversely correlate with spine density (Figures 4 and 5); however, this was not the case for sh78, which could suggest a threshold or “dose-response” effect of decreased CYP51 and/or cholesterol biosynthesis. As the phenotype was observed with two each of the three hairpins employed for each enzyme, and these were the hairpins that decreased mRNA levels of FDFT1 or CYP51, I concluded that this phenotype was not due to off-target effects of gene silencing.

Increased spine density may be indicative of increased membrane surface area or redistribution of existing membranes. As sufficient cholesterol is necessary for membrane expansion, increased spine density may suggest an increase in total neuronal cholesterol levels; however, I did not assess cellular cholesterol levels. Thus, it is possible that decreased FDFT1- or CYP51-mediated disruptions to neuronal cholesterol synthesis or levels of intermediates increased neuronal uptake of glia-derived cholesterol. Glia promote synaptogenesis ²¹ and synapse strength ¹²² by supplying cholesterol to neurons ²⁰. Thus, increased neuronal uptake of glial cholesterol may be responsible for increased spine density. Neurons take up glia-derived cholesterol through LDLr and LRP1, which

contain SREs and are sterol-regulated. LRP1 is located on dendritic spines and depletion of LRP1 decreases spine numbers¹²³. Upon decreased FDFT1 or CYP51, neurons may increase LDLr and/or LRP1 expression, thereby promoting uptake of exogenous cholesterol. Alternatively, decreased FDFT1 or CYP51 may induce oxidative stress, thereby increasing CYP46A1 expression and 24OHC production⁵⁹. 24OHC stimulates expression of glial cholesterol efflux genes including *AbcA1* and *ApoE*, which could increase neuronal uptake of glial cholesterol. However, 24OHC production also results in cholesterol loss from neurons, so an alternative possibility is that decreased FDFT1 or CYP51 prevents 24OHC synthesis and cholesterol loss.

While increased spine density may be the result of increased cholesterol levels in neurons, it is also possible that the predicted loss or depletion of neuronally synthesized cholesterol (as a result of decreased neuronal FDFT1 or CYP51) may be responsible for increased spine density, ultimately implicating neuronal cholesterol synthesis in the regulation of spine formation, dynamics, or maturation. Cholesterol is synthesized in the ER, and the ER is present in dendrites and spines¹²⁴. Indeed, neurons express late-stage cholesterol biosynthetic intermediates³², which could suggest that neurons maintain a readily accessible pool of intermediates for local cholesterol synthesis. Dendritic lipid microdomains regulate spine formation and morphology (as reviewed in¹²¹). It is possible that neuronally synthesized cholesterol incorporates locally into dendritic lipid microdomains and is involved in spine turnover or spine development. Thus, decreased FDFT1 or CYP51 may prevent sufficient neuronal cholesterol synthesis, which in turn prevents incorporation of locally synthesized cholesterol into lipid microdomains and either prevents signalling cascades necessary for spine regression and/or elimination, or

promotes signalling involved in spine formation. Indeed, decreases in neuronal cholesterol synthesis have been shown to increase tropomyosin receptor kinase B (TrkB) signalling ¹²⁵, which is a receptor for brain-derived neurotrophic factor (BDNF), and BDNF promotes spine survival ¹²⁶. Qualitatively, downregulation of FDFT1 or CYP51 seemed to increase the number of filopodia spines, which are immature spine types, thereby supporting the notion that neuronal cholesterol synthesis promotes spine maturation; however, further investigations are necessary to determine the role of neuronal cholesterol biosynthesis in dendritic spine formation and dynamics through cell signalling and other mechanisms.

In neurons, mitochondria are involved in spine formation, as they supply ATP and buffer cytosolic Ca²⁺ levels to facilitate polymerization of filamentous actin (F-actin) ¹²⁷, and the presence of mitochondria in dendritic spines positively correlates with synapse number ¹²⁸. Given the high energy demands of neurons and their reliance on mitochondria for ATP ^{114, 129, 130}, I investigated the effects of decreased FDFT1 or CYP51 on mitochondrial size.

Downregulation of FDFT1 or CYP51 differentially alter cholesterol biosynthetic intermediate profiles, which may have variable effects on mitochondria. Inhibition of FDFT1 prevents lanosterol and DHL synthesis and is predicted to increase isoprenoid levels. Ubiquinone is an isoprenoid and an important component of the electron transport chain, which facilitates mitochondrial oxidative phosphorylation and ATP production (as reviewed in ¹³¹). Thus, increased isoprenoid formation is expected to have effects on mitochondrial function. Inhibition of CYP51 accumulates lanosterol, which has been shown to uncouple mitochondria and promote mitochondrial clearance in dopaminergic

neurons⁷⁴; however, mitochondrial size did not change with decreased FDFT1 or CYP51 relative to control (Figure 9), and attempts to investigate mitochondrial function were unsuccessful. Mitochondria are morphologically dynamic organelles whose structure and size is related to function. While I cannot conclude that the unaltered mitochondrial morphological phenotype is indicative of unaltered mitochondrial function, it is possible that the observed decreases in FDFT1 or CYP51 were insufficient to cause mitochondrial phenotypes. Given that neurons were assessed ten days after transfection, it is possible that immediate insults to mitochondria were rectified by the time of imaging due to biogenesis, mitophagy or other regulatory mechanisms. Investigations into the effects of inhibiting other late-stage biosynthetic enzymes, such as 7DHCR or LS, may be valuable in further elucidating a specific role of neuronal cholesterol biosynthesis.

4.3 THE ROLE OF ORP4 IN HIPPOCAMPAL NEURONS AND GLIA

ORP4 is highly expressed in the brain, particularly in the hippocampus^{81, 98}. I employed primary hippocampal cultures to investigate the role of ORP4, as these cells were expected to have high endogenous levels of ORP4 relative to other brain cell types. Based on mRNA isolated from total brain tissue, there are comparable levels of ORP4S and ORP4L in the brain⁸¹, but this does not speak to the relative contribution of neurons and glia to ORP4 isoform expression. I investigated ORP4 isoform levels at different developmental stages in cultures containing predominantly neurons (+cytC) and cultures containing neurons and glia (-cytC). Neurons and glia expressed ORP4L and ORP4S at each developmental stage (Figure 7A) and the levels of ORP4 isoforms were not significantly different between developmental stages (Figure 7C). At DIV8, predominantly neuronal cultures had significantly less ORP4L than co-cultures (Figure

7B), which could suggest that proliferating glia express higher levels of ORP4L than neurons of the same developmental age. I acknowledge that my analysis treats neurons and glia as independent entities within cultures and ignores the possibility of neuron-glia inter-regulation of ORP4 expression. Neuronal ORP4 isoform levels can be assessed in cultures treated with cytC, as evidenced by undetectable GFAP levels in these cultures (Figure 7A), but it is possible that these neurons are exhibiting compensatory expression of ORP4 isoforms in the absence of glia and/or glia-derived factors. Similarly, glia may exhibit different ORP4 isoform expression patterns in the absence of neurons. The use of primary hippocampal glial cultures would allow assessment of glial ORP4 isoform expression in the absence of neurons and may be useful in determining the relative contribution of neurons and glia to total ORP4 isoform expression at different developmental stages.

4.3.1 ORP4 Is Required For Glial Cell Proliferation But Not Neuronal Survival

ORP4 is necessary for cell proliferation in sperm cells and cell lines such as HeLa, HEK 293T, CaSki and C33A^{94, 95, 98}. Recently, these effects on cell proliferation have been attributed to regulation of the inositol 1,4,5-triphosphate receptor (IP3R) by ORP4L^{95, 96}. More specifically, ORP4L silencing decreases IP3R expression, which prevents Ca²⁺ efflux from the ER to the cytosol and mitochondria⁹⁵ and impairs mitochondrial bioenergetics, with detrimental effects on cell growth and proliferation⁹⁶. To my knowledge, the effects of ORP4 depletion on primary hippocampal cells has not been explored in detail.

Glial cells are proliferating at DIV8 but have ceased/slowed proliferation at DIV15. I transduced with shORP4 or shORP4L and found that while gross glial

morphology was unaffected at both developmental stages, glial populations were visibly reduced in cultures with proliferating glia but not when glial proliferation had ceased/slowed (Figure 10), suggesting a role for ORP4 in proliferation or cell death. Hoechst staining revealed that transduction with shORP4 or shORP4L did not increase the proportion of apoptotic cells relative to control (Figure 12A), even upon treatment with rotenone as a positive effector of mitochondrial dysfunction (Figure 12B), and thus, the diminished glial populations were attributable to inhibited glial proliferation. However, determination of the multiplicity of infection in these cultures proved difficult, as lentivirus was prepared with pLKO.1 vectors, which lack a fluorescent reporter, and selection of transduced cells with puromycin was not possible, as this compromises the health and viability of primary hippocampal cultures. Therefore, the assessment of only the cells remaining in culture after transduction with shORP4 or shORP4L may not be entirely representative of cells with decreased ORP4, but rather of cells surviving the insult or of cells that were not transduced. The development of shORP4 and shORP4L vectors with fluorescent reporter constructs is expected to remedy this issue.

Cell division requires sufficient cholesterol for membrane expansion and lipid-dependent signalling¹³². ORP4 shares high sequence similarity with OSBP⁹³, which is a cholesterol sensor/transfer protein, and overexpression of OSBP increases cholesterol biosynthesis¹⁰⁹ by sequestering oxysterols¹¹⁰. I investigated whether ORP4 regulates cholesterol biosynthesis, which could limit cholesterol for membrane formation and inhibit cell proliferation. Transduction with shORP4 or shORP4L did not alter the relative mRNA levels of HMGR, FDFT1 or CYP51 (Figure 9), suggesting that ORP4 does not regulate these cholesterol biosynthetic enzymes at the transcriptional level. The

relative protein expression levels of CYP51 were unchanged with shORP4 or shORP4L, suggesting that ORP4 does not regulate cholesterol synthesis via CYP51 at the translational level (Figure 9). While it is possible that I did not observe changes in cholesterol biosynthesis due to increases in one cell type with balanced decreases in the other, this seems unlikely and suggests that ORP4 does not regulate cholesterol biosynthesis.

Unlike glia, neurons do not proliferate, yet neurons express ORP4L and ORP4S at this developmental stage (Figure 7A), suggesting a role of ORP4 outside of cell proliferation. *ORP4*^{-/-} mice exhibit defects in the apical dendrites of the hippocampus⁹⁸, which suggests that ORP4 is involved in gross neuronal morphology, but I did not observe alterations in neuronal morphology with shORP4 or shORP4L, nor did I observe decreased neuronal cell counts (Figure 11), or increased apoptosis (Figure 12) in these cultures.

4.3.2 ORP4 Regulates Glial And Neuritic Mitochondrial Length

ORP4S contains an FFAT motif, which targets the ER through interactions with VAP¹³³, while ORP4L contains an FFAT motif and PH domain, which interacts with the PI4P in the Golgi¹³⁴. The localization of Golgi proteins is regulated by the levels of cholesterol in the Golgi and thus, OSBP regulates Golgi structure by sensing and transferring cholesterol¹³⁵. ORP4L with a mutated ORD binds the ER protein, VAP, but localizes to the plasma membrane, which could suggest altered ER structure¹⁰⁸. Additionally depletion of ORP4L decreases IP3R expression, which could disrupt ER-mitochondria contacts and/or alter ER or mitochondrial structure^{95, 96}. I found that

transduction with shORP4 or shORP4L did not alter the gross structural morphology of Golgi or ER (Figures 13 and 14).

Members of the ORP superfamily are present and functional at membrane contact sites (MCS) (as reviewed in ⁹⁰). Two highly similar ORPs, ORP5 and ORP8, are present at ER-mitochondria MCS known as the mitochondria-associated ER membrane (MAM), and this localization is facilitated by a functional ORD ¹¹⁵. I investigated the effects of shORP4 or shORP4L on mitochondrial size. Immunostaining with anti-TOM20 antibodies visualizes both neuronal and glial mitochondria, and I focused on mitochondrial length in glia and neurites.

Transduction with shORP4 or shORP4L significantly increased the proportion of elongated mitochondria relative to control (Figure 15B), and increased the distribution range of mitochondrial lengths (Figure 15C). I considered that the increased proportion of elongated mitochondria was in part due to a decreased proportion of fragmented or “small” mitochondria. Small mitochondria are difficult to reliably measure, as image resolution is limited by software pixilation; thus, the proportions of fragmented mitochondria were not assessed but may have been altered as well.

The loss of mitochondrial fission selectively depletes axonal mitochondria in dopaminergic neurons ¹³⁶. Axonal mitochondria are smaller than dendritic mitochondria; thus, the absence of small, axonal mitochondria may be perceived as an increase in elongated mitochondria. Therefore, it is possible that decreased ORP4 prevents fission, which leads to both the elongation of mitochondria and the depletion of small, axonal mitochondria. Alterations to fission and/or fusion could also explain the inhibited proliferation of glial cells transduced with shORP4 or shORP4L, as mitochondrial fission

and fusion processes are tightly linked to the cell cycle and cell division (as reviewed in ¹³⁷). For example, fission protein 1 (FIS1) recruits cytosolic dynamin-related protein 1 (DRP1) to the mitochondrion for fission ¹³⁸, and FIS1 depletion leads to persistent mitochondrial elongation that triggers cell senescence in mammalian cells ¹³⁹ by preventing mitotic entry ¹⁴⁰. Additionally, mitochondrial biogenesis is coupled with cell division ¹⁴¹ and the survival of daughter cells relies on the proper distribution of mitochondria during division. I investigated the relative mRNA levels of FIS1, mitofusin 2 (MFN2, a mitochondrial fusion protein), and transcription factor A for mitochondrial DNA (TFAM), but found that they were unaltered with shORP4 or shORP4L (Figure 17). Thus, ORP4 likely does not directly regulate FIS1, MFN2 or TFAM at the transcriptional level but may regulate fission and fusion processes involving these proteins.

Mitochondrial elongation can occur independently of alterations in fission and fusion machinery. For instance, α -synuclein is a protein that associates with mitochondria and regulates mitochondrial size. Silencing of α -synuclein elongated mitochondria while overexpression of α -synuclein fragmented mitochondria in *Caenorhabditis elegans* neurons, and these effects occurred independently of alterations to fission and fusion proteins ¹⁴². While I did not explore this avenue, it speaks to the possibility of ORP4-mediated regulation of mitochondrial size independently of alterations to fission and fusion protein levels. Additionally, ORP4L depletion was shown to decrease the expression of IP3R ^{95, 96}, which interacts with VDAC at ER-mitochondria MCS. Given that ER-mitochondria MCS formation facilitates mitochondrial fission, specifically by encircling a mitochondrion at division sites through interactions with mitochondrial

proteins ¹⁴³, it is possible that decreased ORP4L expression could decrease the number and/or strength of ER-mitochondria MCS, in turn decreasing fission events. However, Zhong *et al.* found that while ORP4L controls Ca²⁺ release from the ER, it does not control the number of ER-mitochondria MCS in T-cell acute lymphoblastic leukemia cells ⁹⁶, suggesting this is not the mechanism by which ORP4 regulates mitochondrial size. Alternatively, ORP4 could regulate mitochondrial size through Ca²⁺-dependent signalling. For instance, pyruvate dehydrogenase is activated through Ca²⁺-dependent dephosphorylation. ORP4-depletion-mediated decreases in IP3R could prevent Ca²⁺ efflux from the ER and impair activation of pyruvate dehydrogenase, in turn decreasing ATP production. Insufficient ATP production can induce mitochondrial elongation to avoid autophagy and promote cell survival ¹⁴⁴. Additionally, decreased cytosolic Ca²⁺ prevents dephosphorylation and activation of DRP1 ¹⁴⁵, which could elongate mitochondria by inhibiting fission processes. While these theories are speculative, further investigations into the mechanisms underlying the role of ORP4 in regulating mitochondrial size are warranted.

Mitochondria are major sources of ROS, and elongated mitochondria may contribute to and/or be a consequence of increased ROS production. NRF2 is an antioxidant gene transcription factor regulated by oxidative stress. NRF2 is present in the cytosol bound to Kelch-like ECH-associated protein 1 (KEAP1) ¹⁴⁶, which facilitates its ubiquitination and degradation in the proteasome; however, oxidative stress increases NRF2 expression, which saturates KEAP1-binding and allows nuclear translocation and transcriptional activity of NRF2 (as reviewed in ¹⁴⁷). I investigated the effects of shORP4 or shORP4L on mRNA expression of NRF2 and its target, heme oxygenase 1 (HMOX1),

and found that they were comparable to control (Figure 17), suggesting that ORP4 does not regulate NRF2 and HMOX1 expression at the transcriptional level.

4.3.3 ORP4 Regulates Neuronal PINK1 And NRF2 Protein Levels

Mitophagy is the process of targeted mitochondrial degradation and involves the proteins phosphatase and tensin homolog (PTEN)-induced kinase 1 (PINK1), a serine/threonine kinase, and PARKIN, an E3 ubiquitin ligase (as reviewed in ¹⁴⁸). Under physiological conditions and mitochondrial polarization, PINK1 is imported into mitochondria and cleaved, but under conditions of mitochondrial dysfunction and depolarization, PINK1 stabilizes on the mitochondrial outer membrane and phosphorylates proteins like MFN2. PARKIN ubiquitinates these proteins, which recruits the autophagosomal membrane protein microtubule-associated protein 1A/1B-light chain 3 (LC3). Autophagosomes fuse with lysosomes to facilitate degradation of dysfunctional cellular components.

Fission-mediated mitochondrial fragmentation precedes mitophagy, and there is evidence that mitochondria elongate on induction of autophagy, which increases ATP production and prevents mitochondrial degradation ¹⁴⁴. Given that mitochondria elongate after transduction with shORP4 or shORP4L, I speculated that mitophagy was decreased as well. The soma contains lysosomes and is the major site of mitophagy in neurons ¹⁴⁹, and I assessed the levels of PINK1 in neuronal cell bodies. Transduction with shORP4 or shORP4L significantly decreased PINK1 protein levels in the soma (Figure 18), which suggests decreased PINK1 expression or increased mitochondrial entry of PINK1, and in turn could suggest decreased PINK1 accumulation on mitochondria and thus, decreased mitophagy.

PINK1 exhibits differential localization and regulation based on cell type and function (as reviewed in ¹⁵⁰), and can be cytosolic or localized to mitochondria. For example, cytosolic PINK1 promotes neurite growth and mitochondrial transport in SH-SY5Y neuroblastoma cells as well as cortical and dopaminergic neurons ¹⁵¹. Additionally, cytosolic PINK1 promotes Ca²⁺ efflux from mitochondria ¹¹⁷. Given the role of ORP4 in promoting IP3R expression, it is possible that decreased ORP4 impairs Ca²⁺ efflux from the ER to mitochondria, and PINK1 is downregulated to prevent further Ca²⁺ release from mitochondria and maintain homeostatic mitochondrial Ca²⁺ levels. Additionally, cytosolic PINK1 suppresses protein kinase A (PKA) function and inactivates DRP1, which is necessary for fragmentation of mitochondria and subsequent degradation ¹⁵⁰. Thus, the decreased PINK1 levels apparent with shORP4 or shORP4L could increase PKA activity, thereby preventing mitochondrial fission and elongating mitochondria ¹⁴⁵. However, these theories require further investigations to be corroborated.

PINK1 is also implicated in regulating ROS production, as silencing of PINK1 increases mitochondrial superoxide production in mammalian cells ¹⁵². I assessed neuronal NRF2 levels as an indicator of oxidative stress in these cells and found that shORP4, but not shORP4L, significantly increased somatic NRF2 levels (Figure 19). These results could also suggest that shORP4 i) increases NRF2 expression, ii) impairs the physiological degradation of cytosolic NRF2, and/or iii) impairs nuclear translocation of NRF2. However, NRF2 detected in the soma was largely nuclear (Figure 20), suggesting that nuclear import was not impaired. Taken together, these results suggest

that decreased total ORP4 accumulates and/or inhibits degradation of cytosolic NRF2 without affecting translocation to the nucleus.

4.4 CONCLUSION

Insights into the specific roles of both neuronal cholesterol biosynthesis and the sterol-binding protein, ORP4, are valuable given the widespread use of therapeutics like statins, which inhibit cholesterol biosynthesis, and ORPphilins, which may one day have applications in anti-cancer treatments. The data presented here indicate that neuronal cholesterol biosynthesis influences spine dynamics or development, specifically spine density, but not mitochondrial morphology; however, further investigations are necessary to determine the mechanism(s) underlying this effect.

In addition, the data provide evidence for a role of ORP4 in glial cell proliferation, as decreased ORP4 diminished glial populations without inducing apoptosis. As ORP4 binds PI4P in addition to cholesterol, it is possible that ORP4 maintains or regulates a pool of PI4P for signalling within the cell, and that this signalling is necessary for cell proliferation, but this remains to be determined. The data also suggests that ORP4 regulates mitochondrial size, as decreased total ORP4 or ORP4L elongated mitochondria in both neurons and glia; however, the mechanism(s) involved in mitochondrial elongation are still unclear and it remains to be determined if ORP4 regulates mitochondrial size by regulating fission and fusion machinery at the translational or post-translational level, or independently of fission and fusion machinery, and whether mitochondria-associated proteins, Ca^{2+} signalling or other mechanisms are involved. Finally, the data provide insight into subcellular neuronal protein levels that may be associated with mitochondrial elongation, specifically PINK1 and NRF2.

Decreased total ORP4 or ORP4L decreased somatic PINK1 levels, while decreased total ORP4, but not ORP4L, increased somatic NRF2 levels without altering nuclear NRF2 levels. Further investigations into the isoform-specific effects of ORP4 by brain cell type would be valuable in fully elucidating the role of ORP4 in hippocampal neurons and glia.

REFERENCES

1. Rajmohan, V. & Mohandas, E. The limbic system. *Indian. J. Psychiatry.* **49**, 132-139 (2007).
2. Ferri, C. P. *et al.* Global prevalence of dementia: a Delphi consensus study. *Lancet* **366**, 2112-2117 (2005).
3. Ballabh, P., Braun, A. & Nedergaard, M. The blood-brain barrier: an overview: structure, regulation, and clinical implications. *Neurobiol. Dis.* **16**, 1-13 (2004).
4. Dietschy, J. M. & Turley, S. D. Cholesterol metabolism in the brain. *Curr. Opin. Lipidol.* **12**, 105-112 (2001).
5. Horton, A. C. & Ehlers, M. D. Dual modes of endoplasmic reticulum-to-Golgi transport in dendrites revealed by live-cell imaging. *J. Neurosci.* **23**, 6188-6199 (2003).
6. Sabatini, B. L., Maravall, M. & Svoboda, K. Ca²⁺ signaling in dendritic spines. *Curr. Opin. Neurobiol.* **11**, 349-356 (2001).
7. van Vliet, A. R., Verfaillie, T. & Agostinis, P. New functions of mitochondria associated membranes in cellular signaling. *Biochim. Biophys. Acta* (2014).
8. Saarikangas, J. *et al.* MIM-Induced Membrane Bending Promotes Dendritic Spine Initiation. *Dev. Cell.* **33**, 644-659 (2015).
9. Hering, H. & Sheng, M. Dendritic spines: structure, dynamics and regulation. *Nat. Rev. Neurosci.* **2**, 880-888 (2001).
10. Ziv, N. E. & Smith, S. J. Evidence for a role of dendritic filopodia in synaptogenesis and spine formation. *Neuron* **17**, 91-102 (1996).
11. Fiala, J. C., Feinberg, M., Popov, V. & Harris, K. M. Synaptogenesis via dendritic filopodia in developing hippocampal area CA1. *J. Neurosci.* **18**, 8900-8911 (1998).
12. Barnett, M. W. & Larkman, P. M. The action potential. *Pract. Neurol.* **7**, 192-197 (2007).
13. Couteaux, R. & Pecot-Dechavassine, M. Synaptic vesicles and pouches at the level of "active zones" of the neuromuscular junction. *C. R. Acad. Sci. Hebd. Seances. Acad. Sci. D.* **271**, 2346-2349 (1970).
14. Heuser, J. E. & Reese, T. S. Evidence for recycling of synaptic vesicle membrane during transmitter release at the frog neuromuscular junction. *J. Cell Biol.* **57**, 315-344 (1973).

15. Harris, K. M. & Kater, S. B. Dendritic spines: cellular specializations imparting both stability and flexibility to synaptic function. *Annu. Rev. Neurosci.* **17**, 341-371 (1994).
16. Sorra, K. E. & Harris, K. M. Overview on the structure, composition, function, development, and plasticity of hippocampal dendritic spines. *Hippocampus* **10**, 501-511 (2000).
17. Dong, X. X., Wang, Y. & Qin, Z. H. Molecular mechanisms of excitotoxicity and their relevance to pathogenesis of neurodegenerative diseases. *Acta Pharmacol. Sin.* **30**, 379-387 (2009).
18. Nedergaard, M., Ransom, B. & Goldman, S. A. New roles for astrocytes: redefining the functional architecture of the brain. *Trends Neurosci.* **26**, 523-530 (2003).
19. Belanger, M., Allaman, I. & Magistretti, P. J. Brain energy metabolism: focus on astrocyte-neuron metabolic cooperation. *Cell. Metab.* **14**, 724-738 (2011).
20. Mauch, D. H. *et al.* CNS synaptogenesis promoted by glia-derived cholesterol. *Science* **294**, 1354-1357 (2001).
21. Ullian, E. M., Sapperstein, S. K., Christopherson, K. S. & Barres, B. A. Control of synapse number by glia. *Science* **291**, 657-661 (2001).
22. Steinmetz, C. C., Buard, I., Claudepierre, T., Nagler, K. & Pfrieder, F. W. Regional variations in the glial influence on synapse development in the mouse CNS. *J. Physiol.* **577**, 249-261 (2006).
23. Ventura, R. & Harris, K. M. Three-dimensional relationships between hippocampal synapses and astrocytes. *J. Neurosci.* **19**, 6897-6906 (1999).
24. Xu-Friedman, M. A., Harris, K. M. & Regehr, W. G. Three-dimensional comparison of ultrastructural characteristics at depressing and facilitating synapses onto cerebellar Purkinje cells. *J. Neurosci.* **21**, 6666-6672 (2001).
25. Bradl, M. & Lassmann, H. Oligodendrocytes: biology and pathology. *Acta Neuropathol.* **119**, 37-53 (2010).
26. Gehrmann, J., Matsumoto, Y. & Kreutzberg, G. W. Microglia: intrinsic immune effector cell of the brain. *Brain Res. Brain Res. Rev.* **20**, 269-287 (1995).
27. Ikonen, E. Cellular cholesterol trafficking and compartmentalization. *Nat. Rev. Mol. Cell Biol.* **9**, 125-138 (2008).
28. Chang, T. Y., Chang, C. C., Ohgami, N. & Yamauchi, Y. Cholesterol sensing, trafficking, and esterification. *Annu. Rev. Cell Dev. Biol.* **22**, 129-157 (2006).

29. Lange, B. M., Rujan, T., Martin, W. & Croteau, R. Isoprenoid biosynthesis: the evolution of two ancient and distinct pathways across genomes. *Proc. Natl. Acad. Sci. U. S. A.* **97**, 13172-13177 (2000).
30. Siperstein, M. D. Role of cholesterologenesis and isoprenoid synthesis in DNA replication and cell growth. *J. Lipid Res.* **25**, 1462-1468 (1984).
31. Kandutsch, A. A. & Russell, A. E. Preputial gland tumor sterols. 3. A metabolic pathway from lanosterol to cholesterol. *J. Biol. Chem.* **235**, 2256-2261 (1960).
32. Nieweg, K., Schaller, H. & Pfrieder, F. W. Marked differences in cholesterol synthesis between neurons and glial cells from postnatal rats. *J. Neurochem.* **109**, 125-134 (2009).
33. Waelsch, H. Lipid metabolism in brain during myelination. *J. Biol. Chem.* **135**, 297-302 (1940).
34. Quan, G., Xie, C., Dietschy, J. M. & Turley, S. D. Ontogenesis and regulation of cholesterol metabolism in the central nervous system of the mouse. *Brain Res. Dev. Brain Res.* **146**, 87-98 (2003).
35. Thelen, K. M., Falkai, P., Bayer, T. A. & Lutjohann, D. Cholesterol synthesis rate in human hippocampus declines with aging. *Neurosci. Lett.* **403**, 15-19 (2006).
36. Vance, J. E., Pan, D., Campenot, R. B., Bussiere, M. & Vance, D. E. Evidence that the major membrane lipids, except cholesterol, are made in axons of cultured rat sympathetic neurons. *J. Neurochem.* **62**, 329-337 (1994).
37. Michikawa, M. & Yanagisawa, K. Inhibition of cholesterol production but not of nonsterol isoprenoid products induces neuronal cell death. *J. Neurochem.* **72**, 2278-2285 (1999).
38. Funfschilling, U. *et al.* Critical time window of neuronal cholesterol synthesis during neurite outgrowth. *J. Neurosci.* **32**, 7632-7645 (2012).
39. Korade, Z., Mi, Z., Portugal, C. & Schor, N. F. Expression and p75 neurotrophin receptor dependence of cholesterol synthetic enzymes in adult mouse brain. *Neurobiol. Aging* **28**, 1522-1531 (2007).
40. Lein, E. S. *et al.* Genome-wide atlas of gene expression in the adult mouse brain. *Nature* **445**, 168-176 (2007).
41. Valdez, C. M., Smith, M. A., Perry, G., Phelix, C. F. & Santamaria, F. Cholesterol homeostasis markers are localized to mouse hippocampal pyramidal and granule layers. *Hippocampus* **20**, 902-905 (2010).

42. Vallejo, M. PACAP signaling to DREAM: a cAMP-dependent pathway that regulates cortical astroglialogenesis. *Mol. Neurobiol.* **39**, 90-100 (2009).
43. Dietschy, J. M. & Turley, S. D. Thematic review series: brain Lipids. Cholesterol metabolism in the central nervous system during early development and in the mature animal. *J. Lipid Res.* **45**, 1375-1397 (2004).
44. Hayashi, H., Campenot, R. B., Vance, D. E. & Vance, J. E. Apolipoprotein E-containing lipoproteins protect neurons from apoptosis via a signaling pathway involving low-density lipoprotein receptor-related protein-1. *J. Neurosci.* **27**, 1933-1941 (2007).
45. Boyles, J. K., Pitas, R. E., Wilson, E., Mahley, R. W. & Taylor, J. M. Apolipoprotein E associated with astrocytic glia of the central nervous system and with nonmyelinating glia of the peripheral nervous system. *J. Clin. Invest.* **76**, 1501-1513 (1985).
46. Vance, J. E. Dysregulation of cholesterol balance in the brain: contribution to neurodegenerative diseases. *Dis. Model. Mech.* **5**, 746-755 (2012).
47. Wahrle, S. E. *et al.* ABCA1 is required for normal central nervous system ApoE levels and for lipidation of astrocyte-secreted apoE. *J. Biol. Chem.* **279**, 40987-40993 (2004).
48. Pfriefer, F. W. & Barres, B. A. New views on synapse-glia interactions. *Curr. Opin. Neurobiol.* **6**, 615-621 (1996).
49. Pfriefer, F. W. & Barres, B. A. Synaptic efficacy enhanced by glial cells in vitro. *Science* **277**, 1684-1687 (1997).
50. Hayashi, H., Campenot, R. B., Vance, D. E. & Vance, J. E. Glial lipoproteins stimulate axon growth of central nervous system neurons in compartmented cultures. *J. Biol. Chem.* **279**, 14009-14015 (2004).
51. Liu, Q. *et al.* Neuronal LRP1 knockout in adult mice leads to impaired brain lipid metabolism and progressive, age-dependent synapse loss and neurodegeneration. *J. Neurosci.* **30**, 17068-17078 (2010).
52. Bjorkhem, I., Lutjohann, D., Breuer, O., Sakinis, A. & Wennmalm, A. Importance of a novel oxidative mechanism for elimination of brain cholesterol. Turnover of cholesterol and 24(S)-hydroxycholesterol in rat brain as measured with $^{18}\text{O}_2$ techniques in vivo and in vitro. *J. Biol. Chem.* **272**, 30178-30184 (1997).
53. Lehmann, J. M. *et al.* Activation of the nuclear receptor LXR by oxysterols defines a new hormone response pathway. *J. Biol. Chem.* **272**, 3137-3140 (1997).

54. Russell, D. W., Halford, R. W., Ramirez, D. M., Shah, R. & Kotti, T. Cholesterol 24-hydroxylase: an enzyme of cholesterol turnover in the brain. *Annu. Rev. Biochem.* **78**, 1017-1040 (2009).
55. Abildayeva, K. *et al.* 24(S)-hydroxycholesterol participates in a liver X receptor-controlled pathway in astrocytes that regulates apolipoprotein E-mediated cholesterol efflux. *J. Biol. Chem.* **281**, 12799-12808 (2006).
56. Lutjohann, D. *et al.* Cholesterol homeostasis in human brain: evidence for an age-dependent flux of 24S-hydroxycholesterol from the brain into the circulation. *Proc. Natl. Acad. Sci. U. S. A.* **93**, 9799-9804 (1996).
57. Lund, E. G. *et al.* Knockout of the cholesterol 24-hydroxylase gene in mice reveals a brain-specific mechanism of cholesterol turnover. *J. Biol. Chem.* **278**, 22980-22988 (2003).
58. Pitas, R. E., Boyles, J. K., Lee, S. H., Foss, D. & Mahley, R. W. Astrocytes synthesize apolipoprotein E and metabolize apolipoprotein E-containing lipoproteins. *Biochim. Biophys. Acta* **917**, 148-161 (1987).
59. Ohyama, Y. *et al.* Studies on the transcriptional regulation of cholesterol 24-hydroxylase (CYP46A1): marked insensitivity toward different regulatory axes. *J. Biol. Chem.* **281**, 3810-3820 (2006).
60. Sharpe, L. J. & Brown, A. J. Controlling cholesterol synthesis beyond 3-hydroxy-3-methylglutaryl-CoA reductase (HMGCR). *J. Biol. Chem.* **288**, 18707-18715 (2013).
61. Radhakrishnan, A., Sun, L. P., Kwon, H. J., Brown, M. S. & Goldstein, J. L. Direct binding of cholesterol to the purified membrane region of SCAP: mechanism for a sterol-sensing domain. *Mol. Cell* **15**, 259-268 (2004).
62. Gaylor, J. L. Membrane-bound enzymes of cholesterol synthesis from lanosterol. *Biochem. Biophys. Res. Commun.* **292**, 1139-1146 (2002).
63. Song, B. L., Javitt, N. B. & DeBose-Boyd, R. A. Insig-mediated degradation of HMG CoA reductase stimulated by lanosterol, an intermediate in the synthesis of cholesterol. *Cell. Metab.* **1**, 179-189 (2005).
64. DeBose-Boyd, R. A. Feedback regulation of cholesterol synthesis: sterol-accelerated ubiquitination and degradation of HMG CoA reductase. *Cell Res.* **18**, 609-621 (2008).
65. Zhu, J. *et al.* Effects of FoxO4 overexpression on cholesterol biosynthesis, triacylglycerol accumulation, and glucose uptake. *J. Lipid Res.* **51**, 1312-1324 (2010).

66. Janowski, B. A., Willy, P. J., Devi, T. R., Falck, J. R. & Mangelsdorf, D. J. An oxysterol signalling pathway mediated by the nuclear receptor LXR alpha. *Nature* **383**, 728-731 (1996).
67. Wolf, G. The role of oxysterols in cholesterol homeostasis. *Nutr. Rev.* **57**, 196-198 (1999).
68. Hanley, K. *et al.* Oxysterols induce differentiation in human keratinocytes and increase Ap-1-dependent involucrin transcription. *J. Invest. Dermatol.* **114**, 545-553 (2000).
69. Venkateswaran, A. *et al.* Control of cellular cholesterol efflux by the nuclear oxysterol receptor LXR alpha. *Proc. Natl. Acad. Sci. U. S. A.* **97**, 12097-12102 (2000).
70. Sehayek, E., Butbul, E., Avner, R., Levkovitz, H. & Eisenberg, S. Enhanced cellular metabolism of very low density lipoprotein by simvastatin. A novel mechanism of action of HMG-CoA reductase inhibitors. *Eur. J. Clin. Invest.* **24**, 173-178 (1994).
71. Corsini, A. *et al.* New insights into the pharmacodynamic and pharmacokinetic properties of statins. *Pharmacol. Ther.* **84**, 413-428 (1999).
72. Huneeus, V. Q., Wiley, M. H. & Siperstein, M. D. Isopentenyladenine as a mediator of mevalonate-regulated DNA replication. *Proc. Natl. Acad. Sci. U. S. A.* **77**, 5842-5846 (1980).
73. Higgins, J. B. & Casey, P. J. The role of prenylation in G-protein assembly and function. *Cell. Signal.* **8**, 433-437 (1996).
74. Lim, L. *et al.* Lanosterol induces mitochondrial uncoupling and protects dopaminergic neurons from cell death in a model for Parkinson's disease. *Cell Death Differ.* **19**, 416-427 (2012).
75. Tint, G. S. *et al.* The Smith-Lemli-Opitz syndrome: a potentially fatal birth defect caused by a block in the last enzymatic step in cholesterol biosynthesis. *Subcell. Biochem.* **28**, 117-144 (1997).
76. Cunniff, C., Kratz, L. E., Moser, A., Natowicz, M. R. & Kelley, R. I. Clinical and biochemical spectrum of patients with RSH/Smith-Lemli-Opitz syndrome and abnormal cholesterol metabolism. *Am. J. Med. Genet.* **68**, 263-269 (1997).
77. Vance, J. E. Transfer of cholesterol by the NPC team. *Cell. Metab.* **12**, 105-106 (2010).
78. Sarna, J. R. *et al.* Patterned Purkinje cell degeneration in mouse models of Niemann-Pick type C disease. *J. Comp. Neurol.* **456**, 279-291 (2003).

79. Valenza, M. *et al.* Dysfunction of the cholesterol biosynthetic pathway in Huntington's disease. *J. Neurosci.* **25**, 9932-9939 (2005).
80. Taylor, F. R. & Kandutsch, A. A. Oxysterol binding protein. *Chem. Phys. Lipids* **38**, 187-194 (1985).
81. Wang, C., JeBailey, L. & Ridgway, N. D. Oxysterol-binding-protein (OSBP)-related protein 4 binds 25-hydroxycholesterol and interacts with vimentin intermediate filaments. *Biochem. J.* **361**, 461-472 (2002).
82. Wang, P. Y., Weng, J., Lee, S. & Anderson, R. G. The N terminus controls sterol binding while the C terminus regulates the scaffolding function of OSBP. *J. Biol. Chem.* **283**, 8034-8045 (2008).
83. Ridgway, N. D., Dawson, P. A., Ho, Y. K., Brown, M. S. & Goldstein, J. L. Translocation of oxysterol binding protein to Golgi apparatus triggered by ligand binding. *J. Cell Biol.* **116**, 307-319 (1992).
84. Mesmin, B. *et al.* A four-step cycle driven by PI(4)P hydrolysis directs sterol/PI(4)P exchange by the ER-Golgi tether OSBP. *Cell* **155**, 830-843 (2013).
85. Perry, R. J. & Ridgway, N. D. Oxysterol-binding protein and vesicle-associated membrane protein-associated protein are required for sterol-dependent activation of the ceramide transport protein. *Mol. Biol. Cell* **17**, 2604-2616 (2006).
86. Janowski, B. A., Shan, B. & Russell, D. W. The hypocholesterolemic agent LY295427 reverses suppression of sterol regulatory element-binding protein processing mediated by oxysterols. *J. Biol. Chem.* **276**, 45408-45416 (2001).
87. Kandutsch, A. A. & Chen, H. W. Inhibition of sterol synthesis in cultured mouse cells by cholesterol derivatives oxygenated in the side chain. *J. Biol. Chem.* **249**, 6057-6061 (1974).
88. Schroepfer, G. J., Jr. Oxysterols: modulators of cholesterol metabolism and other processes. *Physiol. Rev.* **80**, 361-554 (2000).
89. Bowden, K. & Ridgway, N. D. OSBP negatively regulates ABCA1 protein stability. *J. Biol. Chem.* **283**, 18210-18217 (2008).
90. Kentala, H., Weber-Boyyat, M. & Olkkonen, V. M. OSBP-Related Protein Family: Mediators of Lipid Transport and Signaling at Membrane Contact Sites. *Int. Rev. Cell. Mol. Biol.* **321**, 299-340 (2016).
91. Lehto, M. *et al.* The OSBP-related protein family in humans. *J. Lipid Res.* **42**, 1203-1213 (2001).

92. Xu, Y., Liu, Y., Ridgway, N. D. & McMaster, C. R. Novel members of the human oxysterol-binding protein family bind phospholipids and regulate vesicle transport. *J. Biol. Chem.* **276**, 18407-18414 (2001).
93. Moreira, E. F., Jaworski, C., Li, A. & Rodriguez, I. R. Molecular and biochemical characterization of a novel oxysterol-binding protein (OSBP2) highly expressed in retina. *J. Biol. Chem.* **276**, 18570-18578 (2001).
94. Charman, M., Colbourne, T. R., Pietrangelo, A., Kreplak, L. & Ridgway, N. D. Oxysterol-binding protein (OSBP)-related protein 4 (ORP4) is essential for cell proliferation and survival. *J. Biol. Chem.* **289**, 15705-15717 (2014).
95. Li, J. W. *et al.* Oxysterol-binding protein-related protein 4L promotes cell proliferation by sustaining intracellular Ca²⁺ homeostasis in cervical carcinoma cell lines. *Oncotarget* (2016).
96. Zhong, W. *et al.* ORP4L is essential for T-cell acute lymphoblastic leukemia cell survival. *Nat. Commun.* **7**, 12702 (2016).
97. Wyles, J. P., Perry, R. J. & Ridgway, N. D. Characterization of the sterol-binding domain of oxysterol-binding protein (OSBP)-related protein 4 reveals a novel role in vimentin organization. *Exp. Cell Res.* **313**, 1426-1437 (2007).
98. Udagawa, O. *et al.* Oligo-astheno-teratozoospermia in mice lacking ORP4, a sterol-binding protein in the OSBP-related protein family. *Genes Cells* **19**, 13-27 (2014).
99. Burgett, A. W. *et al.* Natural products reveal cancer cell dependence on oxysterol-binding proteins. *Nat. Chem. Biol.* **7**, 639-647 (2011).
100. Karra, D. & Dahm, R. Transfection techniques for neuronal cells. *J. Neurosci.* **30**, 6171-6177 (2010).
101. Sattler, W., Mohr, D. & Stocker, R. Rapid isolation of lipoproteins and assessment of their peroxidation by high-performance liquid chromatography postcolumn chemiluminescence. *Methods Enzymol.* **233**, 469-489 (1994).
102. Smith, P. K. *et al.* Measurement of protein using bicinchoninic acid. *Anal. Biochem.* **150**, 76-85 (1985).
103. Dotti, C. G., Esteban, J. A. & Ledesma, M. D. Lipid dynamics at dendritic spines. *Front. Neuroanat.* **8**, 76 (2014).
104. Papa, M., Bundman, M. C., Greenberger, V. & Segal, M. Morphological analysis of dendritic spine development in primary cultures of hippocampal neurons. *J. Neurosci.* **15**, 1-11 (1995).

105. Golomb, B. A. & Evans, M. A. Statin adverse effects : a review of the literature and evidence for a mitochondrial mechanism. *Am. J. Cardiovasc. Drugs* **8**, 373-418 (2008).
106. Littarru, G. P. & Langsjoen, P. Coenzyme Q10 and statins: biochemical and clinical implications. *Mitochondrion* **7 Suppl**, S168-74 (2007).
107. Hernandez, G. *et al.* MitoTimer: a novel tool for monitoring mitochondrial turnover. *Autophagy* **9**, 1852-1861 (2013).
108. Kentala, H., Pfisterer, S. G., Olkkonen, V. M. & Weber-Boyvat, M. Sterol liganding of OSBP-related proteins (ORPs) regulates the subcellular distribution of ORP-VAPA complexes and their impacts on organelle structure. *Steroids* **99**, 248-258 (2015).
109. Lagace, T. A., Byers, D. M., Cook, H. W. & Ridgway, N. D. Altered regulation of cholesterol and cholesteryl ester synthesis in Chinese-hamster ovary cells overexpressing the oxysterol-binding protein is dependent on the pleckstrin homology domain. *Biochem. J.* **326 (Pt 1)**, 205-213 (1997).
110. Nishimura, T. *et al.* Inhibition of cholesterol biosynthesis by 25-hydroxycholesterol is independent of OSBP. *Genes Cells* **10**, 793-801 (2005).
111. Banerji, S. *et al.* Oxysterol binding protein-dependent activation of sphingomyelin synthesis in the golgi apparatus requires phosphatidylinositol 4-kinase IIalpha. *Mol. Biol. Cell* **21**, 4141-4150 (2010).
112. Nhek, S. *et al.* Regulation of oxysterol-binding protein Golgi localization through protein kinase D-mediated phosphorylation. *Mol. Biol. Cell* **21**, 2327-2337 (2010).
113. Erecinska, M. & Silver, I. A. Ions and energy in mammalian brain. *Prog. Neurobiol.* **43**, 37-71 (1994).
114. Bolanos, J. P., Almeida, A. & Moncada, S. Glycolysis: a bioenergetic or a survival pathway? *Trends Biochem. Sci.* **35**, 145-149 (2010).
115. Galmes, R. *et al.* ORP5/ORP8 localize to endoplasmic reticulum-mitochondria contacts and are involved in mitochondrial function. *EMBO Rep.* **17**, 800-810 (2016).
116. Ashrafi, G., Schlehe, J. S., LaVoie, M. J. & Schwarz, T. L. Mitophagy of damaged mitochondria occurs locally in distal neuronal axons and requires PINK1 and Parkin. *J. Cell Biol.* **206**, 655-670 (2014).
117. Gandhi, S. *et al.* PINK1-associated Parkinson's disease is caused by neuronal vulnerability to calcium-induced cell death. *Mol. Cell* **33**, 627-638 (2009).

118. Pinton, P. *et al.* The Ca²⁺ concentration of the endoplasmic reticulum is a key determinant of ceramide-induced apoptosis: significance for the molecular mechanism of Bcl-2 action. *EMBO J.* **20**, 2690-2701 (2001).
119. Han, D., Antunes, F., Canali, R., Rettori, D. & Cadenas, E. Voltage-dependent anion channels control the release of the superoxide anion from mitochondria to cytosol. *J. Biol. Chem.* **278**, 5557-5563 (2003).
120. Mailman, T., Hariharan, M. & Karten, B. Inhibition of neuronal cholesterol biosynthesis with lovastatin leads to impaired synaptic vesicle release even in the presence of lipoproteins or geranylgeraniol. *J. Neurochem.* **119**, 1002-1015 (2011).
121. Allen, J. A., Halverson-Tamboli, R. A. & Rasenick, M. M. Lipid raft microdomains and neurotransmitter signalling. *Nat. Rev. Neurosci.* **8**, 128-140 (2007).
122. Nagler, K., Mauch, D. H. & Pfrieder, F. W. Glia-derived signals induce synapse formation in neurones of the rat central nervous system. *J. Physiol.* **533**, 665-679 (2001).
123. Nakajima, C. *et al.* Low density lipoprotein receptor-related protein 1 (LRP1) modulates N-methyl-D-aspartate (NMDA) receptor-dependent intracellular signaling and NMDA-induced regulation of postsynaptic protein complexes. *J. Biol. Chem.* **288**, 21909-21923 (2013).
124. Spacek, J. & Harris, K. M. Three-dimensional organization of smooth endoplasmic reticulum in hippocampal CA1 dendrites and dendritic spines of the immature and mature rat. *J. Neurosci.* **17**, 190-203 (1997).
125. Martin, M. G. *et al.* Cholesterol loss enhances TrkB signaling in hippocampal neurons aging in vitro. *Mol. Biol. Cell* **19**, 2101-2112 (2008).
126. Ji, Y., Pang, P. T., Feng, L. & Lu, B. Cyclic AMP controls BDNF-induced TrkB phosphorylation and dendritic spine formation in mature hippocampal neurons. *Nat. Neurosci.* **8**, 164-172 (2005).
127. Fukumitsu, K. *et al.* Synergistic action of dendritic mitochondria and creatine kinase maintains ATP homeostasis and actin dynamics in growing neuronal dendrites. *J. Neurosci.* **35**, 5707-5723 (2015).
128. Li, Z., Okamoto, K., Hayashi, Y. & Sheng, M. The importance of dendritic mitochondria in the morphogenesis and plasticity of spines and synapses. *Cell* **119**, 873-887 (2004).
129. Attwell, D. & Laughlin, S. B. An energy budget for signaling in the grey matter of the brain. *J. Cereb. Blood Flow Metab.* **21**, 1133-1145 (2001).

130. Mironov, S. L. Complexity of mitochondrial dynamics in neurons and its control by ADP produced during synaptic activity. *Int. J. Biochem. Cell Biol.* **41**, 2005-2014 (2009).
131. Dallner, G. & Sindelar, P. J. Regulation of ubiquinone metabolism. *Free Radic. Biol. Med.* **29**, 285-294 (2000).
132. Sheng, R. *et al.* Cholesterol modulates cell signaling and protein networking by specifically interacting with PDZ domain-containing scaffold proteins. *Nat. Commun.* **3**, 1249 (2012).
133. Wyles, J. P., McMaster, C. R. & Ridgway, N. D. Vesicle-associated membrane protein-associated protein-A (VAP-A) interacts with the oxysterol-binding protein to modify export from the endoplasmic reticulum. *J. Biol. Chem.* **277**, 29908-29918 (2002).
134. Levine, T. P. & Munro, S. The pleckstrin homology domain of oxysterol-binding protein recognises a determinant specific to Golgi membranes. *Curr. Biol.* **8**, 729-739 (1998).
135. Stuken, E. *et al.* Intra-Golgi protein transport depends on a cholesterol balance in the lipid membrane. *J. Biol. Chem.* **278**, 53112-53122 (2003).
136. Berthet, A. *et al.* Loss of mitochondrial fission depletes axonal mitochondria in midbrain dopamine neurons. *J. Neurosci.* **34**, 14304-14317 (2014).
137. Mitra, K. Mitochondrial fission-fusion as an emerging key regulator of cell proliferation and differentiation. *Bioessays* **35**, 955-964 (2013).
138. Otera, H. *et al.* Mff is an essential factor for mitochondrial recruitment of Drp1 during mitochondrial fission in mammalian cells. *J. Cell Biol.* **191**, 1141-1158 (2010).
139. Lee, S. *et al.* Mitochondrial fission and fusion mediators, hFis1 and OPA1, modulate cellular senescence. *J. Biol. Chem.* **282**, 22977-22983 (2007).
140. Lee, S. *et al.* Human mitochondrial Fis1 links to cell cycle regulators at G2/M transition. *Cell Mol. Life Sci.* **71**, 711-725 (2014).
141. Martinez-Diez, M., Santamaria, G., Ortega, A. D. & Cuezva, J. M. Biogenesis and dynamics of mitochondria during the cell cycle: significance of 3'UTRs. *PLoS One* **1**, e107 (2006).
142. Kamp, F. *et al.* Inhibition of mitochondrial fusion by alpha-synuclein is rescued by PINK1, Parkin and DJ-1. *EMBO J.* **29**, 3571-3589 (2010).
143. Friedman, J. R. *et al.* ER tubules mark sites of mitochondrial division. *Science* **334**, 358-362 (2011).

144. Gomes, L. C., Di Benedetto, G. & Scorrano, L. During autophagy mitochondria elongate, are spared from degradation and sustain cell viability. *Nat. Cell Biol.* **13**, 589-598 (2011).
145. Chang, C. R. & Blackstone, C. Cyclic AMP-dependent protein kinase phosphorylation of Drp1 regulates its GTPase activity and mitochondrial morphology. *J. Biol. Chem.* **282**, 21583-21587 (2007).
146. Itoh, K. *et al.* Keap1 represses nuclear activation of antioxidant responsive elements by Nrf2 through binding to the amino-terminal Neh2 domain. *Genes Dev.* **13**, 76-86 (1999).
147. Bryan, H. K., Olayanju, A., Goldring, C. E. & Park, B. K. The Nrf2 cell defence pathway: Keap1-dependent and -independent mechanisms of regulation. *Biochem. Pharmacol.* **85**, 705-717 (2013).
148. Amadoro, G. *et al.* Morphological and bioenergetic demands underlying the mitophagy in post-mitotic neurons: the pink-parkin pathway. *Front. Aging Neurosci.* **6**, 18 (2014).
149. Cai, Q., Zakaria, H. M., Simone, A. & Sheng, Z. H. Spatial parkin translocation and degradation of damaged mitochondria via mitophagy in live cortical neurons. *Curr. Biol.* **22**, 545-552 (2012).
150. Steer, E. K., Dail, M. K. & Chu, C. T. Beyond mitophagy: cytosolic PINK1 as a messenger of mitochondrial health. *Antioxid. Redox Signal.* **22**, 1047-1059 (2015).
151. Dagda, R. K. *et al.* Beyond the mitochondrion: cytosolic PINK1 remodels dendrites through protein kinase A. *J. Neurochem.* **128**, 864-877 (2014).
152. Dagda, R. K. *et al.* Loss of PINK1 function promotes mitophagy through effects on oxidative stress and mitochondrial fission. *J. Biol. Chem.* **284**, 13843-13855 (2009).